Nuclear Science
NEA/NSC/DOC(2007)6

ISBN 978-92-64-99019-7

Mixed-oxide (MOX) Fuel Performance Benchmark

Summary of the Results for the Halden Reactor Project MOX Rods

Compiled by

Terje Tverberg
OECD Halden Reactor Project

Work carried out within the

Expert Group on Reactor-based Plutonium Disposition (TFRPD)

Abstract

Within the framework of the Expert Group on Reactor-based Plutonium disposition (TFRPD), a fuel modelling code benchmark test for MOX fuel was initiated, with in-pile irradiation data on two short MOX rods provided by the OECD Halden Reactor Project (HRP). This note summarises the provided in-pile data and fuel characteristics for the irradiation, and presents the calculation results provided by the contributors. A limited sensitivity study of the effect of the rod power uncertainty on code predictions of fuel centreline temperature and fuel pin pressure has also been performed and is included in the report.

NEA No. 4450

NUCLEAR ENERGY AGENCY
ORGANISATION FOR ECONOMIC CO-OPERATION AND DEVELOPMENT

ORGANISATION FOR ECONOMIC CO-OPERATION AND DEVELOPMENT

The OECD is a unique forum where the governments of 30 democracies work together to address the economic, social and environmental challenges of globalisation. The OECD is also at the forefront of efforts to understand and to help governments respond to new developments and concerns, such as corporate governance, the information economy and the challenges of an ageing population. The Organisation provides a setting where governments can compare policy experiences, seek answers to common problems, identify good practice and work to co-ordinate domestic and international policies.

The OECD member countries are: Australia, Austria, Belgium, Canada, the Czech Republic, Denmark, Finland, France, Germany, Greece, Hungary, Iceland, Ireland, Italy, Japan, Korea, Luxembourg, Mexico, the Netherlands, New Zealand, Norway, Poland, Portugal, the Slovak Republic, Spain, Sweden, Switzerland, Turkey, the United Kingdom and the United States. The Commission of the European Communities takes part in the work of the OECD.

OECD Publishing disseminates widely the results of the Organisation's statistics gathering and research on economic, social and environmental issues, as well as the conventions, guidelines and standards agreed by its members.

* * *

This work is published on the responsibility of the Secretary-General of the OECD. The opinions expressed and arguments employed herein do not necessarily reflect the official views of the Organisation or of the governments of its member countries.

NUCLEAR ENERGY AGENCY

The OECD Nuclear Energy Agency (NEA) was established on 1st February 1958 under the name of the OEEC European Nuclear Energy Agency. It received its present designation on 20th April 1972, when Japan became its first non-European full member. NEA membership today consists of 28 OECD member countries: Australia, Austria, Belgium, Canada, the Czech Republic, Denmark, Finland, France, Germany, Greece, Hungary, Iceland, Ireland, Italy, Japan, Luxembourg, Mexico, the Netherlands, Norway, Portugal, Republic of Korea, the Slovak Republic, Spain, Sweden, Switzerland, Turkey, the United Kingdom and the United States. The Commission of the European Communities also takes part in the work of the Agency.

The mission of the NEA is:

- to assist its member countries in maintaining and further developing, through international co-operation, the scientific, technological and legal bases required for a safe, environmentally friendly and economical use of nuclear energy for peaceful purposes, as well as
- to provide authoritative assessments and to forge common understandings on key issues, as input to government decisions on nuclear energy policy and to broader OECD policy analyses in areas such as energy and sustainable development.

Specific areas of competence of the NEA include safety and regulation of nuclear activities, radioactive waste management, radiological protection, nuclear science, economic and technical analyses of the nuclear fuel cycle, nuclear law and liability, and public information. The NEA Data Bank provides nuclear data and computer program services for participating countries.

In these and related tasks, the NEA works in close collaboration with the International Atomic Energy Agency in Vienna, with which it has a Co-operation Agreement, as well as with other international organisations in the nuclear field.

Cover credit: NEI.

FOREWORD

The NEA Nuclear Science Committee has established an Expert Group that deals with the status and trends of reactor physics, nuclear fuel performance and fuel cycle issues related to the disposition of weapons-grade plutonium as mixed-oxide fuel. The objectives of the group are to provide NEA member countries with up-to-date information on, and develop consensus regarding, core and fuel cycle issues associated with weapons-grade plutonium disposition in thermal water reactors (PWR, BWR, VVER-1000 and CANDU) and fast reactors (BN-600). These issues concern core physics, fuel performance and reliability, and the capability and flexibility of thermal water reactors and fast reactors to dispose of weapons-grade plutonium in standard fuel cycles.

The activities of the NEA Expert Group on Reactor-based Plutonium Disposition are carried out in close co-operation with the NEA Working Party on Scientific Issues in Reactor Systems (WPRS), and in most cases jointly. An eminent part of these activities include benchmark studies.

This report describes the results of the first benchmark relative to MOX fuel behaviour. The corresponding experimental data have been released, compiled and reviewed for the International Fuel Performance Experiments (IFPE) Database. Other MOX fuel behaviour benchmarks being finalised or in progress are:

- Belgonucléaire and SCK•CEN PRIMO ramped MOX fuel rod performance benchmark (ongoing);
- US Department of Energy weapons-grade MOX fuel irradiation experiment irradiated at the advanced test reactor (ATR) benchmark (started);
- MOX fuel rod behaviour in fast power pulse conditions (started).

At the time of preparation of the report the following benchmarks relative to the reactor physics activities of the Expert Group were completed or in progress:

- VENUS-2 MOX core benchmarks, carried out jointly with the WPRS (completed);
- VVER-1000 LEU and MOX benchmark (completed);
- KRITZ-2 benchmarks, carried out jointly with the WPRS (completed);
- benchmark using dosimetry data from the VENUS-2, MOX core experiments (completed);
- VVER-1000 in-core self-powered neutron detector calculational benchmark (started);
- VENUS-7 weapons-grade MOX core benchmark (started).

Contributors

Text

T. Tverberg, OECD Halden Reactor Project (Norway)

Text review

L.J. Ott, ORNL (United States)

E. Sartori, OECD/NEA

Text processing/layout

A. Costa, OECD/NEA

Participants

V. Sobolev, SCK•CEN (Belgium)

B-H. Lee, Y-H. Koo, J-S. Cheon, J-Y. Oh, KAERI (Korea)

K. Mikityuk, A. Shestopalov, P. Fomitchenko, Kurchatov Institute (Russia)

A. Medvedev, S. Bogatyr, V. Kouznetsov, G. Khvostov, M. Korneev, VNIINM-Bochvar (Russia)

G. Rossiter, Nexia Solutions (UK)

L.J. Ott, ORNL (USA)

TABLE OF CONTENTS

Chapter 1

INTRODUCTION

1.1 Irradiation data

The benchmark exercise was performed on a data set provided by the OECD Halden Reactor Project (HRP) of two short MOX rods (one hollow and one solid). The rods were instrumented with fuel thermocouples (TF) and internal rod pressure transducers (PF) and irradiated in the Halden Boiling Water Reactor (HBWR). The irradiation data were provided in plain text format as local rod power (in kW/m) for each rod as a function of irradiation time comprising a total of ~626 irradiation days. Details of the fuel fabrication data as well as information about the provided irradiation data can be found in Appendix I.

The as-provided power data are shown in Figure 1 and Figure 2 for Rod 1 (solid pellets) and Rod 2 (hollow pellets) respectively. The linear heat rates for each fuel rod were given for three axial locations of the rod: bottom, middle and top. In addition the local heat rate at the axial elevation of the fuel centreline thermocouple (TF) tip were provided (denoted LHRTF). The rod average linear heat generation rate, including power uncertainty, for each rod is illustrated in Figures 3 and 4.

The measured fuel temperatures in the two rods during the irradiation are shown in Figures 5 and 6, Rod 1 (solid pellets) and Rod 2 (hollow pellets) respectively, whereas the corresponding measured rod pressures are given in Figures 7 and 8.

Of special note in the power histories is the short power spike at ~170 irradiation days followed by a ~50 day period with slightly higher power than before, during which notable gas release was observed in the rods as can be seen from the pressure curves in Figures 7 and 8. Also notable is the power increase towards the later stages of irradiation (at about ~525 days), which caused large gas release in both rods (see again Figures 7 and 8). The step-wise pressure increase seen for both rods during this period is an indication that the gap is closed at-power here.

It should be noted that the internal pressure measured in the rods during rod puncturing after irradiation was in good agreement with the end-of-life (EOL) pressure from the in-pile measurements shown in these figures.

1.2 Notes about the provided data

1.2.1 Radial power and burn-up profiles

The evolution of radial power and burn-up profiles with burn-up in the hollow and solid pellets has been calculated with the HELIOS code [1]. The results are summarised in Appendix II.

1.2.2 Considerations on the experimental uncertainty in power determination

In general, the irradiation of an instrumented fuel assembly (IFA) in the HBWR starts off with a calorimetric power calibration of the thermal power produced by the fuel in the experiment rig. The experimental uncertainty of this power calibration is generally considered to be within 5%, but somewhat dependent on the actual power produced in the rig (low power means higher uncertainty). Subsequent power calibrations at various stages of irradiation of the IFA are not always possible, and the power change with irradiation will always be reliant, to some degree, on neutronics calculations that are routinely performed for all experiments before start of irradiation.

In the case of the HRP, these neutronics calculations are performed with the HELIOS code [1]. Such calculations will always be dependent on the choice of local geometry (i.e. local surroundings of the irradiation rig) to best describe the actual physical irradiation conditions the rig is subject to throughout its time in-reactor. To evaluate the sensitivity of the HELIOS calculations with respect to the choice of surrounding fuel elements in-core, calculations have been performed for the two extreme cases actually seen by the rig during operation in-pile.

In Figures 3 and 4 the implication on average linear heat rate from the combined uncertainty of the 5% experimental uncertainty of an in-pile power calibration, and the sensitivity of neutronics calculations to changes in local surroundings are plotted for Rod 1 and Rod 2, respectively.

The estimated error increases with burn-up error from the initial 5% (power calibration uncertainty) to ca. 10% at the end of the data set.

The results of a limited sensitivity study of the effects of a ±5% power uncertainty on the computed fuel pin centerline temperature and fuel pin internal pressure are presented in Appendix IV.

1.3 Contributing organisations and codes

The following countries and organisations, and the respective fuel modelling codes they have used, have provided contributions to the benchmark exercise.

Organisation	Fuel modelling code
BNFL (UK)	ENIGMA
KAERI (Korea)	COSMOS
Kurchatov institute (RU)	FRED
ORNL(USA)	FRAPCON-3 v1.3
SCK•CEN (Belgium)	FEMAXI-V MACROS (*not yet included*)
VNIINM-Bochvar (Russia)	START-3

1.4 PIE on irradiated fuel rods

The two MOX rods were subjected to PIE after the end of irradiation. The results of the gas puncturing and mass spectrometry of the extracted gas are summarised in Appendix III.

Figure 1. Power data for Rod 1 (solid)

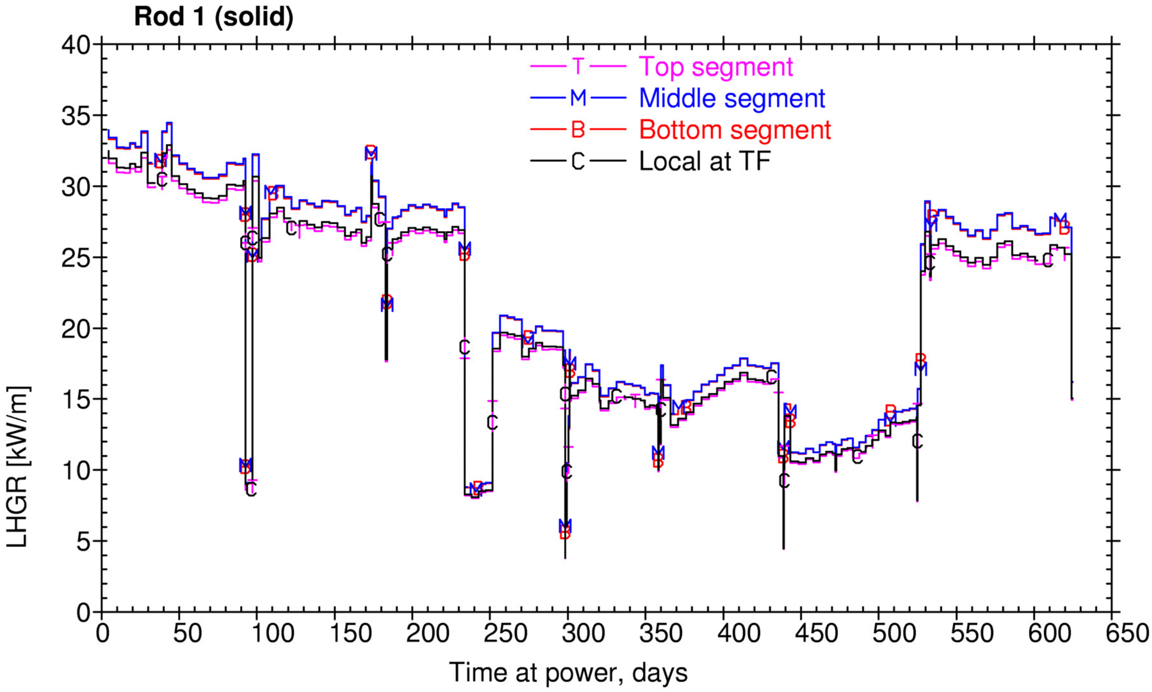

Figure 2. Power data for Rod 2 (hollow)

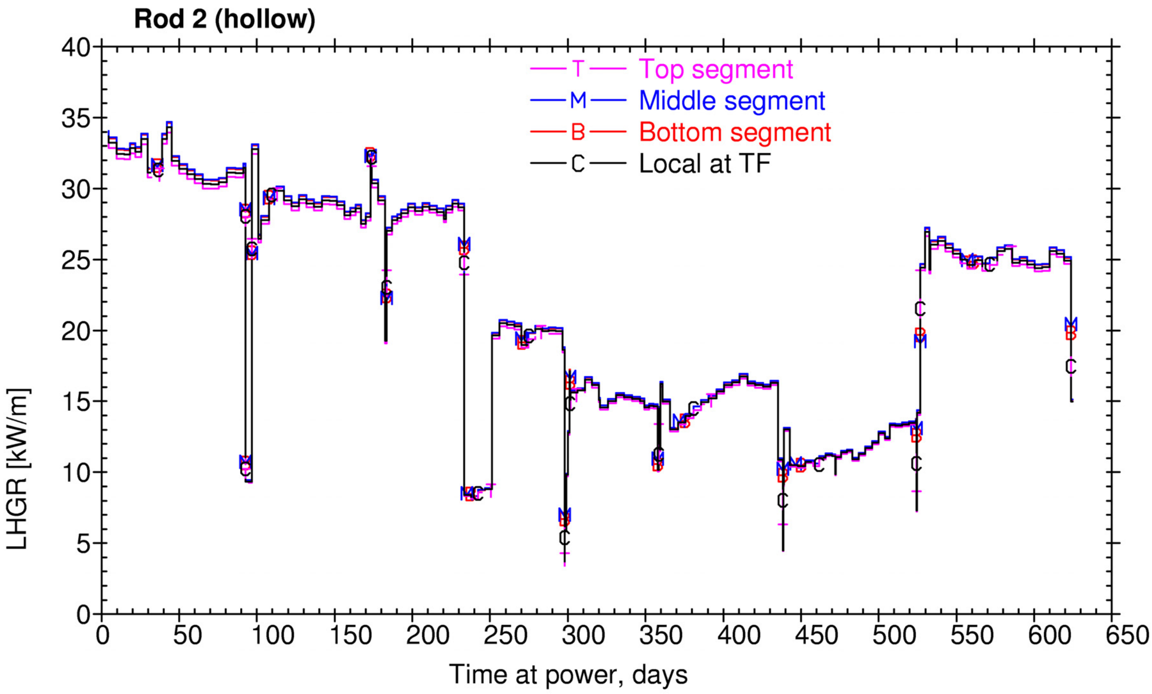

Figure 3. ALHR for Rod 1 (solid) including power uncertainty

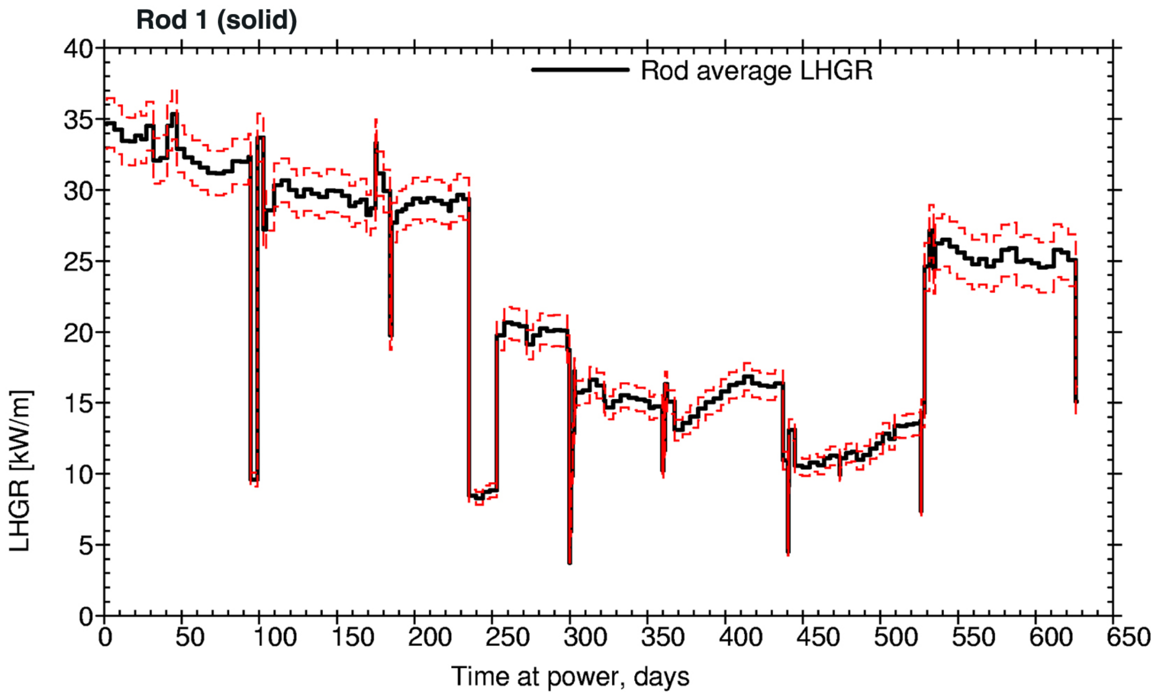

Figure 4. ALHR for Rod 2 (hollow) including power uncertainty

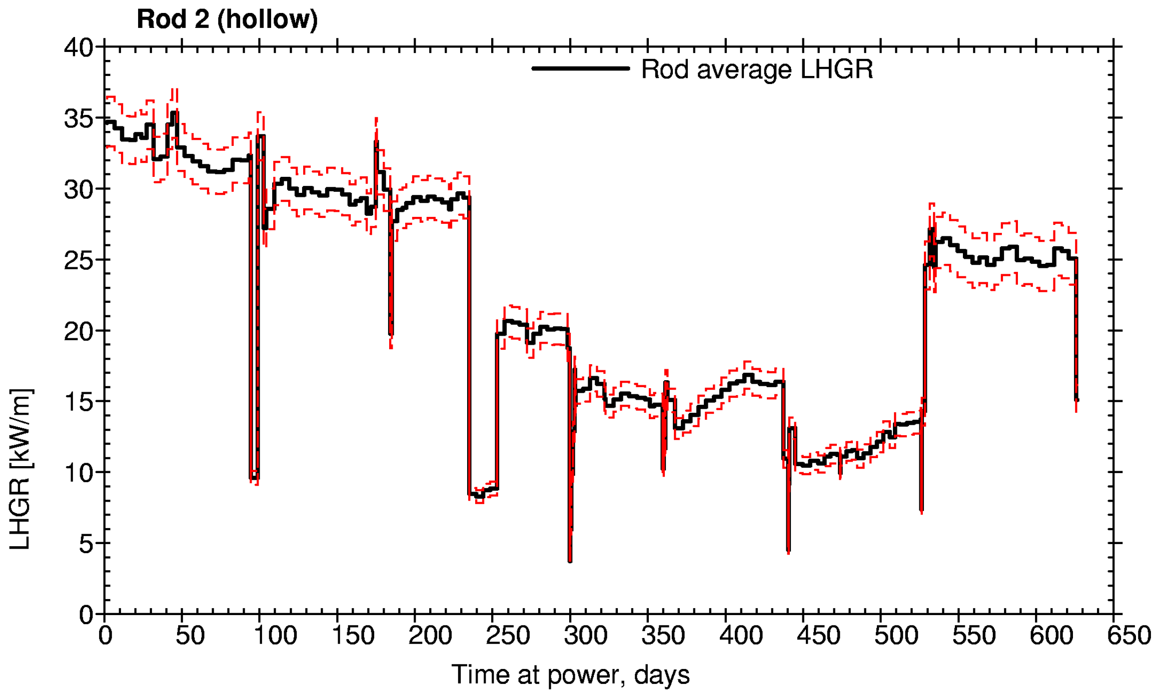

Figure 5. Measured fuel centre temperature for Rod 1 (solid)

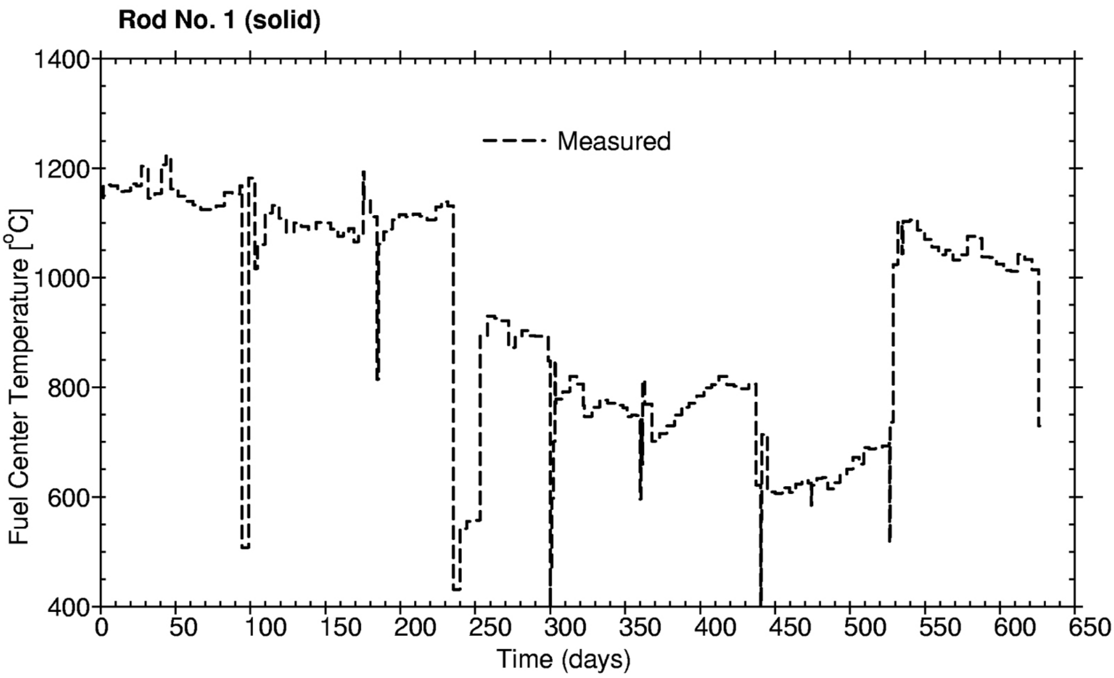

Figure 6. Measured fuel centre temperature for Rod 2 (hollow)

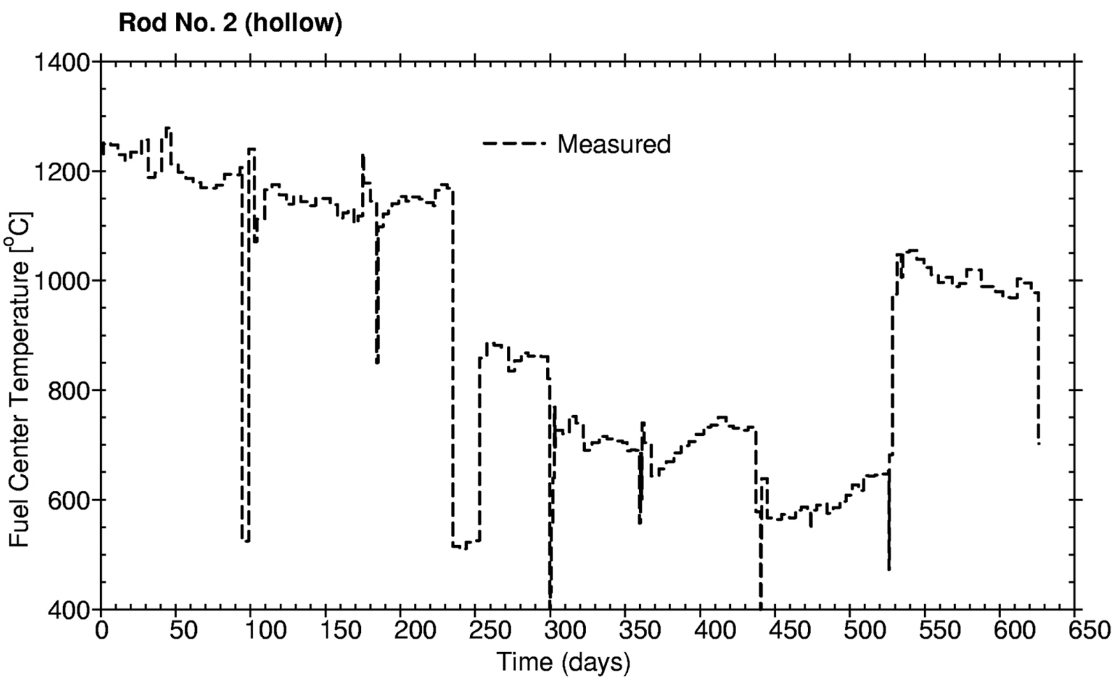

Figure 7. Measured rod pressure for Rod 1 (solid)

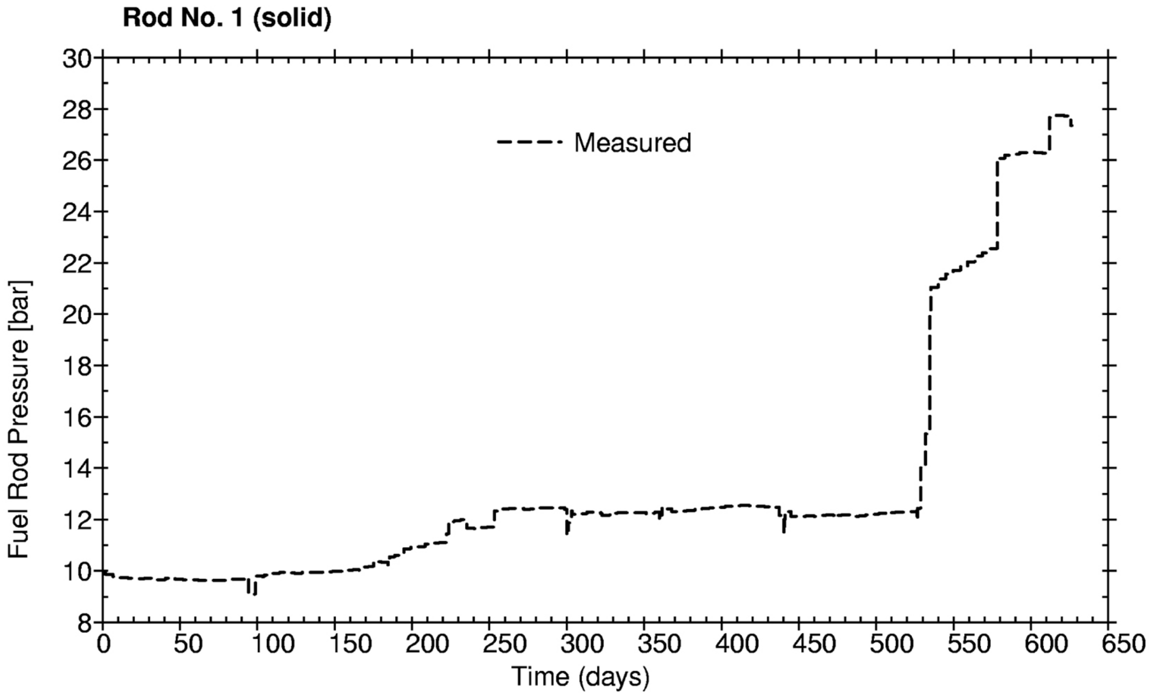

Figure 8. Measured rod pressure for Rod 2 (hollow)

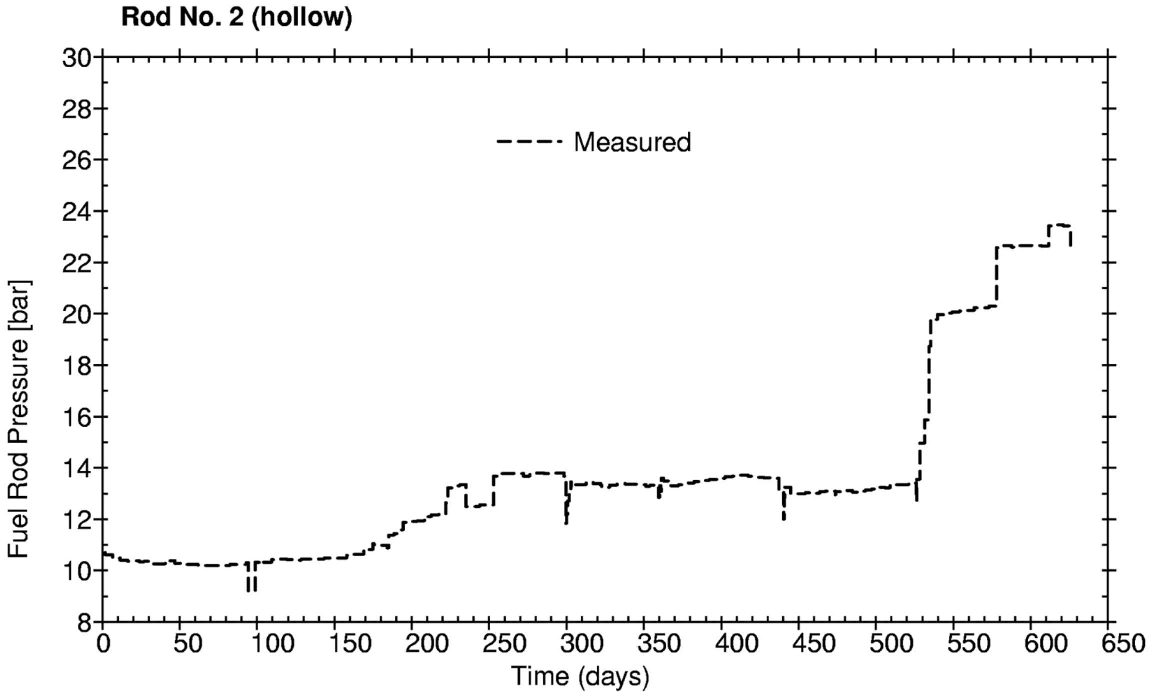

Chapter 2

BRIEF DESCRIPTION OF SOME IMPORTANT PARAMETERS OF THE CODES

2.1 Thermal conductivity of MOX

In the following subsections, a brief summary of the various codes' models for the thermal conductivity of MOX as compared to that of UO_2 fuel is described for each of the codes, as provided by the participants.

2.1.1 BNFL (UK) – ENIGMA

In the ENIGMA code used by BNFL, the thermal conductivity of MOX is reduced by a fixed value of 8% as compared to that of UO_2:

$$k_{MOX} = 0.92 \cdot k_{UO_2}$$

where k_{MOX} is the thermal conductivity of MOX and k_{UO_2} is the thermal conductivity of UO_2.

The low temperature behaviour of the fuel thermal conductivity is modelled by an equation of the form $1/(a + bT)$, where a describes the phonon-impurity scattering, b represents the phonon-phonon scattering and T is the absolute temperature. The conductivity in ENIGMA is modified to an equation of the form $1/(a_0 + a_1B(1 – f) + bT)$ to represent the effects of fission products (i.e. degradation with burn-up), where B is the burn-up and f is the fraction of fission gas atoms not in solution in the matrix, i.e. the fractional sum of all gas which is either in bubbles or has been released. The same degradation is assumed for both MOX and UO_2 fuel [2].

2.1.2 KAERI (Korea) – COSMOS

The COSMOS code uses a thermal conductivity of MOX fuel that takes into account the amount of heterogeneity of the MOX fuel:

$$k_{MOX} = k_{matrix} \cdot \left\{ 1 - a \cdot P_{PuR}^{\frac{2}{3}} \cdot \left[1 - 1 \Big/ \left(1 + \frac{1}{a} \cdot P_{PuR}^{\frac{1}{3}} \left(\frac{k_{matrix}}{k_{PuR}} - 1 \right) \right) \right] \right\}$$

where k_{MOX} is the thermal conductivity of MOX, k_{matrix} is the thermal conductivity of a matrix with only a small amount of Pu, k_{PuR} is the thermal conductivity of Pu rich particles, P_{PuR} is the volumetric fraction of Pu rich particles and a is the anisotropy factor (a = 1 means isotropic pore distribution).

The net effect of the above model is a reduction of 4-8% of the thermal conductivity as compared to UO_2 fuel [3].

2.1.3 Kurchatov Institute (RU) – FRED

The thermal and mechanical properties of LWR MOX fuel in the FRED code are based on available test data and the MATPRO-V11 material property library [4]. The table below summarises the formulation of the fuel thermal conductivity for MOX fuel used in the present calculations.

<table>
<tr><th>Thermal conductivity λ =[W/m K]</th><th>Units</th></tr>
<tr><td rowspan="3">

$$\lambda = \lambda_0 \cdot FD \cdot FP \cdot FR \cdot FM$$

where:

$\lambda_0 = 1.1579 \cdot (A + C \cdot T)^{-1} + \{2.3434 \cdot 10^{11}/T^{2.5}\} \exp[-16350/T]$

$A = 2.85\ (O/M) + 0.035$, $C = (-7.15\ (O/M) + 2.86) \cdot 10^{-4}$

$$FD = \left[\frac{1.09}{B^{3.265}} + \frac{0.0643}{\sqrt{B}}\sqrt{T}\right] \cdot \arctan\left[\frac{1}{\left[\frac{1.09}{B^{3.265}} + \frac{0.0643}{\sqrt{B}}\sqrt{T}\right]}\right]$$

$$FP = 1 + \left[\frac{0.0198}{3 - 0.019B}\right] \cdot \left[\frac{1}{1 + \exp(-\frac{T - 1200}{100})}\right]$$

$$FR = 1 - \frac{0.2}{1 + \exp(\frac{T - 900}{80})}$$

$$FM = \frac{1 - p}{1 + (s - 1)p}$$

</td><td>T – temperature, K
B – burn-up, % h.a.
p – fuel porosity, rel. units
s – shape factor, s = 1.5
O/M – oxygen-to-metal ration, relative units
Y – PuO_2 content, %</td></tr>
<tr><td>Constraints</td></tr>
<tr><td>$3 < Y < 15$
$700 < T < 3\,100$ K</td></tr>
</table>

2.1.4 ORNL (USA) – FRAPCON-3 v1.3

In the version of FRAPCON-3 (v1.3, modified by ORNL for MOX applications) used by ORNL for these simulations, the MOX thermal conductivity used is a combination of the Duriez stoichiometry-dependent correlation [9] plus the burn-up degradation contained in a modified version of the NFI fuel thermal conductivity model. This combined model is described in [5].

2.1.5 ORNL (USA) – TRANSURANUS version v1m3j04

In version v1m3j04 of TRANSURANUS, used by ORNL for these simulations, a new best-estimate MOX thermal conductivity correlation has been implemented (LAMBDA=31) which is a combination of the Duriez stoichiometry-dependent correlation for fresh MOX fuel and new data (obtained via a laser flash technique at ITU) on irradiated MOX fuel with burn-up values between 20 and 45 MWd/kgHM. This model is described in [6]. Five MOX thermal conductivity correlations are available in v1m3j04, these simulations use the new best-estimate correlation (LAMBDA=31) for MOX fuel.

2.1.6 SCK•CEN (Belgium) – FEMAXI-V

The FEMAXI code has three options for the thermal conductivity, which can be selected by means of the MTHCN parameter:

- MTHCN=1: Martin's model [7];
- MTHCN=2: MATPRO-11 model [4];
- MTHCN=3: Baron's model [8].

The provided results use the Baron model [MTHCN=3] for the thermal conductivity.

2.1.7 VNIINM-Bochvar (Russia) – START-3

The START-3 code used by the VNIINM for these calculations, uses a similar model as [9] (Duriez) for the thermal conductivity of (fresh) MOX fuel. In this formulation, the conductivity is constant with Pu content (a maximum Pu content of 15% is considered as the upper range for the model), but is dependent on the amount of hypostoichiometry of the fuel. The burn-up dependence of the thermal conductivity is modelled as [10] with an extra factor in the phonon term $1/(a + bT)$.

2.2 Fission gas release model

2.2.1 BNFL (UK) – ENIGMA

The fission gas release model in the ENIGMA code used by BNFL is the same as for UO_2, but the *fission gas generation model* is modified for MOX fuel [2].

2.2.2 KAERI (Korea) – COSMOS

The fission gas release model used for MOX fuel in the COSMOS code is the same as that used for UO_2, but the Pu content in the matrix is taken into account assuming that Pu-rich particles are distributed uniformly in the UO_2 matrix. The local fission rates inside the fuel are then calculated considering the effective Pu content in each zone [3].

2.2.3 Kurchatov Institute (RU) – FRED

For the calculation of FGR with the FRED code, the FASTGRASS model [11] is used. FASTGRASS is a mechanistic code that predicts atomic and bubble behaviour of fission gas in UO_2 fuel under steady-state and transient conditions. The model is employed on MOX fuel without modification. The model accounts for amount of atoms of inert gases during fission, migration of atoms, formation and migration of gas bubbles, their coalescence and solution, influence of grain boundaries and other traps on bubble behaviour. The code allows the calculation of fuel swelling vs. time as result of fission gas accumulation in the matrix and fission gas release from fuel during base-irradiation, transient and accident conditions. The area of code applicability is up to a fuel average burn-up of 50 MWd/kgU.

2.2.4 ORNL (USA) – FRAPCON-3 v1.3

The FRAPCON-3 model for FGR employed in these simulations is the Massih/Forsberg model [12]. The model is employed on MOX fuel without modification.

2.2.5 ORNL (USA) – TRANSURANUS version v1m3j04

The recommended TRANSURANUS model for FGR (FGRMOD=6), employed by ORNL for these simulations, uses the URGAS algorithm [13] with the diffusion coefficients of Hj. Matzke [14] and a constant athermal diffusion coefficient. This model option is used in conjunction with a model for intragranular fission gas release.

2.2.6 SCK•CEN (Belgium) – FEMAXI-V

The FEMAXI-V code has two model options for calculating fission gas release:

- MOX=1: The fission gas is composed of 86% Xe and 14% Kr, and the FGR, which is predicted by the same model as that for UO_2 fuel, is multiplied by 1.3.

- MOX=2: The fission gas is composed of 87% Xe and 13% Kr, and the FGR is predicted by the same model as that for UO_2 fuel without modification.

Results with both models are provided.

2.2.7 VNIINM-Bochvar (Russia) – START-3

The fission gas release model utilised in the START-3 code is based on solution of a two-stage diffusion problem for fission gas in polycrystal fuel. The fission gas release is determined by diffusive flow of fission gas atoms to grain boundaries, and subsequent “quasi-diffusive” percolation of the intergranular gas to fuel-free surface. The model also takes into account the possibility of gas release by the athermal “direct recoil” and “knock-out” mechanisms [15]. Recently the model has been updated to improve its prediction at extended burn-ups [15]. Here the model is employed on MOX fuel without modification.

Chapter 3

RESULTS

The results from each of the contributors are presented and briefly discussed.

3.1 Fuel temperatures

3.1.1 BNFL (UK) – ENIGMA code

The results of the ENIGMA calculations of fuel temperature (calculated at the LHRTF node) are shown in Figure 9 for Rod 1 (solid) and Figure 10 for Rod 2 (hollow).

In general (i.e. for both rods) the temperatures are under-predicted when compared to the measurements from the start of irradiation. As the irradiation proceeds, the difference between predictions and measurements gradually become smaller, and in the low power period (from ~230 to ~525 irradiation days), the predicted temperatures for the hollow rod (Rod 2) reproduce the measurements very well. For the final high power period, starting at ~525 irradiation days, the predictions and measurements start to deviate again, this time with the predicted temperatures exceeding the measured values. This is particularly the case for the solid rod (Rod 1).

As noted above, the rod pressure data indicate significant fission gas release (FGR) in both rods during the high power period towards the end of the data set (from ~525 days) (see Section 1.1).

3.1.2 KAERI (Korea) – COSMOS

The results of the COSMOS calculations of fuel temperature (calculated at the LHRTF node) are shown in Figure 11 for Rod 1 (solid) and Figure 12 for Rod 2 (hollow).

As can be seen by the figures, two calculation results have been provided:

1. Inclusion of thermal conductivity recovery after ~525 irradiation days after which significant FGR is seen from the pressure data (see Section 1.1). These calculations are denoted “no pressure adj.” in the figures (solid red curve).

2. Inclusion of the above thermal recovery effect above *and* an adjustment of the saturation gas atom number in the FGR model. These calculations are denoted “pressure adj.” in the figures (dashed red curve).

In general both the calculations above reproduce the measured temperatures fairly well (within ca. ±25°C), with a slight tendency of over-prediction after ~525 days.

3.1.3 *Kurchatov Institute (RU) – FRED*

The results of the FRED calculations of fuel temperature (calculated at the LHRTF node) are shown in Figure 13 for Rod 1 (solid) and Figure 14 for Rod 2 (hollow).

For the solid rod (Rod 1) the FRED calculations over-estimate the measurements by ~100°C at the very beginning, but between ~50 and 100 irradiation days the agreement between measurements and predictions is very good. After this the tendency for this rod is to underestimate the measurements up to the power up-rating from ~525 days, when the agreement is somewhat better.

For the hollow rod, the agreement between calculations and measurements is very good at start of life, but the calculations start to undershoot (~50°C) the measurements after ~50 days. The discrepancy between measurements and calculations gradually decreases with time, and from ~300 irradiation days, the agreement between predictions and measurements is very good. The temperature increase during the power up-rating from ~525 days is also generally well reproduced in the data.

3.1.4 *ORNL (USA) – FRAPCON-3 v1.3*

The results of the FRAPCON-3 calculations of fuel temperature (calculated at the LHRTF node) are shown in Figure 15 for Rod 1 (solid) and Figure 16 for Rod 2 (hollow).

The agreement with measurements is very good for both the solid and the hollow rod at BOL. After ~50-100 days a tendency of under-prediction of the measurements can be seen for both rods. During the low power period from ~230 to ~525 days, however, the agreement for the hollow rod is excellent, whereas for the solid rod the temperature estimates are still below the measurements (by ~25-50°C). After the FGR occurs at ~525, the measured temperatures are over-predicted by up to ~125°C for both the solid and the hollow rod.

3.1.5 *ORNL (USA) – TRANSURANUS version v1m3j04*

The results of the TRANSURANUS calculations of fuel temperature (calculated at the LHRTF node) are shown in Figure 17 for Rod 1 (solid) and Figure 18 for Rod 2 (hollow).

The TRANSURANUS results are very similar to the COSMOS results (see Section 3.1.2). There is a tendency of under-prediction in the first and middle part of the irradiation, while towards the end of the final high power period (after ~525 days) the temperatures are slightly over-predicted. Overall the agreement with measurements is within ±25°C, apart from for Rod 1 during the first part of the low power period (from ~230 days), when the temperatures are under-predicted by up to ~100°C.

3.1.6 *SCK•CEN (Belgium) – FEMAXI-V*

The results of the FEMAXI-V calculations of fuel temperature (calculated at the LHRTF node) are shown in Figure 19 for Rod 1 (solid) and Figure 20 for Rod 2 (hollow).

As mentioned in Section 2.1.6 above, two sets of calculations with the FEMAXI-V code (parameter MOX=1 and MOX=2) have been provided, and both results are shown in the figures.

There is little difference between the two calculation sets for both rods, and the agreement with the measurements is generally good up to the power up-rating at ~525 days. Some tendency of under-predicting the measurements can be seen however, particularly during the first ~230 days. After the power increase at ~525 days, temperatures are overestimated for both rods, but most significantly for the solid rod (Rod 1).

3.1.7 VNIINM-Bochvar (Russia) – START-3

The results of START-3 calculations of fuel temperature (calculated at the LHRTF node) are shown in Figure 21 for Rod 1 (solid) and Figure 22 for Rod 2 (hollow).

At the time of this writing, only data up to ~230 days of irradiation were provided.

For both rods the temperatures are overestimated (ca. 50-100°C) at BOL but the overshoot decreases gradually and at ~175 days the agreement between calculations and measurements is excellent for both rods. After this a slight under-prediction is seen for the solid rod, whereas for the hollow rod the agreement also stays good here.

3.2 Fuel rod internal pressure

In this section the results of the calculations of rod internal fuel pressure is presented and compared with the measured data. The discussion focuses mainly on the above-mentioned period from ~525 days to EOL when the measured pressure rises substantially in both rods and significant FGR is seen.

3.2.1 BNFL (UK) – ENIGMA

The results of the ENIGMA calculations of rod internal pressure are shown in Figure 23 for Rod 1 (solid) and Figure 24 for Rod 2 (hollow).

For both of the rods, ENIGMA predicts a pressure step from the high power period at ~525 days, but the magnitude of the pressure step is lower than what is seen from the measurements. For the solid rod, the subsequent increase seen from the pressure measurements is reproduced somewhat by the calculations, but again the magnitude is lower than the measurements. For the hollow rod, the pressure steps seen in the measured data at ~570 and ~610 days (interpreted as an indication of a closed gap at power conditions) are not reproduced by the calculations. The more or less continuous pressure increase seen from the calculations would suggest that the code does not predict a closed gap for the rods at this power and burn-up.

For both rods the EOL pressure is underestimated by the calculations.

3.2.2 KAERI (Korea) – COSMOS

The results of the COSMOS calculations of rod internal pressure are shown in Figure 25 for Rod 1 (solid) and Figure 26 for Rod 2 (hollow).

For the COSMOS calculations, the EOL pressure for the hollow rod (Rod 2) is predicted excellently with Option 2 (see Section 3.1.2 above) for the fission gas release calculations, whereas Option 1 underestimates the EOL pressure. For the solid rod, both options predict an EOL pressure below what was measured. As for the ENIGMA code discussed above, the step-wise pressure increase during the final high power period is not reproduced by the calculations, and a more or less continuous pressure increase is predicted. However, during the period from ~525 to ~570 days, when the measured pressure in the solid rod also shows a steady increase, the calculated rates of pressure increase (for both options) are close to parallel to the increase rate of the measured pressure (Figure 25).

3.2.3 Kurchatov Institute (RU) – FRED

The results of the FRED calculations of rod internal pressure are shown in Figure 27 for Rod 1 (solid) and Figure 28 for Rod 2 (hollow).

For the high-power period after ~525 days, the FRED calculations predict pressure increase and FGR, but smaller than what was measured in-pile. The step-wise pressure increase in the measured pressures during this period is not particularly visible in the calculations. For both rods, the EOL pressure is underestimated in the calculations, mostly so for the solid rod (Rod 1).

3.2.4 ORNL (USA) – FRAPCON-3 v1.3

The results of the FRAPCON-3 calculations of rod internal pressure are shown in Figure 29 for Rod 1 (solid) and Figure 30 for Rod 2 (hollow).

The code predicts a pressure step at ~525 days for both the hollow and the solid rod, but for both rods the step is smaller than the measured increase. For both rods, a more step-wise pressure increase after the high power period starts at ~525 is calculated by the code than the results from both ENIGMA and COSMOS showed.

The pressure at EOL is best met for the hollow rod, but for both rods the predicted EOL pressure is somewhat below the measurements.

3.2.5 ORNL (USA) – TRANSURANUS version v1m3j04

The results of the TRANSURANUS calculations of rod internal pressure are shown in Figure 31 for Rod 1 (solid) and Figure 32 for Rod 2 (hollow).

For the high-power period after ~525 days, TRANSURANUS results show a small pressure increase, but this is much lower than what the in-pile measurements show. The step-wise pressure increase in the measured pressures during this period is not seen in the calculations. For both rods, the EOL pressure is underestimated in the calculations, mostly so for the solid rod (Rod 1).

3.2.6 SCK•CEN (Belgium) – FEMAXI-V

The results of the FEMAXI-V calculations of rod internal pressure are shown in Figure 33 for Rod 1 (solid) and Figure 34 for Rod 2 (hollow).

As for the temperature calculations (see Section 3.1.5), two sets of calculations are provided, where the difference is in the FGR model. For the hollow rod, the difference between the two models is insignificant, and the EOL pressure is underestimated quite a bit in both cases. For the solid rod (Rod 1) however, the two models yield different results. In the case of this rod, the highest pressure increase is predicted by the MOX=1 option, coming relatively close to the measurements in predicting the EOL pressure.

As for the COSMOS and ENIGMA code, the pressure development after ~525 days shows a more or less steady increase for the solid rod (both for the MOX=1 and MOX=2 option), and does not reproduce very well the stair-steps seen in the measured pressure for this rod.

3.2.7 VNIINM-Bochvar (Russia) – START-3

The results of the START-3 calculations of rod internal pressure are shown in Figure 35 for Rod 1 (solid) and Figure 36 for Rod 2 (hollow).

As for the temperature data only data up to ~225 days are provided at the time of this writing. During this irradiation period, there is not much development in the measured pressure, and it is thus difficult to make any judgement of how well the code is able to reproduce the in-pile behaviour of these rods.

Figure 9. Fuel temperature for Rod 1 (solid) calculated by ENIGMA (BNFL)

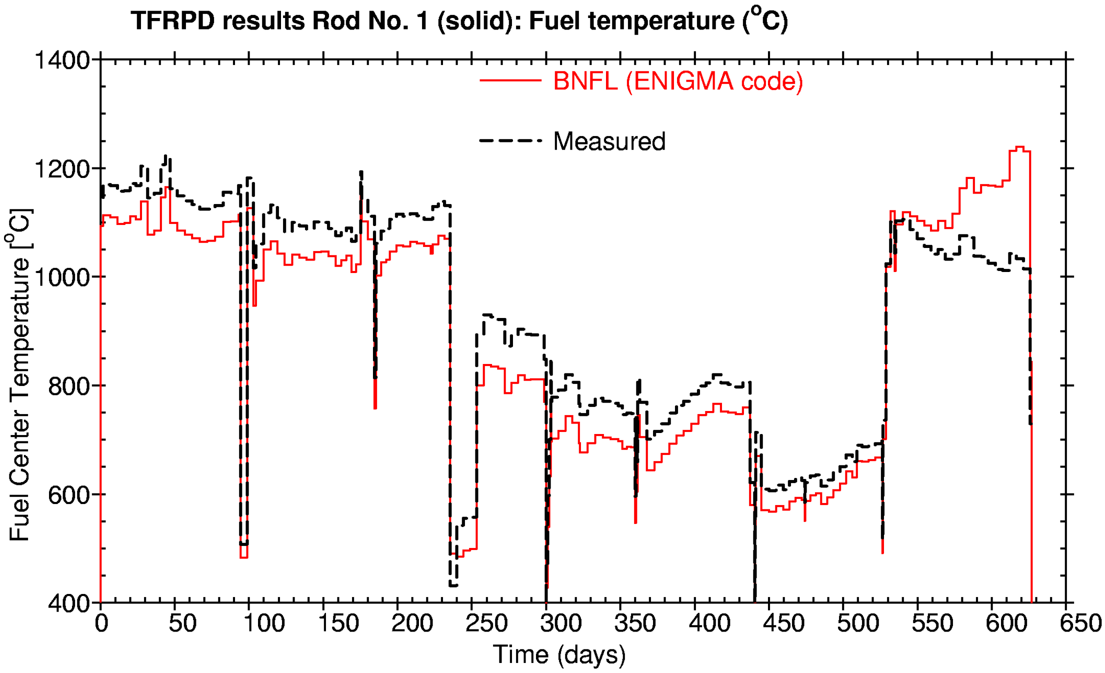

Figure 10. Fuel temperature for Rod 2 (hollow) calculated by ENIGMA (BNFL)

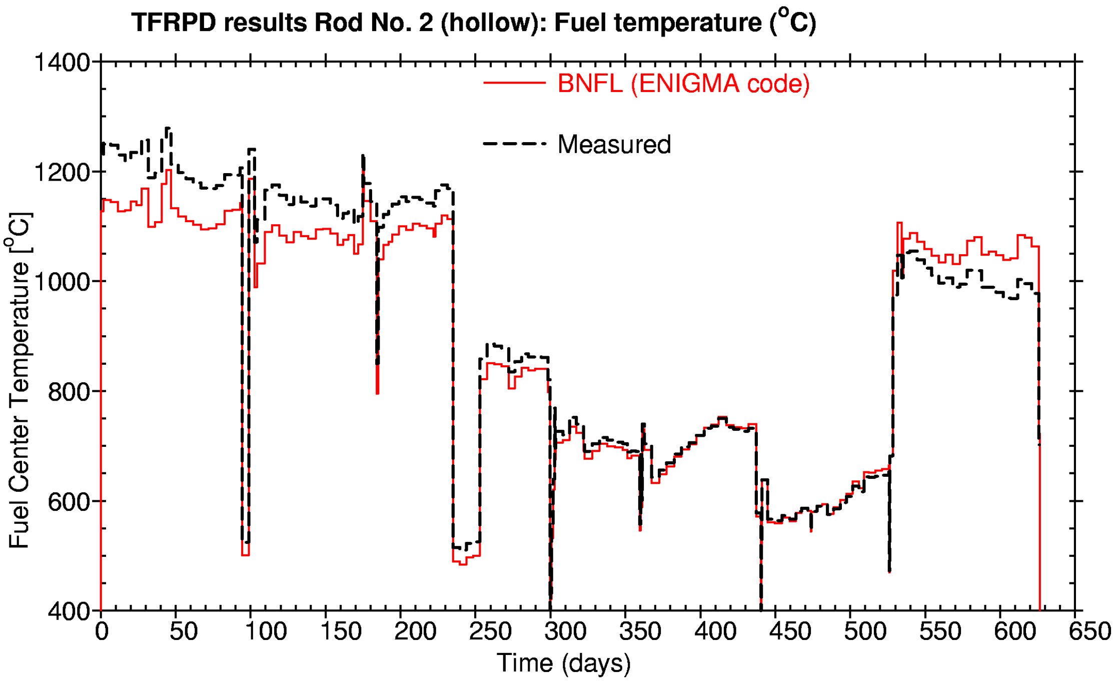

Figure 11. Fuel temperature for Rod 1 (solid) calculated by COSMOS (KAERI)

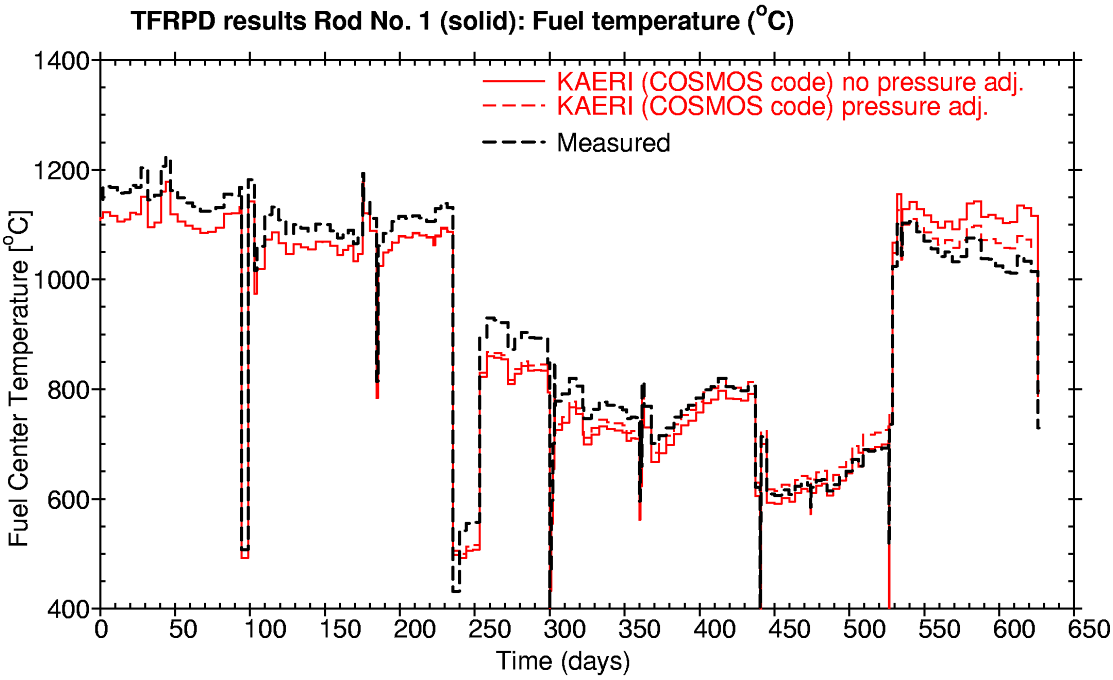

Figure 12. Fuel temperature for Rod 2 (hollow) calculated by COSMOS (KAERI)

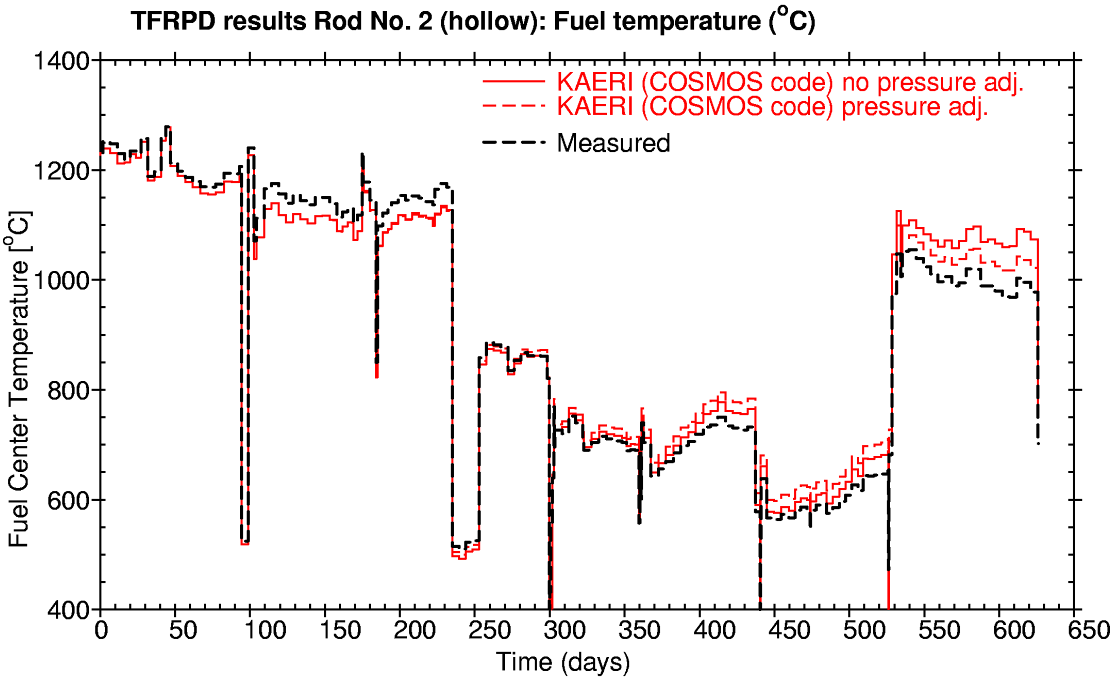

Figure 13. Fuel temperature for Rod 1 (solid) calculated by FRED (Kurchatov)

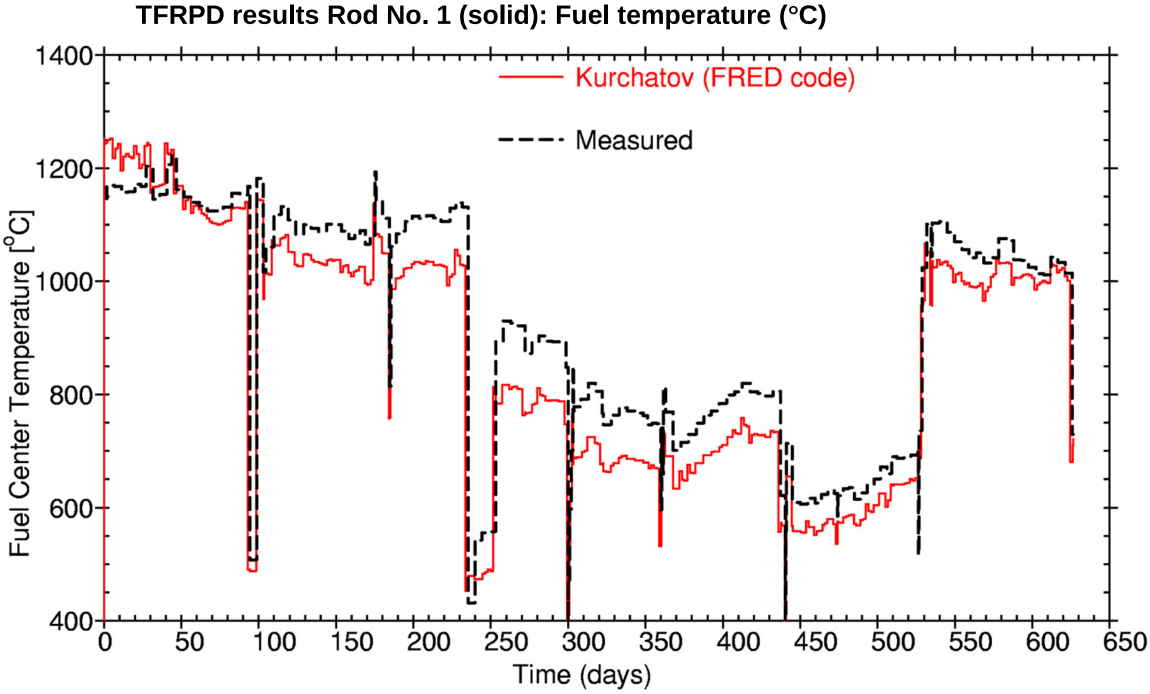

Figure 14. Fuel temperature for Rod 2 (hollow) calculated by FRED (Kurchatov)

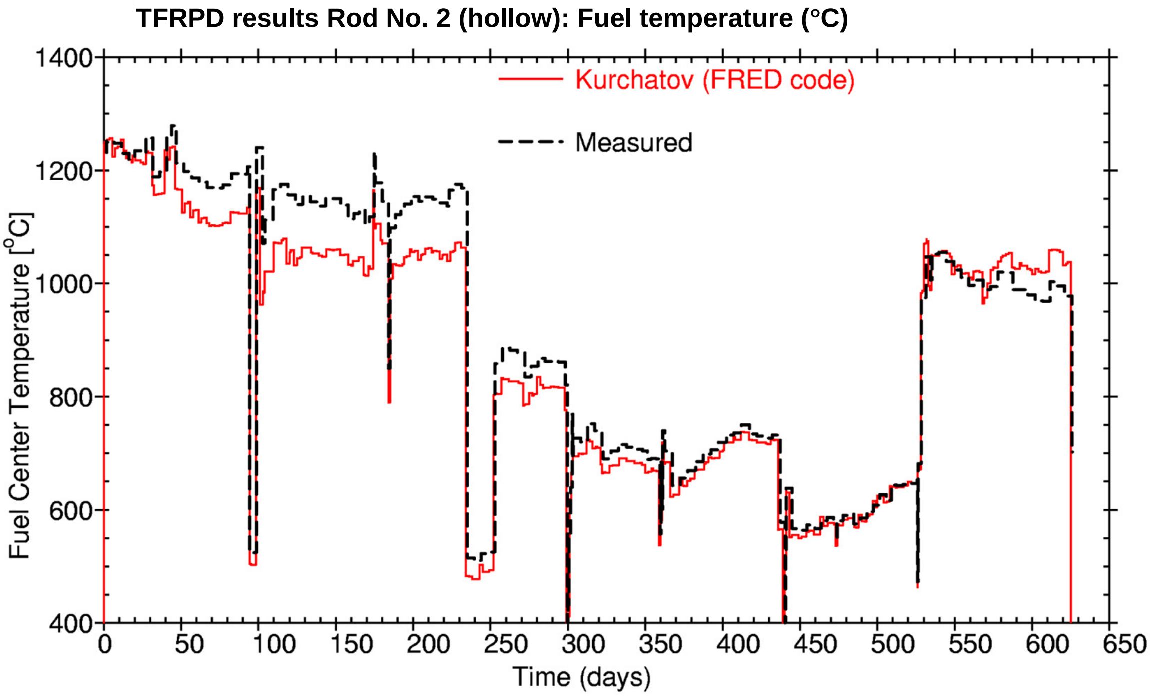

Figure 15. Fuel temperature for Rod 1 (solid) calculated by FRAPCON-3 (ORNL)

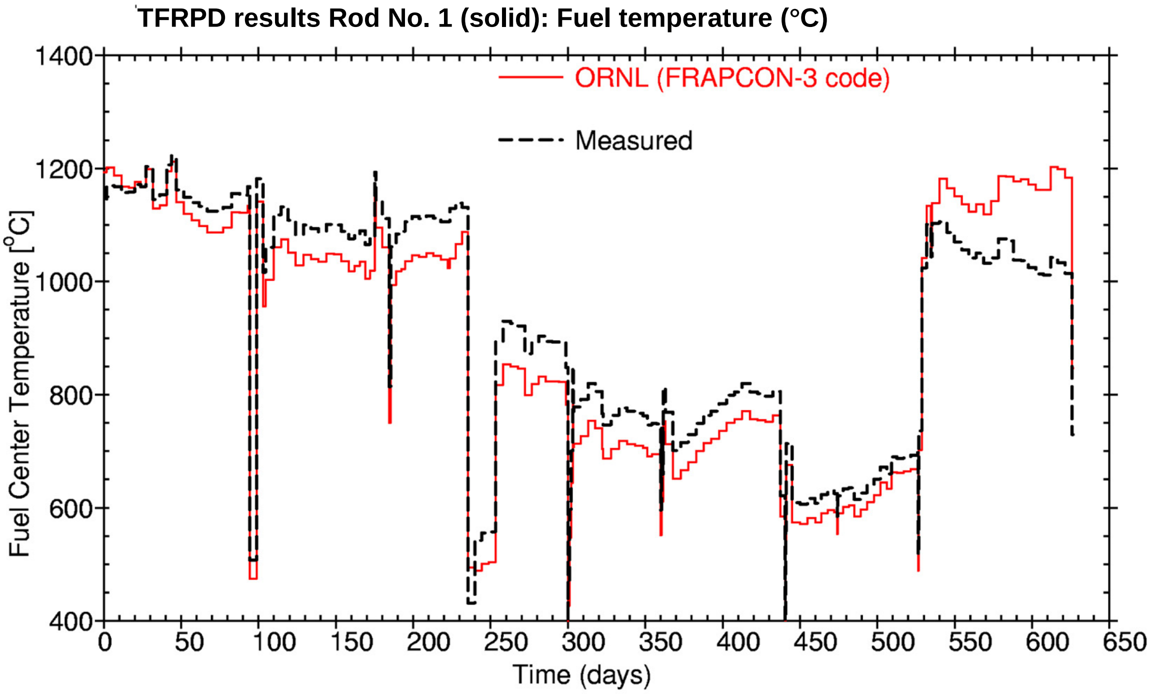

Figure 16. Fuel temperature for Rod 2 (hollow) calculated by FRAPCON-3 (ORNL)

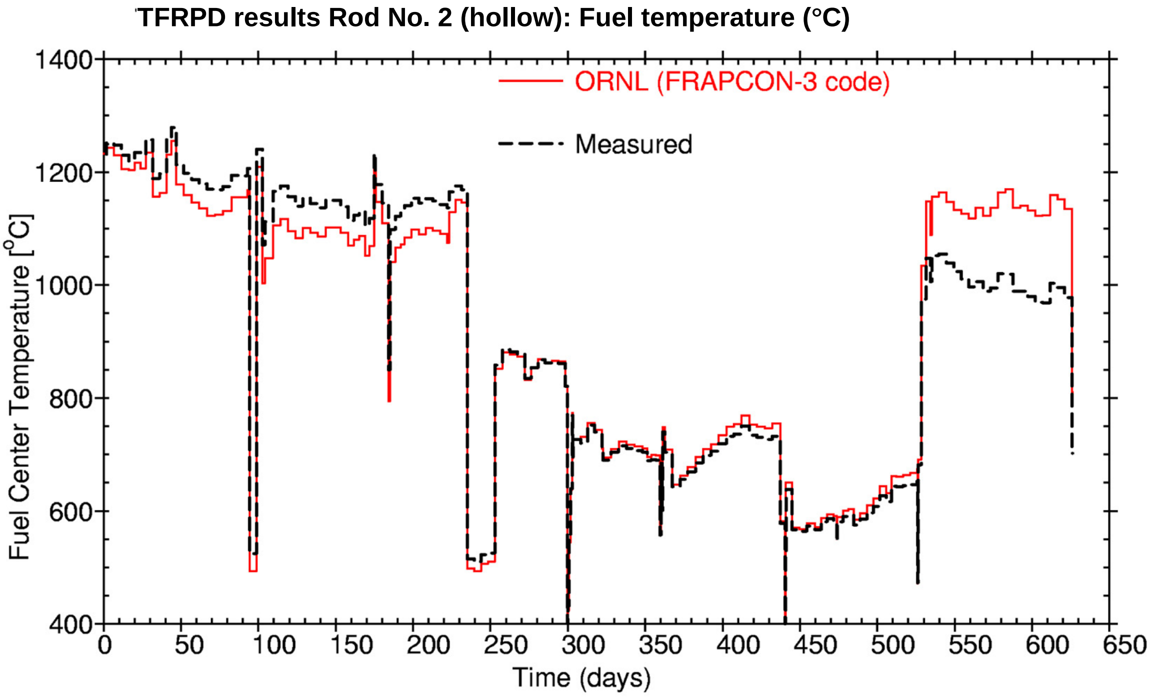

Figure 17. Fuel temperature for Rod 1 (solid) calculated by TRANSURANUS (ORNL)

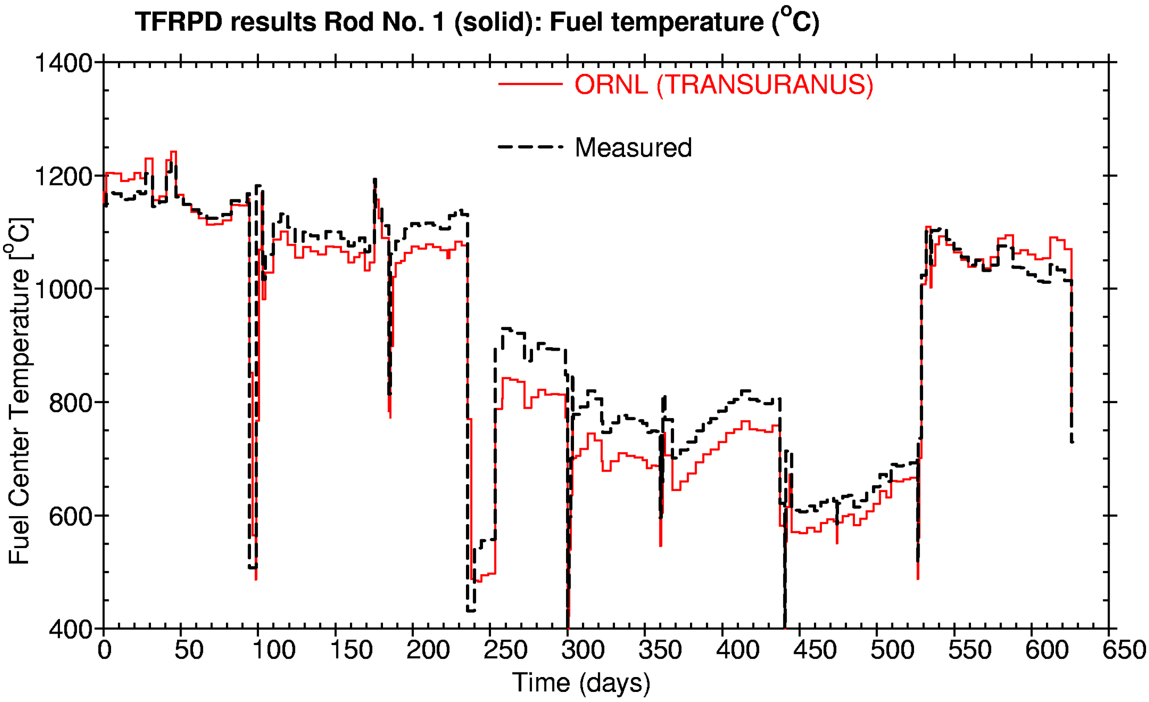

Figure 18. Fuel temperature for Rod 2 (hollow) calculated by TRANSURANUS (ORNL)

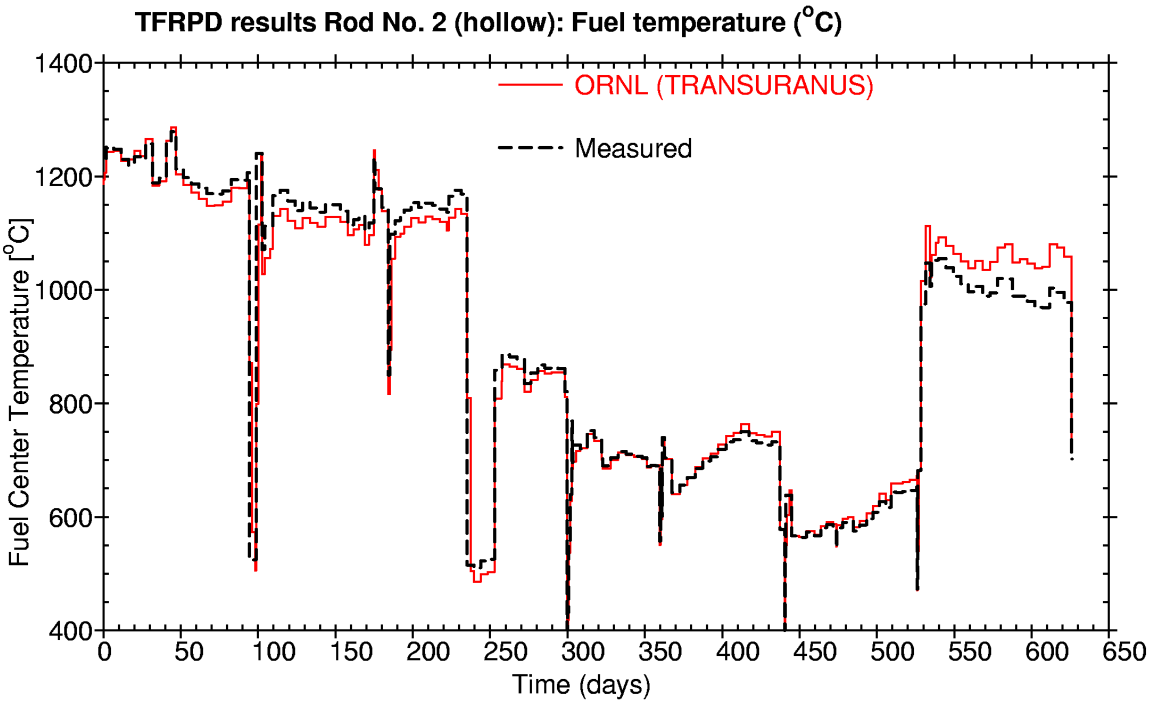

Figure 19. Fuel temperature for Rod 1 (solid) calculated by FEMAXI-V (SCK•CEN)

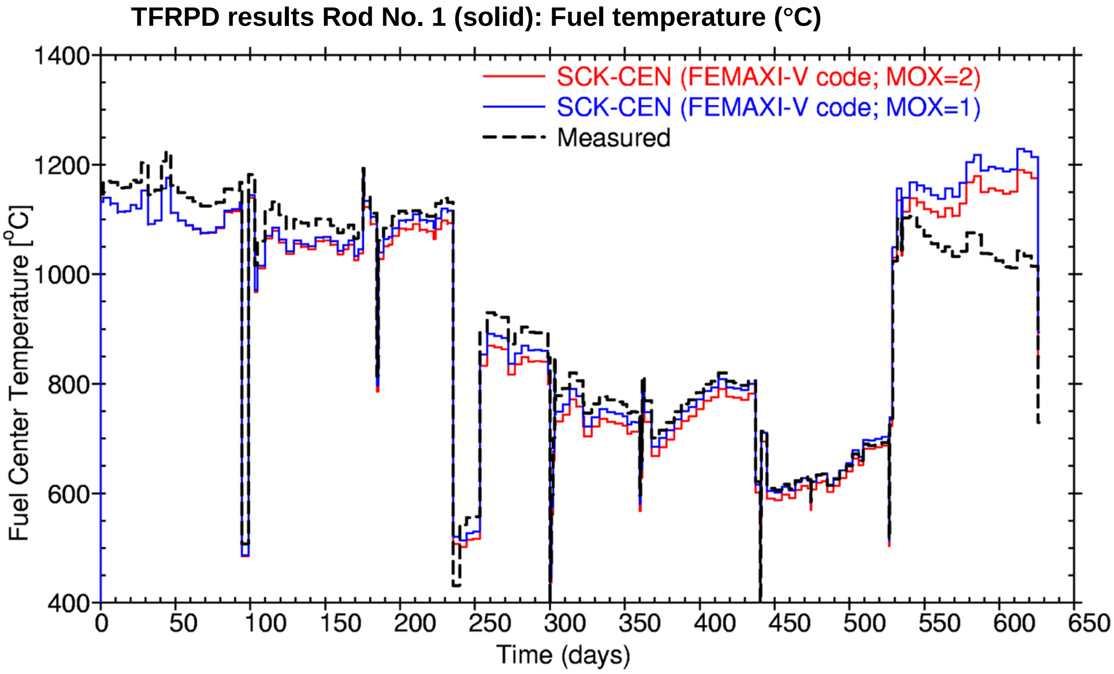

Figure 20. Fuel temperature for Rod 2 (hollow) calculated by FEMAXI-V (SCK•CEN)

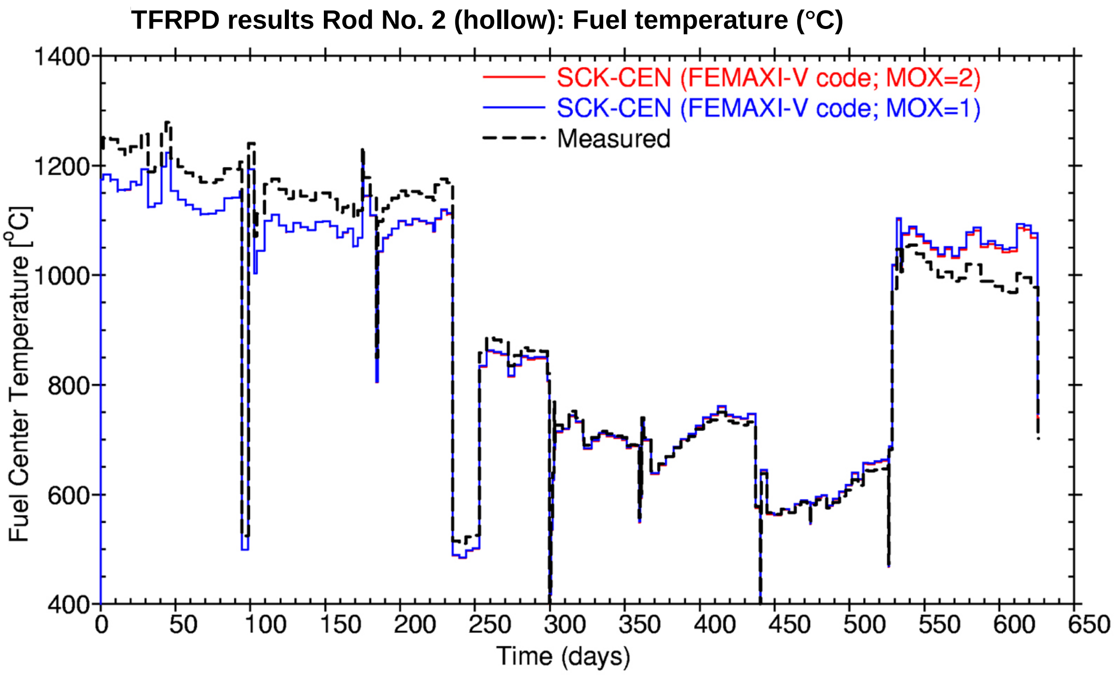

Figure 21. Fuel temperature for Rod 1 (solid) calculated by START-3 (VNIINM)

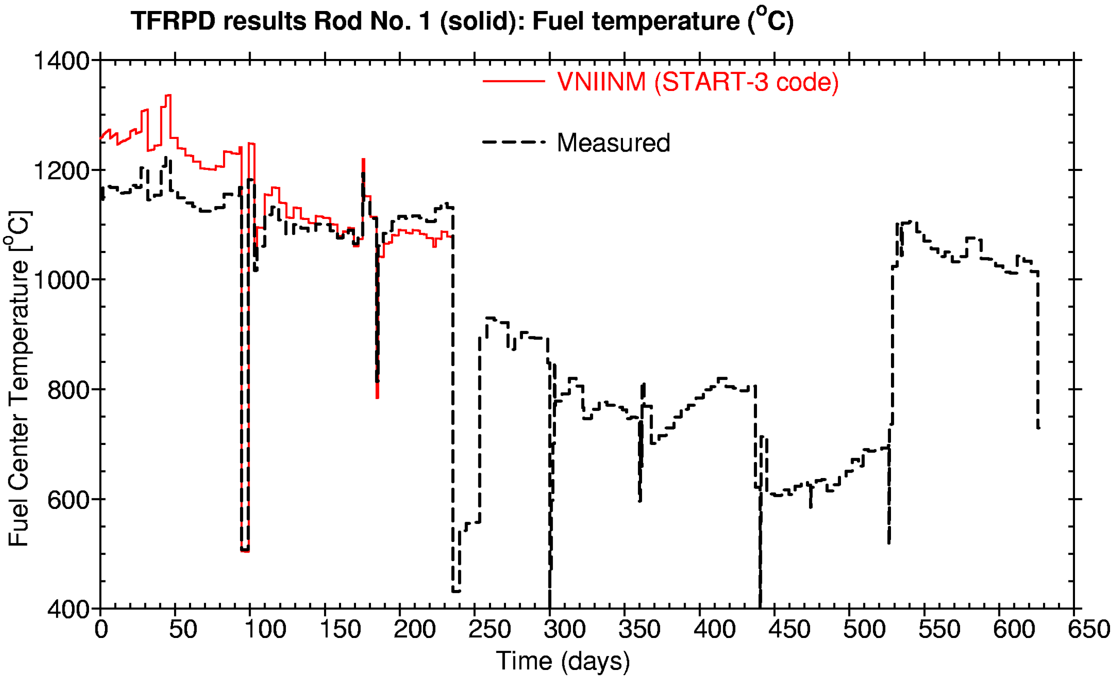

Figure 22. Fuel temperature for Rod 2 (hollow) calculated by START-3 (VNIINM)

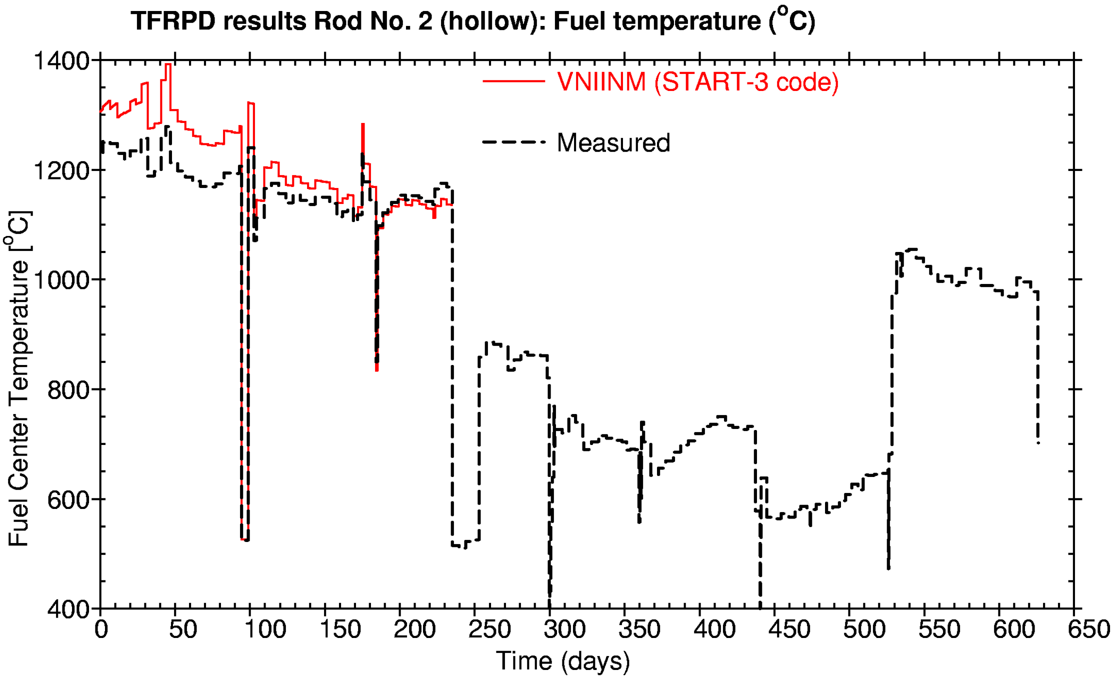

Figure 23. Internal rod pressure for Rod 1 (solid) calculated by ENIGMA (BNFL)

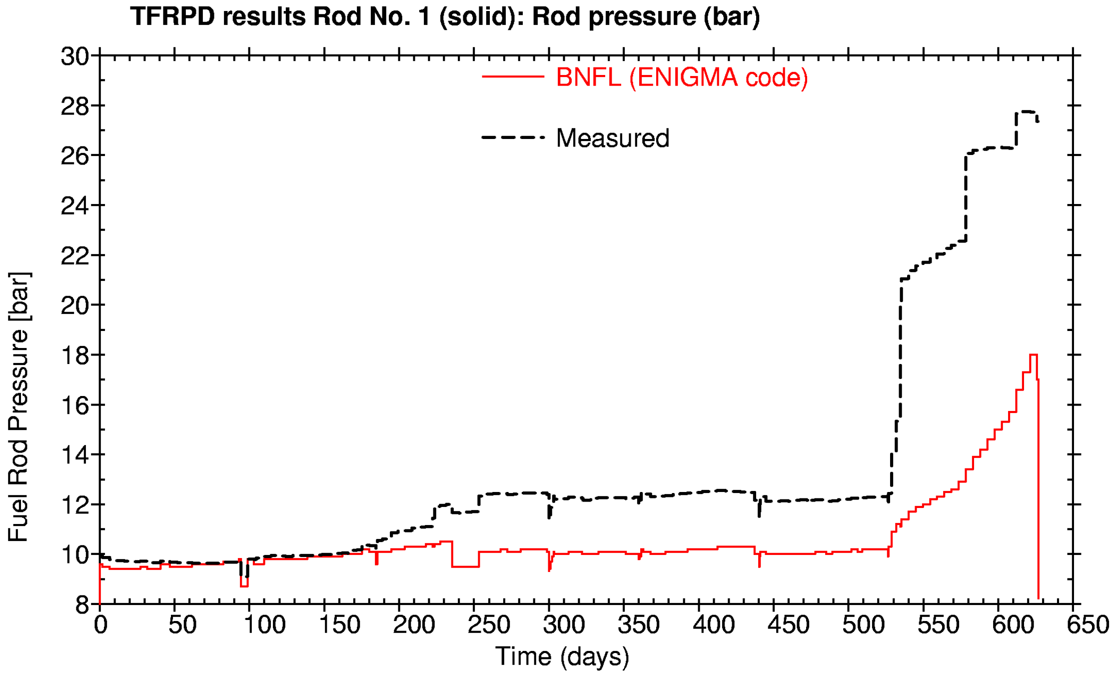

Figure 24. Internal rod pressure for Rod 2 (hollow) calculated by ENIGMA (BNFL)

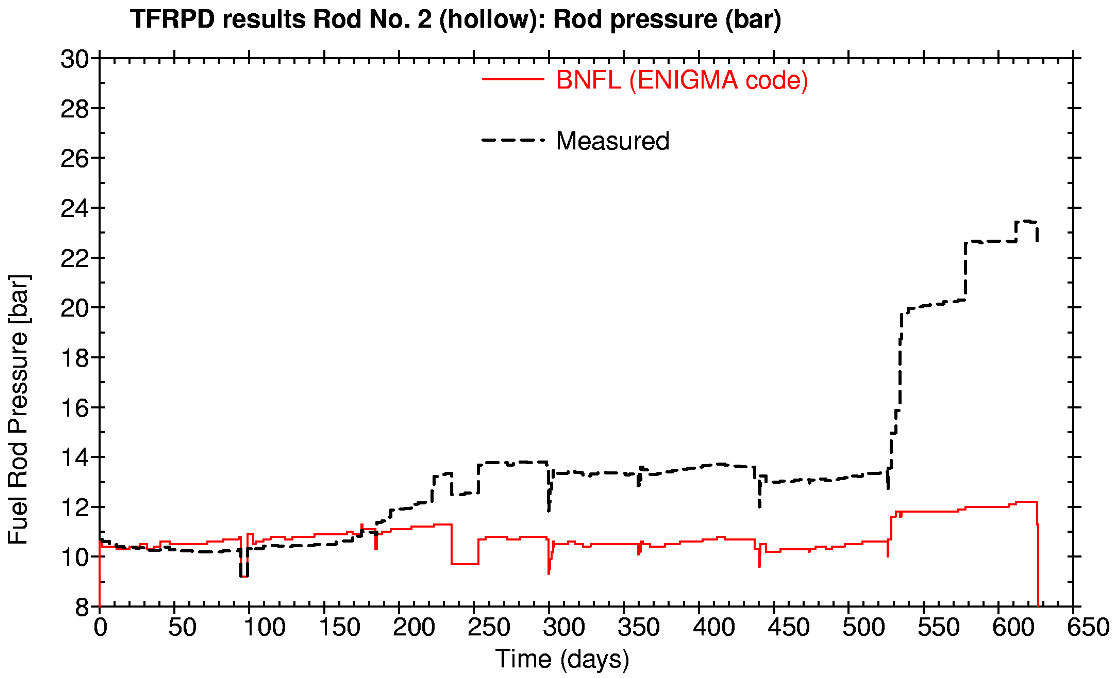

Figure 25. Internal rod pressure for Rod 1 (solid) calculated by COSMOS (KAERI)

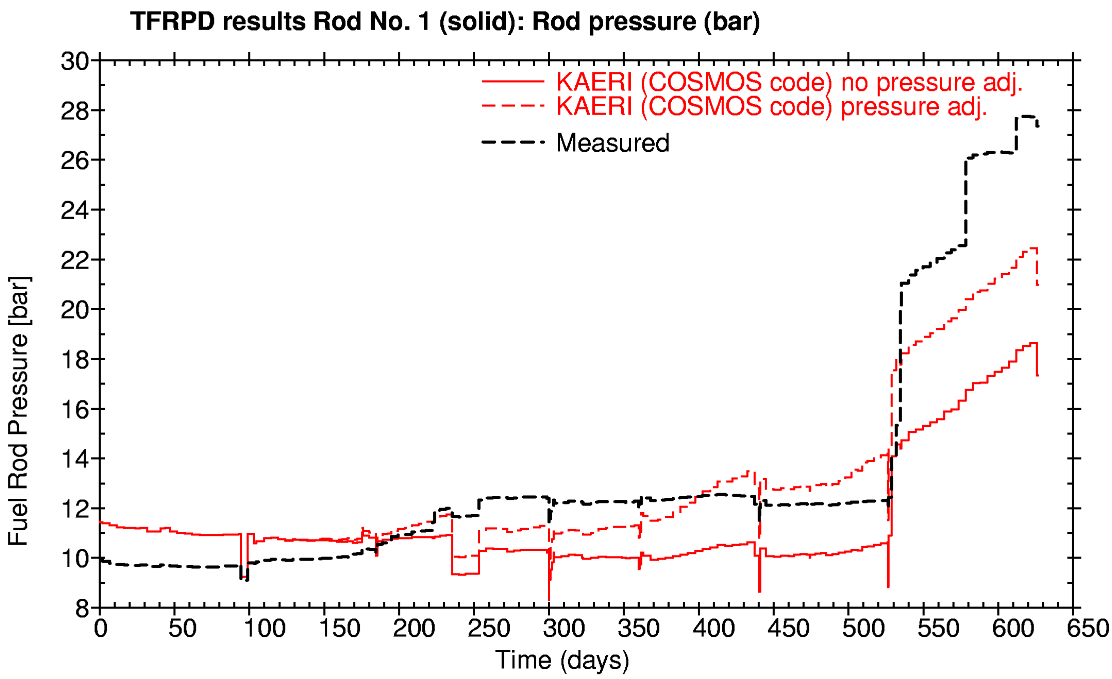

Figure 26. Internal rod pressure for Rod 2 (hollow) calculated by COSMOS (KAERI)

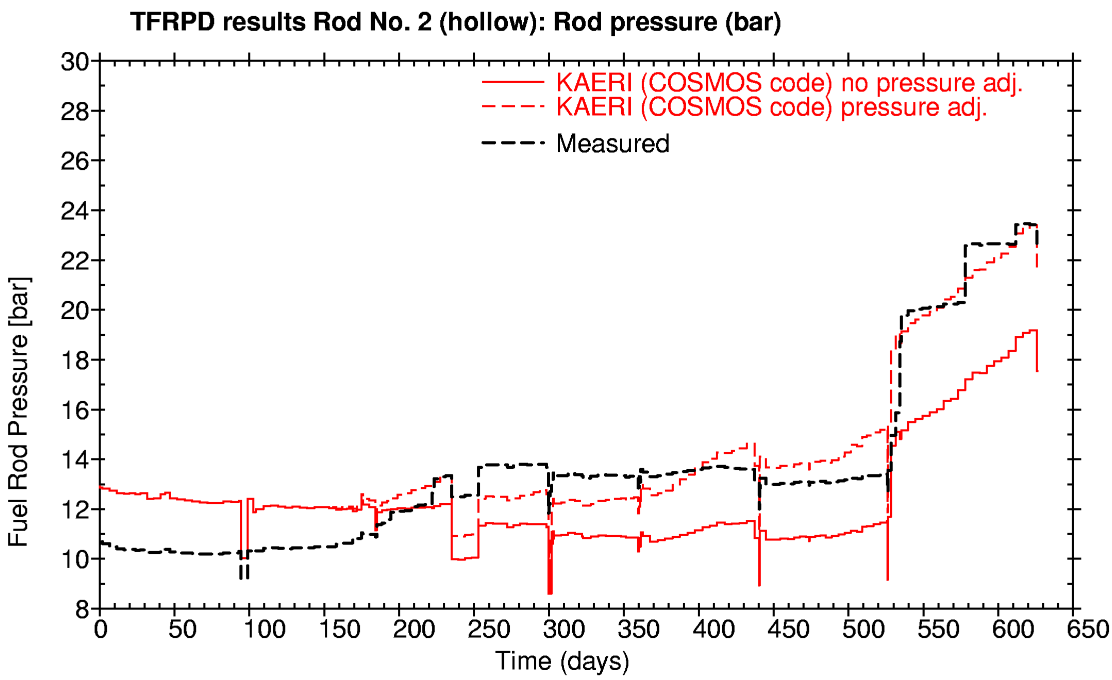

Figure 27. Internal rod pressure for Rod 1 (solid) calculated by FRED (Kurchatov)

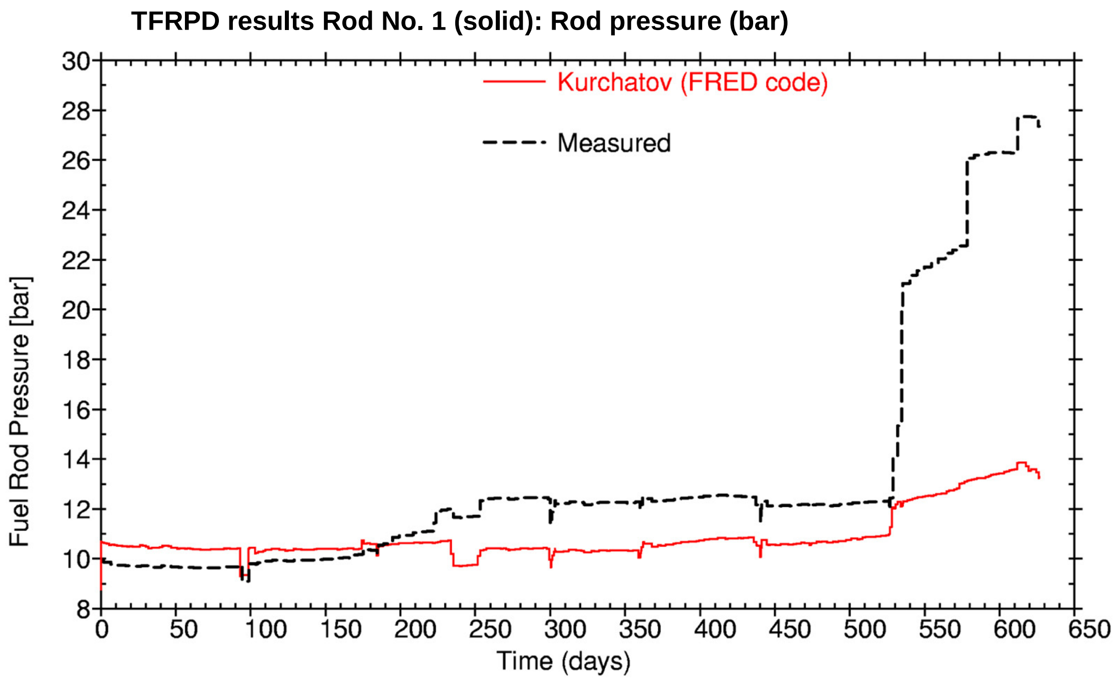

Figure 28. Internal rod pressure for Rod 2 (hollow) calculated by FRED (Kurchatov)

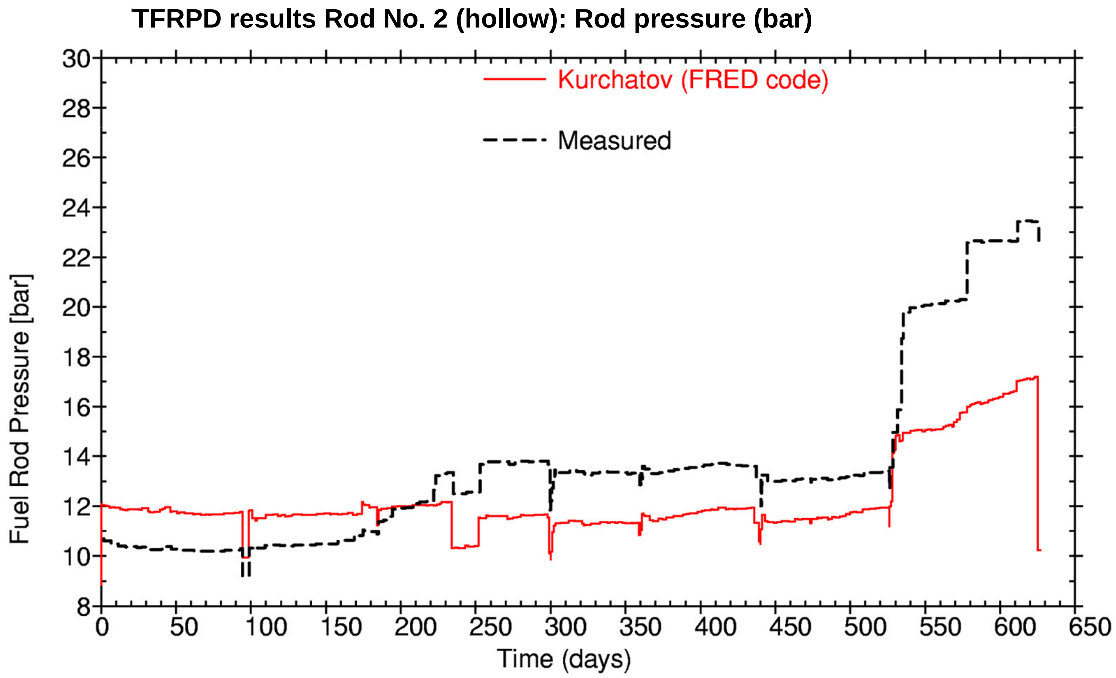

Figure 29. Internal rod pressure for Rod 1 (solid) calculated by FRAPCON-3 (ORNL)

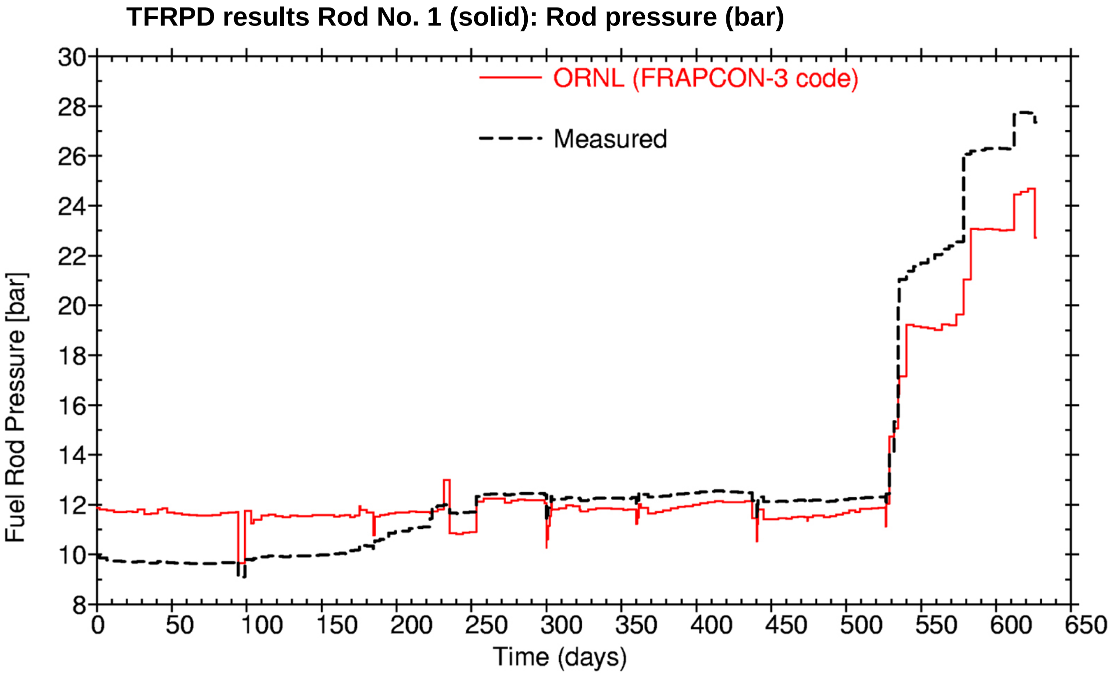

Figure 30. Internal rod pressure for Rod 2 (hollow) calculated by FRAPCON-3 (ORNL)

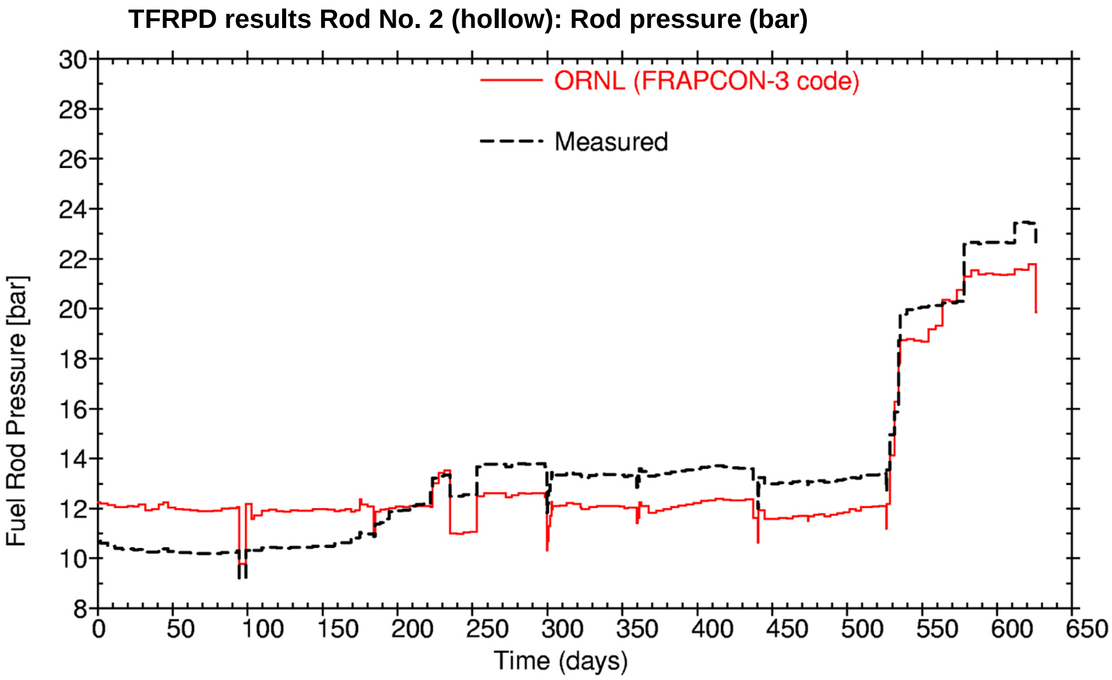

Figure 31. Internal rod pressure for Rod 1 (solid) calculated by TRANSURANUS (ORNL)

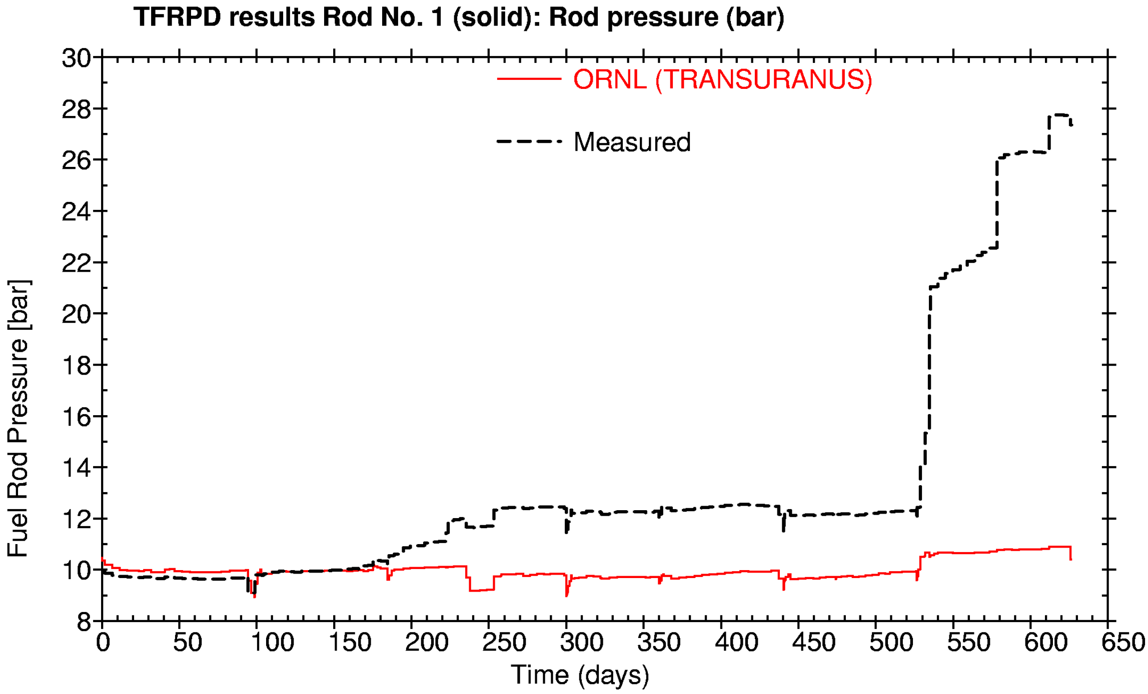

Figure 32. Internal rod pressure for Rod 2 (hollow) calculated by TRANSURANUS (ORNL)

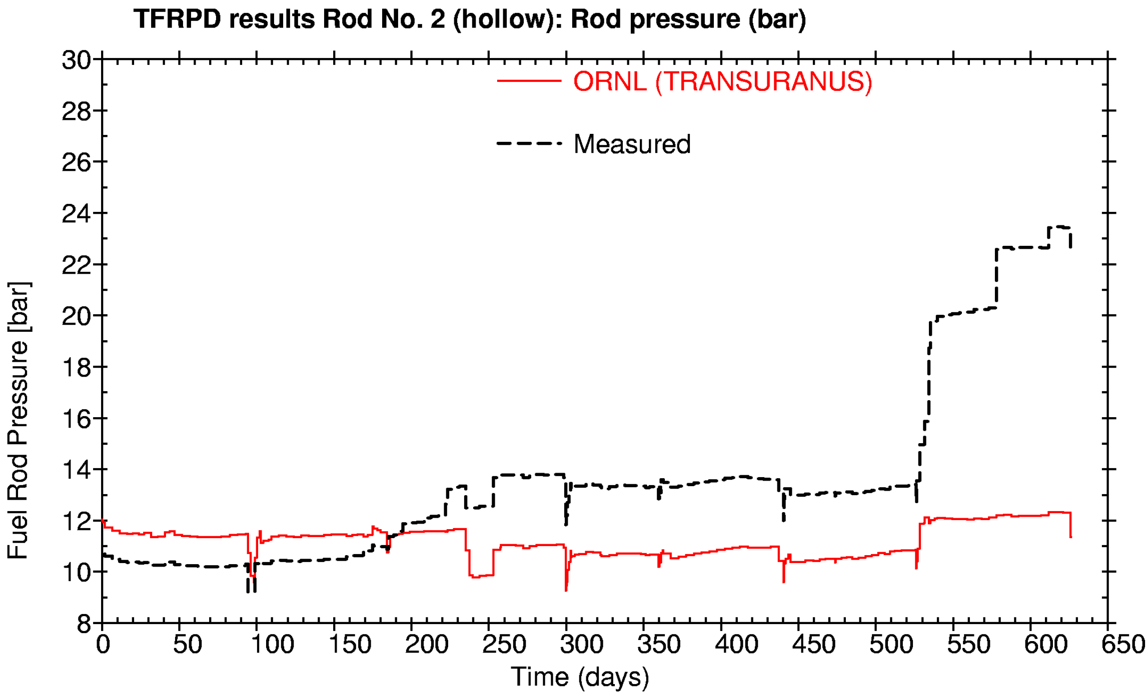

Figure 33. Internal rod pressure for Rod 1 (solid) calculated by FEMAXI-V (SCK•CEN)

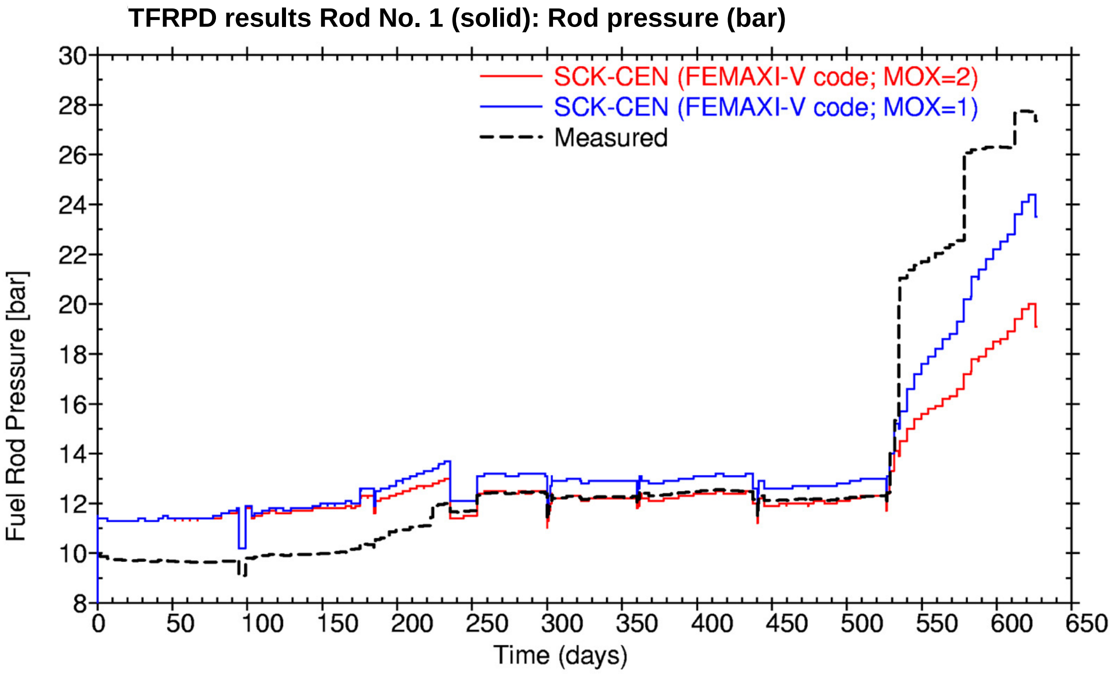

Figure 34. Internal rod pressure for Rod 2 (hollow) calculated by FEMAXI-V (SCK•CEN)

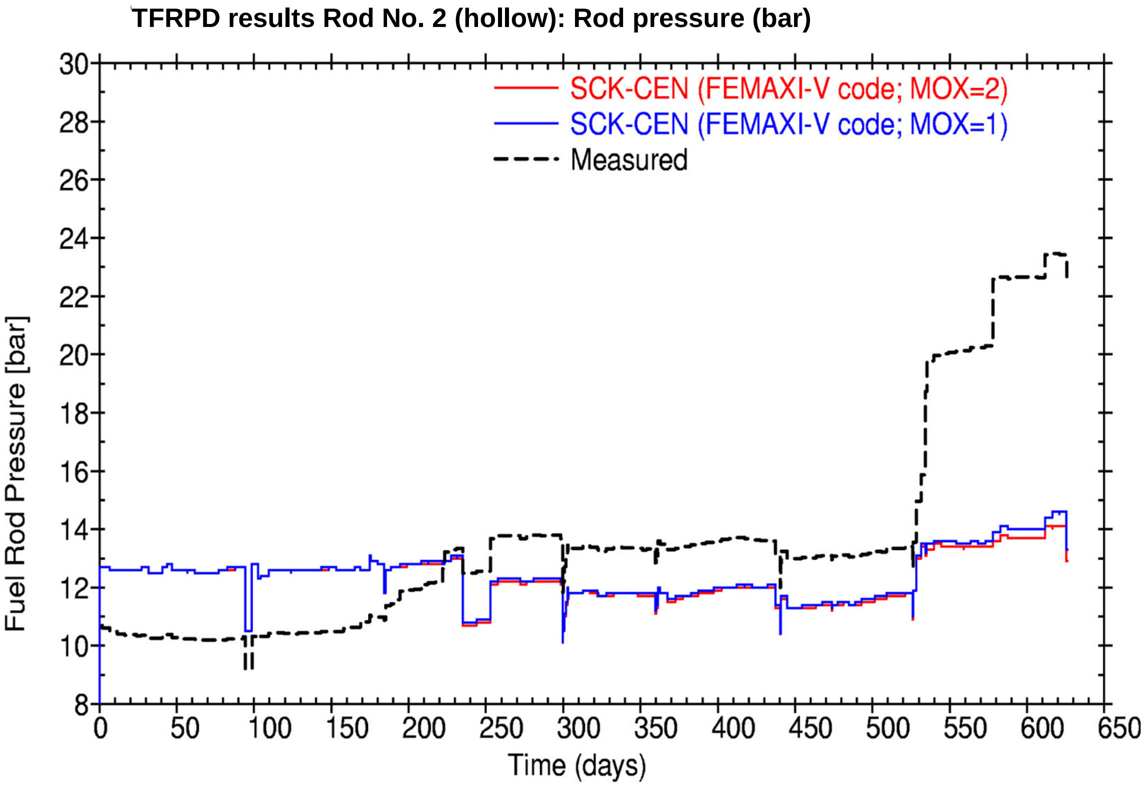

Figure 35. Internal rod pressure for Rod 1 (solid) calculated by START-3 (VNIINM)

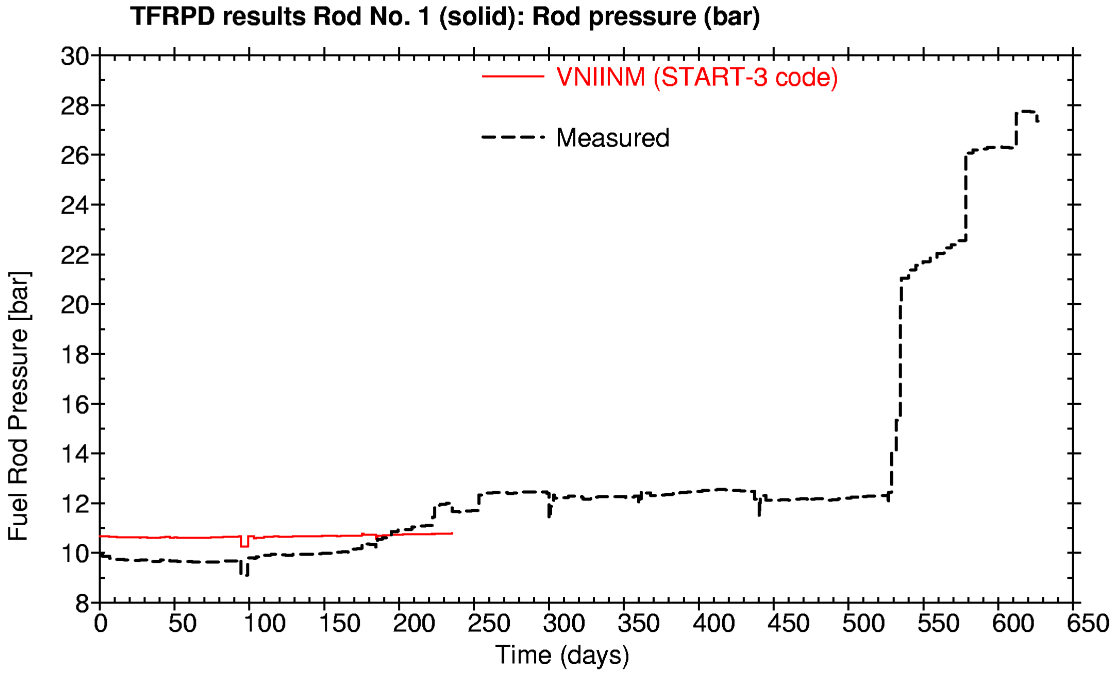

Figure 36. Internal rod pressure for Rod 2 (hollow) calculated by START-3 (VNIINM)

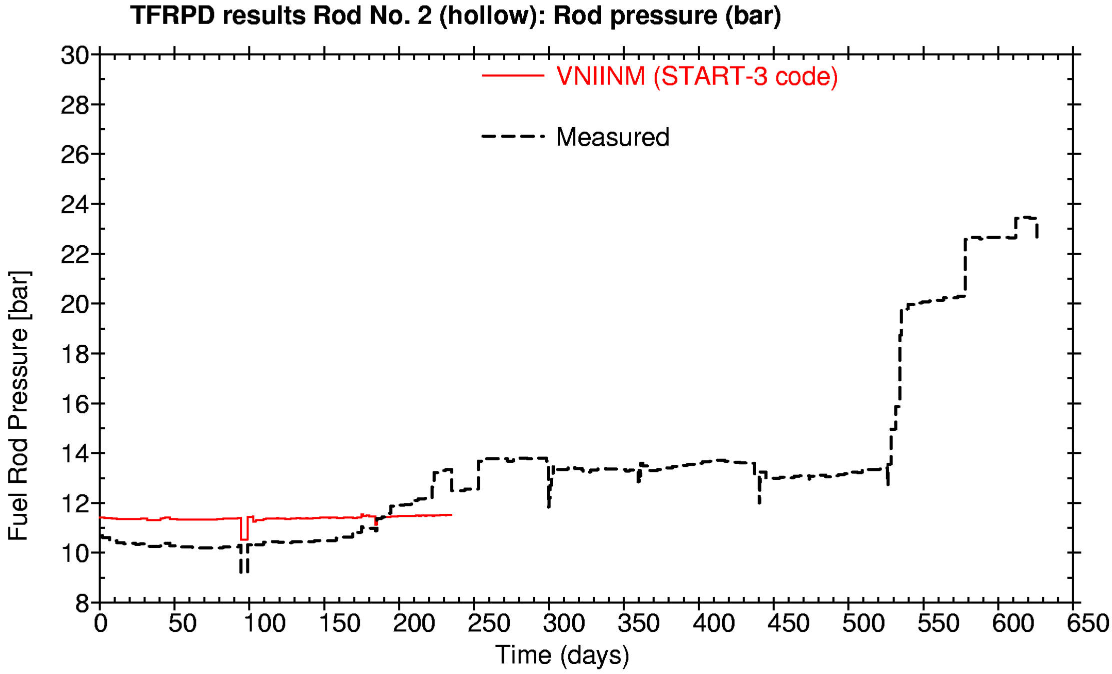

REFERENCES

[1] Skardhamar, T., U. Kasemeyer, "Introduction of HELIOS to the Halden Reactor Project", *Studsvik Scandpower European CMS/FMS Users Group Meeting*, Madrid (1998).

[2] Palmer, I., G. Rossiter, R. White, *Development and Validation of the ENIGMA Code for MOX Fuel Performance Modelling*, IAEA-SM-358/20.

[3] Lee, B-H., Y-H. Koo, J-S. Cheon, J-Y. Oh, D-S. Sohn, "COSMOS Code Benchmark by Using a Solid and Hollow MOX Fuel Behaviour", Contribution to the MOX Benchmark Test (2003).

[4] Hagrman, D.L., G.A. Reymann, R.E. Mason, *MATPRO-Version 11 (Revision 1): A Handbook of Material Properties for Use in the Analysis of Light Water Reactor Fuel Rod Behavior*, NUREG/CR-0497, Rev 1, February 1980.

[5] Lanning, D.D., C.E. Beyer, "Revised Fuel Thermal Conductivity for NRC Fuel Performance Codes", Transactions of the American Nuclear Society, 2002 Annual Meeting, Hollywood, Florida, Vol. 86, pp. 285-287, June 2002.

[6] Schubert, A., P.V. Uffelen, J.V.D. Laar, M. Sheindlin, L. Ott, "Present Status of the MOX Version of the TRANSURANUS Code (F2.5)", *Enlarged Halden Programme Group Meeting on High Burn-up Fuel Performance, Safety and Reliability*, Rica Park Hotel, Sandefjord, Norway, 9-14 May 2004.

[7] Martin, D.G., "A Re-appraisal of the Thermal Conductivity of UO_2 and Mixed (U,Pu) Oxide Fuels", *J. Nucl. Mat*., 110, pp. 73-94 (1982).

[8] Baron, D., "About the Modelling of Fuel Thermal Conductivity Degradation at High-burn-up Accounting for Recovering Process with Temperature", *Proc Sem. Thermal Performance of High-burn-up LWR Fuel*, Cadarache, France, 3-6 March 1998, pp. 129-143.

[9] Duriez, C., J-P. Alessandri, T. Gervais, Y. Philipponneau, "Thermal Conductivity of Hypostoichiometric Low Pu Content $(U,Pu)O_{2-x}$ Mixed Oxide", *J. Nucl. Mat*., 277, pp. 143-158 (2000).

[10] Wiesenack, W., T. Tverberg, "Thermal Performance of High Burn-up Fuel", *ANS Topical Meeting on LWR Fuel Performance* (2000).

[11] Rest, J., S.A. Zawadzki, *FASTGRASS: A Mechanistic Model for the Prediction of Xe, I, Cs, Te, Ba, and Sr Release from Nuclear Fuel Under Normal and Severe Accident Condition*, NUREG/CR-5840 ANL-92/3, September 1992.

[12] Lanning, D.D., C.E. Beyer, C.L. Painter, *FRAPCON-3: Modifications to Fuel Rod Material Properties and Performance Models for High-burn-up Application*, NUREG/CR-6534, Chapter 2, October 1997.

[13] Lassmann, K., H. Benk, "Numerical Algorithms for Intragranular Fission Gas Release", *J. Nucl. Mater.*, 280, pp. 127-135 (2000).

[14] Matzke, Hj., "Gas Release Mechanisms in UO_2 – A Critical Overview", *Radiation Effects*, 53, pp. 219-242 (1980).

[15] Bibilashvili, Yu.K., A.V. Medvedev, G.A. Khvostov, S.M. Bogatyr, L.V. Korystin, "Development of the Fission Gas Behaviour Model in the START-3 Code and its Experimental Support", *Seminar on Fission Gas Behaviour in Water Reactor Fuels*, Cadarache, France, 26-29 September 2000.

Appendix I

SPECIFICATION FOR A SOLID AND HOLLOW MOX PELLET BEHAVIOUR BENCHMARK

Revision 4 – 2 June 2003

(Revision 3 – 19 November 2002)

(Revision 2 – 9 October 2001 – ~235 irradiation days)

(Revision 1 – 6 June 2000)

Wolfgang Wiesenack, Terje Tverberg
OECD/IFE Halden Reactor Project
Halden, Norway

This version includes data up to ~626.5 irradiation days and the total free volume for the 2 rods.

```
Contents : Brief description of important operational data, fabrication data and
           Contents of the data files for the condensed data history of the rods.

Reactor Conditions
  Coolant/Moderator                                D2O
  Coolant Pressure              (bar)              33.6
  Coolant temperature           (deg C)            240
  Boiling can be assumed for the entire length of a fuel rod.

  Rod design                                       Rod 1           Rod 2
  Pellet radius, inner          (mm)               0.9 / 0.0        0.9
  Pellet radius, outer          (mm)               4.025            4.025
  Pellet length:                (mm)               10.5            10.5
  Fuel rod length               (mm)               224 enriched     220 enriched
  Length of drilled section     (mm)               ~43              220
  (measured from top of fuel rod)                 (4/21 pellets)  (21/21 pellets)

  Pellet end geometry    (both rods)                  Dished both ends
  Dishing depth                 (mm)                       0.26
  Land width                    (mm)                       5.3
  Chamfer Height                (mm)                       0.15
  Chamfer Width                 (mm)                       0.3

  Cladding radius, inner        (mm)               4.11             4.11
  Cladding radius, outer        (mm)               4.75             4.75
  Total free volume             (ccm)              2.6              2.8
  Filling gas                                      He               He
  Filling gas pressure          (bar)              5                5
  Fuel surface roughness        (microm)           1.4              1.4
  Cladding surface roughness    (microm)           < 0.15           < 0.15
  Fast flux level:              (n/cm2s)           1.6*E11*LHR *)
  (Both rods)                                      *) LHR=Linear Heat Rate (kW/m)
```

```
  Material Characteristics (valid for both rods)
  Cladding type                                              Zr-4
  Fuel density                  (g/ccm)                      10.54
  Enrichment PU-fissile         (%)                          6.07 w/o
  Isotopic composition:
              wt% U             (%)                         80.568
              wt% Pu            (%)                          7.424
              wt% Am            (%)                          0.04

  Pu composition:
              Pu238             (% of total Pu)              0.914
              Pu239             (% of total Pu)             65.340
              Pu240             (% of total Pu)             23.675
              Pu241             (% of total Pu)              6.570
              Pu242             (% of total Pu)              3.494
              Am241             (% 0f total Pu)              0.595

  U  composition:
              U234              (% of total U )              0.002
              U235              (% of total U )              0.252
              U236              (% of total U )              0.001
              U238              (% of total U )             99.745

  Grain size:
              4.3 to 6.6 micrometer.

  Pore size distribution:
              1.9 to 3.0 micrometer.

  PuO2 spot size:
              Mean    :  15.2 micrometer
              Median  :   5.1 micrometer
              Maximum : 231.4 micrometer


  Initial density:
              Average      : 95.86% of TD
              Standard dev.:  0.28% of TD


  Re-sintering test:
              Conditions           : 1700 deg. C for 24hr in Helium
              Average densification: 0.445% of TD (from 0.35 to 0.55% of TD)

  O/M ratio:
              Average      : 1.999
              Standard dev.: 0.001


VARIABLES IN CONDENSED DATA FILES


ROD 1              Data File:      rod1.dat


Local heat rates:

  Name:            Units:  Pos (measured from bottom of rod):
  LHRB1            kW/m    0.0     (bottom)
  LHRM1            kW/m    112     (mid)
  LHRT1            kW/m    224     (top)
  LHRTF1           kW/m    184     (at TF tip pos.)

Other Variables

  Name:            Units:
  Timeinc          s               Time interval

ROD 2              Data File:      rod2.dat
```

Local heat rates:

Name:	Units:	Pos (measured from bottom of rod):	
LHRB2	kW/m	0.0	(bottom)
LHRM2	kW/m	110	(mid)
LHRT2	kW/m	220	(top)
LHRTF	kW/m	180	(at TF tip pos.)

Other Variables

Name:	Units:	
Timeinc	s	Time interval

ROD1.dat

timeinc	LHRB1	LHRM1	LHRT1	LHRTF1
154356.	33.7906	33.8906	32.0997	32.4545
411223.	33.8296	33.9294	32.1288	32.4827
417697.	33.3083	33.4061	31.6219	31.9685
426071.	32.6566	32.7521	30.9918	31.3299
321709.	32.6166	32.7116	30.9437	31.2798
318469.	32.9507	33.0464	31.2520	31.5903
320965.	32.6966	32.7912	31.0025	31.3369
364610.	33.7655	33.8628	32.0049	32.3487
390047.	31.5658	31.6565	29.9106	30.2306
387765.	31.7539	31.8448	30.0797	30.4003
272723.	33.7804	33.8767	31.9904	32.3301
268005.	34.3769	34.4747	32.5477	32.8923
422167.	32.0933	32.1842	30.3760	30.6963
429730.	31.5311	31.6201	29.8333	30.1465
434798.	31.1662	31.2538	29.4778	29.7858
439003.	30.8702	30.9566	29.1877	29.4913
443928.	30.5303	30.6154	28.8565	29.1553
444049.	30.5244	30.6092	28.8413	29.1386
462840.	30.7241	30.8090	29.0197	29.3173
450660.	31.5572	31.6440	29.7960	30.1000
451450.	31.5047	31.5909	29.7359	30.0377
113919.	31.8793	31.9662	30.0825	30.3868
405201.	9.0785	9.1032	8.5658	8.6522
345279.	32.1756	32.2630	30.3533	30.6590
150942.	26.1770	26.2480	24.6903	24.9383
438937.	27.6732	27.7480	26.0964	26.3577
411809.	29.4983	29.5777	27.8093	28.0865
405837.	29.9347	30.0148	28.2121	28.4918
416830.	29.1473	29.2250	27.4618	27.7327
428142.	28.3793	28.4546	26.7304	26.9928
419622.	28.9575	29.0340	27.2672	27.5335
423452.	28.6977	28.7731	27.0147	27.2771
426395.	28.5016	28.5761	26.8226	27.0817
420331.	28.9148	28.9900	27.2038	27.4652
421028.	28.8691	28.9437	27.1530	27.4125
425813.	28.5466	28.6200	26.8423	27.0973
312728.	27.9174	27.9889	26.2444	26.4925
309601.	28.2009	28.2728	26.5056	26.7551
307172.	28.4252	28.4974	26.7112	26.9616
260116.	27.4319	27.5013	25.7729	26.0135
256149.	27.8578	27.9280	26.1690	26.4125
76510.	32.3930	32.4745	30.4256	30.7079
358696.	30.3189	30.3950	28.4731	28.7364
372581.	29.1908	29.2637	27.4071	27.6592
83248.	18.7906	18.8373	17.6398	17.8015
308001.	26.9676	27.0345	25.3129	25.5442
299390.	27.7443	27.8129	26.0377	26.2748
189806.	27.8363	27.9048	26.1201	26.3570
401081.	28.2729	28.3423	26.5250	26.7645
396581.	28.5955	28.6652	26.8211	27.0619
398361.	28.4695	28.5385	26.6965	26.9347
395703.	28.6625	28.7316	26.8711	27.1094

398115.	28.4906	28.5589	26.7035	26.9389
400912.	28.2935	28.3609	26.5126	26.7448
120809.	27.8095	27.8754	26.0550	26.2823
337021.	28.3034	28.3703	26.5142	26.7447
332040.	28.7294	28.7970	26.9080	27.1407
335015.	28.4756	28.5423	26.6650	26.8948
388105.	8.7758	8.8018	8.2018	8.2931
387918.	8.5805	8.6058	8.0194	8.1086
387908.	9.0089	9.0354	8.4200	8.5134
386108.	9.0882	9.1150	8.4944	8.5885
411301.	19.6340	19.6917	18.3519	18.5548
411338.	20.8393	20.9004	19.4797	19.6943
411319.	20.7131	20.7735	19.3628	19.5754
407721.	20.5736	20.6334	19.2336	19.4440
379993.	19.0265	19.0817	17.7884	17.9823
379816.	19.6414	19.6981	18.3643	18.5638
379827.	20.0833	20.1411	18.7784	18.9818
379827.	19.7813	19.8380	18.4971	18.6968
379810.	19.7967	19.8534	18.5126	18.7118
376253.	19.7433	19.7996	18.4637	18.6617
113358.	18.3875	18.4398	17.1965	17.3804
18012.	4.0221	4.0335	3.7616	3.8018
80096.	6.3639	6.3820	5.9518	6.0154
88254.	10.4824	10.5122	9.8036	9.9083
74700.	13.7605	13.7995	12.8695	13.0069
30595.	18.4156	18.4678	17.2233	17.4072
46785.	15.9152	15.9603	14.8850	15.0438
396870.	16.1111	16.1567	15.0686	15.2291
396909.	16.5193	16.5660	15.4512	15.6153
396984.	17.4168	17.4658	16.2915	16.4640
395068.	16.9913	17.0389	15.8943	16.0620
57651.	15.7668	15.8110	14.7494	14.9047
443772.	15.1835	15.2259	14.2041	14.3534
443744.	15.7379	15.7817	14.7236	14.8778
443768.	16.1900	16.2349	15.1473	15.3055
443731.	16.0187	16.0630	14.9879	15.1439
441095.	15.9029	15.9467	14.8804	15.0347
251979.	15.7610	15.8043	14.7483	14.9008
251089.	15.2726	15.3144	14.2917	14.4392
245718.	15.4018	15.4439	14.4131	14.5615
225877.	15.3693	15.4112	14.3831	14.5310
55670.	10.5985	10.6274	9.9186	10.0205
77415.	15.1248	15.1660	14.1547	14.3000
21601.	12.5834	12.6176	11.7764	11.8972
111616.	17.3244	17.3715	16.2136	16.3798
429261.	15.9665	16.0098	14.9433	15.0961
429301.	13.9211	13.9588	13.0297	13.1625
429354.	14.4267	14.4656	13.5036	13.6408
429277.	14.8922	14.9322	13.9400	14.0812
429370.	15.5126	15.5541	14.5215	14.6681
429410.	15.9827	16.0253	14.9624	15.1129
429416.	16.2320	16.2750	15.1966	15.3489
429398.	16.6754	16.7195	15.6127	15.7686
429331.	17.1592	17.2044	16.0666	16.2264
429297.	17.3602	17.4057	16.2558	16.4168
429282.	17.8239	17.8704	16.6911	16.8558
431171.	17.3420	17.3870	16.2408	16.4004
429219.	17.2675	17.3122	16.1721	16.3304
429393.	17.1595	17.2037	16.0720	16.2286
425672.	17.5110	17.5559	16.4023	16.5614
269173.	11.6142	11.6439	10.8794	10.9846
26947.	4.7397	4.7518	4.4399	4.4828
27861.	9.6456	9.6702	9.0355	9.1227
332108.	14.6254	14.6627	13.7006	13.8327
426698.	11.2300	11.2586	10.5204	10.6216
426676.	11.1377	11.1660	10.4344	10.5344
425661.	11.4714	11.5004	10.7474	10.8502

352936.	11.2440	11.2723	10.5348	10.6353
348325.	11.7416	11.7711	11.0014	11.1061
346565.	11.9521	11.9821	11.1991	11.3054
173758.	11.8127	11.8422	11.0688	11.1736
41390.	10.5297	10.5561	9.8667	9.9601
307905.	11.7368	11.7661	10.9980	11.1019
307907.	12.1315	12.1617	11.3682	11.4754
305139.	12.2180	12.2484	11.4497	11.5574
362017.	11.5675	11.5962	10.8405	10.9422
361805.	11.9470	11.9766	11.1966	11.3014
361951.	12.3825	12.4131	11.6052	11.7135
361684.	12.7930	12.8245	11.9904	12.1020
357173.	13.5354	13.5687	12.6868	12.8046
289729.	13.1478	13.1800	12.3240	12.4381
283598.	14.1206	14.1551	13.2364	13.3585
384230.	14.0902	14.1245	13.2084	13.3299
384362.	14.1818	14.2162	13.2949	13.4168
383485.	14.2909	14.3255	13.3979	13.5204
36028.	14.4814	14.5163	13.5769	13.7007
29664.	8.4720	8.4971	7.7832	7.8693
173970.	15.6798	15.7262	14.4055	14.5648
257632.	25.8508	25.9271	23.7519	24.0138
256513.	28.8423	28.9271	26.5038	26.7950
64804.	25.4268	25.5014	23.3676	23.6236
410542.	27.8311	27.9123	25.5805	25.8597
410411.	28.2611	28.3431	25.9812	26.2630
410449.	27.7537	27.8337	25.5201	25.7952
411348.	27.3117	27.3900	25.1189	25.3880
410413.	26.8703	26.9468	24.7180	24.9812
412161.	26.4568	26.5316	24.3427	24.6003
410418.	26.8210	26.8964	24.6829	24.9425
410405.	26.2823	26.3557	24.1921	24.4450
405005.	26.8739	26.9485	24.7419	24.9988
418532.	27.9089	27.9858	25.7007	25.9658
418485.	28.0552	28.1319	25.8414	26.1060
418528.	27.0006	27.0739	24.8756	25.1286
418539.	27.1401	27.2132	25.0097	25.2623
418551.	26.8706	26.9425	24.7669	25.0153
418532.	26.5777	26.6483	24.5024	24.7464
417610.	26.6235	26.6937	24.5502	24.7929
398775.	27.7535	27.8260	25.5981	25.8493
398721.	27.5672	27.6387	25.4320	25.6798
398735.	27.0458	27.1155	24.9566	25.1979
69244.	16.1740	16.2155	14.9266	15.0703

ROD2.dat

timeinc	LHRB2	LHRM2	LHRT2	LHRTF2
154541.	33.8929	33.9682	33.2202	33.5874
411217.	33.9830	34.0583	33.3106	33.6776
416952.	33.5153	33.5892	32.8553	33.2155
426789.	32.7425	32.8144	32.1007	32.4511
322252.	32.7116	32.7831	32.0730	32.4216
318156.	33.1326	33.2048	32.4880	32.8399
320694.	32.8701	32.9415	32.2328	32.5807
363475.	33.7856	33.8586	33.1333	33.4894
391132.	31.3964	31.4640	30.7926	31.1222
388673.	31.5948	31.6625	30.9894	31.3199
273518.	33.7967	33.8690	33.1515	33.5038
267029.	34.6179	34.6917	33.9589	34.3188
421627.	32.2305	32.2989	31.6194	31.9531
429427.	31.6448	31.7117	31.0476	31.3737
434626.	31.2660	31.3317	30.6786	30.9994
439043.	30.9512	31.0160	30.3724	30.6885
444336.	30.5823	30.6460	30.0130	30.3239
444741.	30.5541	30.6175	29.9880	30.2972
461610.	30.6966	30.7599	30.1307	30.4398
451420.	31.3892	31.4537	30.8135	31.1280
451868.	31.3578	31.4218	30.7857	31.0982
114045.	31.7150	31.7795	31.1383	31.4534
377508.	9.4180	9.4372	9.2471	9.3405
345395.	33.0343	33.1012	32.4363	32.7630
151235.	26.6882	26.7421	26.2064	26.4696
440054.	28.0111	28.0674	27.5070	27.7824
414053.	29.7698	29.8294	29.2366	29.5279
409530.	30.0983	30.1582	29.5620	29.8550
419084.	29.4119	29.4702	28.8905	29.1754
425389.	28.9757	29.0328	28.4647	28.7440
418060.	29.4834	29.5412	28.9662	29.2489
422484.	29.1745	29.2313	28.6654	28.9436
425825.	28.9453	29.0014	28.4430	28.7175
419298.	29.3956	29.4522	28.8883	29.1656
419601.	29.3741	29.4304	28.8701	29.1456
424237.	29.0528	29.1082	28.5572	28.8281
312470.	28.3294	28.3831	27.8486	28.1115
309482.	28.6028	28.6568	28.1194	28.3837
307301.	28.8056	28.8597	28.3209	28.5859
260547.	27.7196	27.7714	27.2551	27.5091
255982.	28.2137	28.2663	27.7426	28.0002
76506.	32.7133	32.7741	32.1686	32.4665
358351.	30.5953	30.6520	30.0877	30.3652
372916.	29.4001	29.4542	28.9151	29.1803
85965.	19.4005	19.4361	19.0815	19.2559
308302.	27.2080	27.2578	26.7621	27.0060
299747.	27.9844	28.0354	27.5276	27.7775
190165.	28.1441	28.1952	27.6863	27.9367
401605.	28.4798	28.5313	28.0187	28.2709
395924.	28.8882	28.9401	28.4233	28.6776
399562.	28.6249	28.6759	28.1671	28.4175
395485.	28.9197	28.9710	28.4601	28.7115
397897.	28.7442	28.7948	28.2903	28.5386
400571.	28.5520	28.6020	28.1040	28.3491
120811.	28.0625	28.1114	27.6240	27.8639
336858.	28.7450	28.7949	28.2975	28.5424
332151.	29.1521	29.2025	28.7007	28.9477
335208.	28.8860	28.9356	28.4412	28.6846
388178.	8.4754	8.4942	8.3071	8.3995
387837.	8.3092	8.3276	8.1444	8.2349
387893.	8.7510	8.7704	8.5777	8.6729
386128.	8.8719	8.8915	8.6965	8.7928
411274.	19.8071	19.8508	19.4165	19.6311
411306.	20.7086	20.7542	20.3017	20.5253

411300.	20.5862	20.6313	20.1832	20.4046
407685.	20.4528	20.4975	20.0539	20.2730
379969.	19.1457	19.1874	18.7737	18.9781
379801.	19.7811	19.8240	19.3981	19.6085
379810.	20.2720	20.3158	19.8808	20.0957
379822.	20.1074	20.1507	19.7208	19.9332
379645.	20.1544	20.1977	19.7682	19.9804
376205.	20.1258	20.1688	19.7415	19.9526
113328.	18.7841	18.8242	18.4264	18.6229
17946.	3.7191	3.7270	3.6483	3.6872
80127.	5.9498	5.9625	5.8366	5.8988
88267.	9.8925	9.9136	9.7044	9.8077
74716.	12.8987	12.9261	12.6535	12.7882
30589.	17.2562	17.2929	16.9282	17.1084
46798.	14.7281	14.7594	14.4484	14.6021
396911.	15.7456	15.7790	15.4470	15.6111
396891.	15.8945	15.9281	15.5940	15.7591
396933.	16.6632	16.6983	16.3492	16.5217
395042.	16.2673	16.3014	15.9617	16.1296
57627.	15.2135	15.2454	14.9283	15.0850
443735.	14.6983	14.7290	14.4233	14.5744
443695.	15.1536	15.1852	14.8710	15.0263
443883.	15.5635	15.5958	15.2742	15.4332
443677.	15.3990	15.4308	15.1138	15.2705
440930.	15.2880	15.3196	15.0059	15.1609
252043.	15.1596	15.1908	14.8806	15.0339
251151.	14.6806	14.7108	14.4110	14.5592
245752.	14.7945	14.8249	14.5234	14.6724
225845.	14.7687	14.7990	14.4985	14.6471
55668.	10.2540	10.2749	10.0666	10.1696
77373.	14.5572	14.5870	14.2913	14.4375
21590.	11.7029	11.7268	11.4893	11.6067
111654.	16.3439	16.3772	16.0459	16.2097
429271.	15.1039	15.1346	14.8291	14.9801
429259.	13.1158	13.1425	12.8780	13.0088
429370.	13.6149	13.6424	13.3688	13.5041
429317.	14.0792	14.1076	13.8255	13.9650
429338.	14.6266	14.6560	14.3639	14.5083
429290.	15.0782	15.1084	14.8085	14.9568
429383.	15.3482	15.3788	15.0745	15.2250
429400.	15.8232	15.8546	15.5421	15.6966
429339.	16.2889	16.3211	16.0007	16.1591
429330.	16.4482	16.4806	16.1583	16.3177
429318.	16.8975	16.9306	16.6009	16.7640
431020.	16.3846	16.4166	16.0983	16.2557
429320.	16.2591	16.2907	15.9761	16.1317
429289.	16.1650	16.1963	15.8848	16.0389
425759.	16.4133	16.4450	16.1300	16.2858
269280.	10.9627	10.9838	10.7741	10.8778
27028.	4.5254	4.5341	4.4476	4.4904
27859.	9.2053	9.2229	9.0471	9.1341
332001.	13.1292	13.1544	12.9040	13.0279
426722.	10.5770	10.5973	10.3961	10.4956
426765.	10.4975	10.5175	10.3184	10.4169
425691.	10.8249	10.8455	10.6407	10.7420
352957.	10.6137	10.6338	10.4336	10.5327
348403.	11.1083	11.1293	10.9203	11.0237
346530.	11.3178	11.3391	11.1267	11.2318
173712.	11.2223	11.2434	11.0332	11.1372
41409.	9.9426	9.9614	9.7753	9.8673
307944.	11.1400	11.1610	10.9527	11.0558
307814.	11.5003	11.5218	11.3073	11.4135
304958.	11.5894	11.6111	11.3955	11.5022
361829.	11.0001	11.0206	10.8165	10.9175
361778.	11.3643	11.3854	11.1751	11.2792
361937.	11.7850	11.8069	11.5893	11.6970
361718.	12.1712	12.1937	11.9697	12.0805

357242.	12.8659	12.8896	12.6535	12.7704
289691.	12.4792	12.5021	12.2737	12.3868
283451.	13.4166	13.4412	13.1963	13.3176
384406.	13.3824	13.4068	13.1633	13.2839
384368.	13.4778	13.5023	13.2579	13.3789
383260.	13.5748	13.5994	13.3541	13.4756
36037.	13.7750	13.8000	13.5516	13.6745
29639.	7.3740	7.3904	7.2275	7.3075
173953.	14.3295	14.3613	14.0450	14.2003
257587.	24.6526	24.7073	24.1646	24.4310
256522.	27.1805	27.2406	26.6445	26.9371
64785.	24.4750	24.5289	23.9937	24.2564
410474.	26.2714	26.3291	25.7569	26.0378
410450.	26.5389	26.5967	26.0225	26.3044
410408.	26.0549	26.1112	25.5511	25.8261
411287.	25.6318	25.6869	25.1393	25.4082
410384.	25.2181	25.2720	24.7367	24.9996
412190.	24.8241	24.8768	24.3532	24.6103
410433.	25.1806	25.2337	24.7062	24.9653
410378.	24.6720	24.7236	24.2101	24.4624
404999.	25.0880	25.1402	24.6214	24.8762
418473.	25.8141	25.8674	25.3375	25.5978
418511.	25.9549	26.0081	25.4792	25.7390
418506.	24.9807	25.0315	24.5262	24.7745
418520.	25.1144	25.1651	24.6607	24.9085
418535.	24.8651	24.9149	24.4192	24.6628
418502.	24.5971	24.6460	24.1592	24.3984
417597.	24.6525	24.7012	24.2168	24.4548
398799.	25.8041	25.8546	25.3515	25.5988
398713.	25.6158	25.6656	25.1699	25.4136
398703.	25.1213	25.1698	24.6872	24.9245
69275.	15.1032	15.1322	14.8434	14.9854

Appendix II

RADIAL POWER AND BURN-UP PROFILES

Figure A.1. Relative power and burn-up distribution in Rod 1 (solid pellet) as function of radius

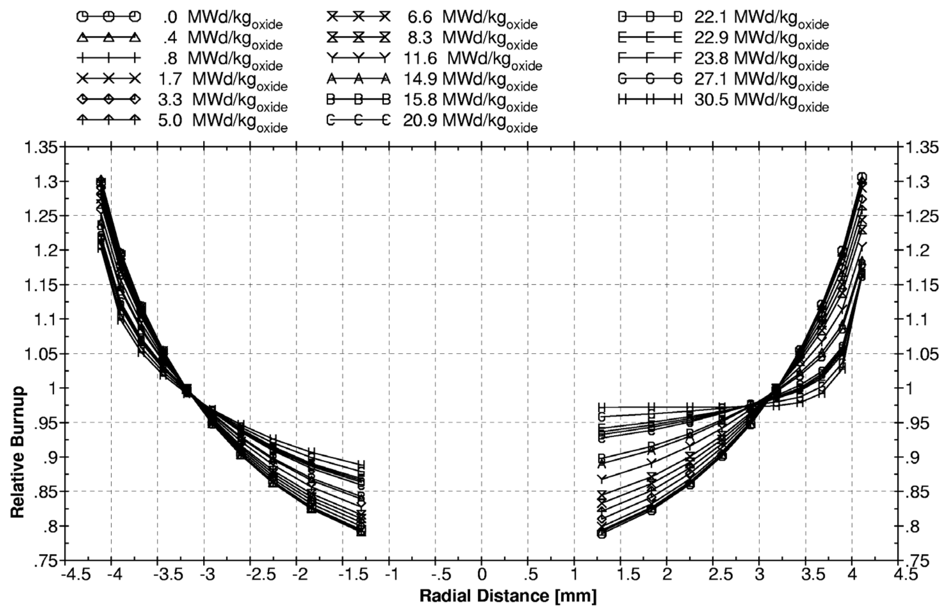

Figure A.2. Relative power and burn-up distribution in Rod 2 (hollow pellet) as function of radius

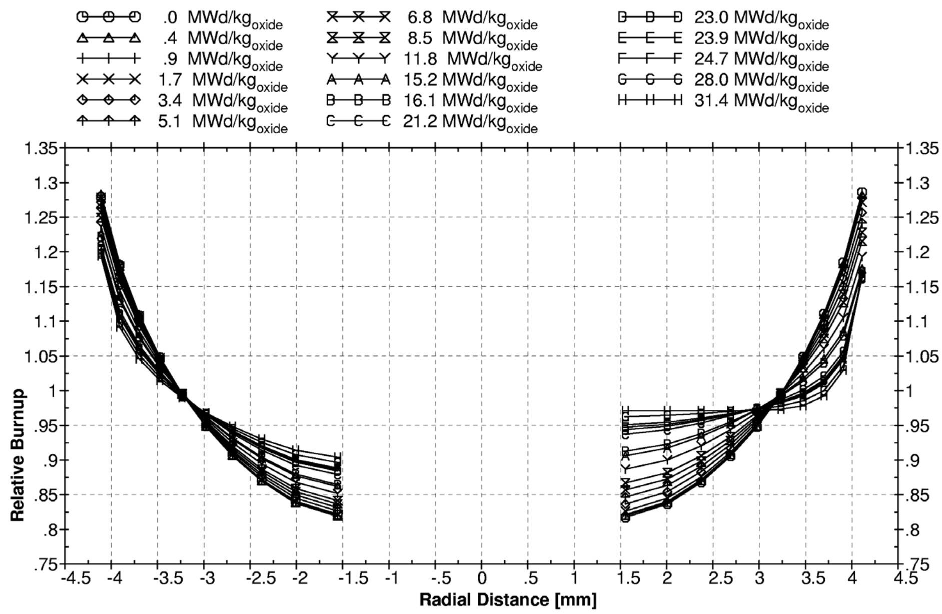

Figure A3. Relative power and burn-up distribution in Rod 1 (solid pellet) as function of burn-up

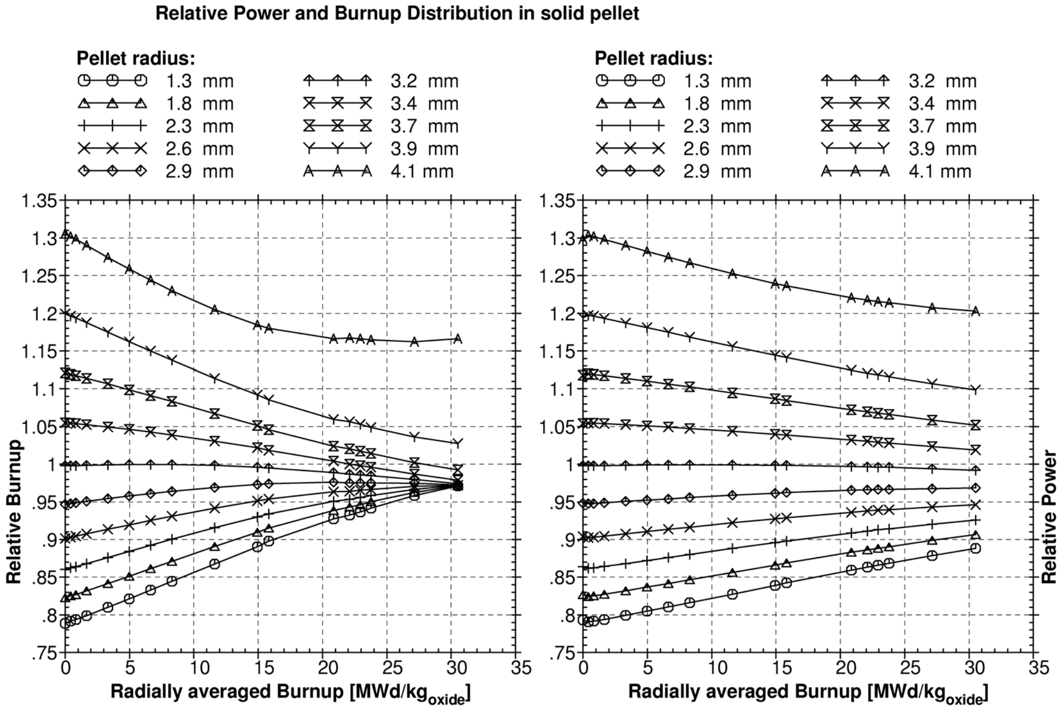

Figure A.4. Relative power and burn-up distribution in Rod 2 (hollow pellet) as function of burn-up

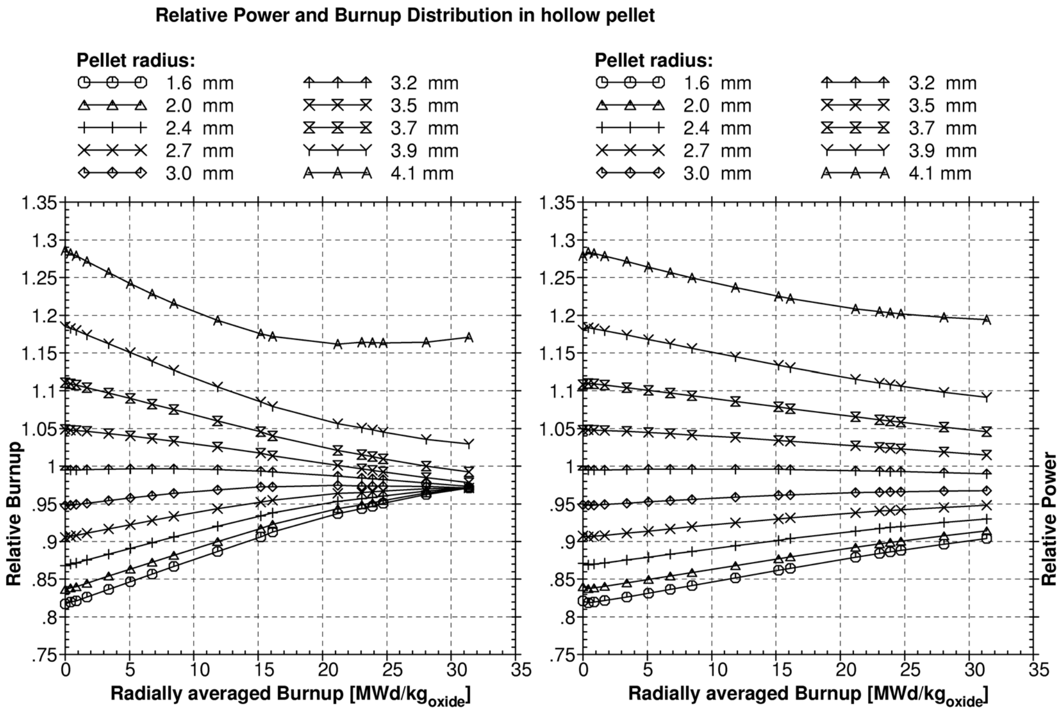

Table A.1. Radial power distribution for Rod 1 (solid pellet)

	Radially averaged burn-up [MWd/kgOX]																
	0.00	0.41	0.83	1.66	3.31	4.97	6.63	8.29	11.61	14.94	15.83	20.86	22.10	22.94	23.78	27.15	30.51
Radius [mm]	**Relative power**																
1.3000	0.7890	0.7917	0.7937	0.7991	0.8102	0.8215	0.8330	0.8445	0.8675	0.8902	0.8980	0.9276	0.9324	0.9368	0.9416	0.9583	0.9714
1.8380	0.8228	0.8252	0.8271	0.8318	0.8415	0.8514	0.8614	0.8712	0.8907	0.9096	0.9152	0.9388	0.9430	0.9464	0.9501	0.9626	0.9719
2.2510	0.8605	0.8625	0.8641	0.8681	0.8762	0.8843	0.8924	0.9003	0.9156	0.9301	0.9341	0.9510	0.9536	0.9559	0.9585	0.9666	0.9720
2.5990	0.9017	0.9032	0.9044	0.9075	0.9135	0.9195	0.9254	0.9310	0.9416	0.9511	0.9540	0.9635	0.9642	0.9654	0.9667	0.9704	0.9721
2.9060	0.9470	0.9479	0.9487	0.9506	0.9542	0.9577	0.9609	0.9639	0.9690	0.9730	0.9743	0.9761	0.9752	0.9752	0.9753	0.9747	0.9727
3.1840	0.9979	0.9981	0.9983	0.9987	0.9993	0.9996	0.9997	0.9996	0.9985	0.9963	0.9950	0.9889	0.9870	0.9858	0.9847	0.9797	0.9744
3.4390	1.0551	1.0544	1.0539	1.0525	1.0495	1.0461	1.0426	1.0388	1.0306	1.0218	1.0182	1.0040	1.0003	0.9981	0.9958	0.9870	0.9790
3.6760	1.1209	1.1191	1.1177	1.1141	1.1066	1.0989	1.0911	1.0832	1.0672	1.0514	1.0457	1.0242	1.0206	1.0174	1.0141	1.0021	0.9924
3.8990	1.1992	1.1962	1.1937	1.1874	1.1749	1.1623	1.1499	1.1377	1.1141	1.0921	1.0857	1.0598	1.0563	1.0527	1.0488	1.0362	1.0276
4.1100	1.3060	1.3018	1.2985	1.2903	1.2741	1.2585	1.2438	1.2299	1.2050	1.1845	1.1798	1.1661	1.1674	1.1663	1.1646	1.1624	1.1664

Table A.2. Radial power distribution for Rod 2 (hollow pellet)

	Radially averaged burn-up [MWd/kgOX]																
	0.00	0.42	0.85	1.69	3.39	5.08	6.77	8.46	11.84	15.21	16.11	21.19	23.05	23.88	24.72	28.05	31.38
Radius [mm]	**Relative power**																
1.5550	0.8172	0.8196	0.8215	0.8264	0.8364	0.8466	0.8568	0.8669	0.8870	0.9063	0.9128	0.9369	0.9438	0.9470	0.9506	0.9625	0.9710
2.0070	0.8363	0.8385	0.8403	0.8449	0.8541	0.8634	0.8727	0.8819	0.9000	0.9172	0.9231	0.9438	0.9487	0.9514	0.9544	0.9643	0.9710
2.3740	0.8681	0.8700	0.8715	0.8754	0.8831	0.8909	0.8985	0.9060	0.9205	0.9339	0.9382	0.9533	0.9567	0.9586	0.9607	0.9672	0.9711
2.6910	0.9054	0.9069	0.9080	0.9110	0.9168	0.9225	0.9281	0.9335	0.9436	0.9525	0.9551	0.9638	0.9653	0.9662	0.9673	0.9702	0.9711
2.9750	0.9476	0.9484	0.9492	0.9510	0.9545	0.9578	0.9609	0.9638	0.9687	0.9725	0.9729	0.9748	0.9738	0.9738	0.9739	0.9731	0.9712
3.2340	0.9948	0.9950	0.9951	0.9955	0.9961	0.9965	0.9966	0.9965	0.9956	0.9937	0.9924	0.9869	0.9844	0.9834	0.9823	0.9779	0.9733
3.4740	1.0487	1.0481	1.0475	1.0462	1.0433	1.0401	1.0368	1.0332	1.0256	1.0175	1.0140	1.0012	0.9966	0.9947	0.9926	0.9851	0.9783
3.6980	1.1108	1.1091	1.1078	1.1043	1.0972	1.0899	1.0826	1.0752	1.0603	1.0457	1.0403	1.0209	1.0155	1.0128	1.0100	1.0001	0.9924
3.9090	1.1851	1.1823	1.1799	1.1740	1.1621	1.1503	1.1386	1.1272	1.1054	1.0853	1.0795	1.0566	1.0511	1.0482	1.0451	1.0355	1.0296
4.1100	1.2861	1.2822	1.2791	1.2714	1.2564	1.2419	1.2283	1.2157	1.1933	1.1753	1.1717	1.1618	1.1642	1.1639	1.1631	1.1641	1.1710

Table A.3. Radial burn-up distribution for Rod 1 (solid pellet)

	Radially averaged burn-up [MWd/kgOX]																
	0.00	0.41	0.83	1.66	3.31	4.97	6.63	8.29	11.61	14.94	15.83	20.86	22.10	22.94	23.78	27.15	30.51
Radius [mm]	**Relative burn-up**																
1.3000	0.7936	0.7907	0.7917	0.7941	0.7994	0.8049	0.8105	0.8161	0.8276	0.8390	0.8424	0.8595	0.8635	0.8661	0.8687	0.8788	0.8883
1.8380	0.8268	0.8243	0.8252	0.8273	0.8320	0.8368	0.8417	0.8467	0.8565	0.8662	0.8690	0.8831	0.8863	0.8885	0.8906	0.8988	0.9064
2.2510	0.8638	0.8617	0.8625	0.8643	0.8682	0.8722	0.8763	0.8803	0.8882	0.8960	0.8981	0.9089	0.9114	0.9130	0.9145	0.9205	0.9259
2.5990	0.9041	0.9026	0.9032	0.9046	0.9075	0.9106	0.9135	0.9165	0.9222	0.9276	0.9291	0.9363	0.9379	0.9389	0.9399	0.9434	0.9465
2.9060	0.9485	0.9476	0.9479	0.9488	0.9506	0.9524	0.9541	0.9558	0.9589	0.9616	0.9624	0.9655	0.9661	0.9665	0.9668	0.9678	0.9685
3.1840	0.9982	0.9980	0.9981	0.9983	0.9986	0.9989	0.9991	0.9992	0.9992	0.9988	0.9986	0.9970	0.9965	0.9962	0.9958	0.9941	0.9922
3.4390	1.0540	1.0547	1.0544	1.0538	1.0524	1.0509	1.0492	1.0475	1.0439	1.0399	1.0387	1.0320	1.0304	1.0292	1.0281	1.0235	1.0190
3.6760	1.1182	1.1198	1.1191	1.1175	1.1139	1.1102	1.1064	1.1025	1.0947	1.0868	1.0844	1.0724	1.0696	1.0677	1.0659	1.0587	1.0519
3.8990	1.1944	1.1974	1.1961	1.1933	1.1872	1.1810	1.1748	1.1685	1.1563	1.1444	1.1411	1.1245	1.1207	1.1183	1.1159	1.1068	1.0985
4.1100	1.2982	1.3033	1.3017	1.2980	1.2901	1.2821	1.2743	1.2668	1.2526	1.2396	1.2361	1.2207	1.2176	1.2157	1.2139	1.2076	1.2027

Table A.4. Radial burn-up distribution for Rod 2 (hollow pellet)

	Radially averaged burn-up [MWd/kgOX]																
	0.00	0.42	0.85	1.69	3.39	5.08	6.77	8.46	11.84	15.21	16.11	21.19	23.05	23.88	24.72	28.05	31.38
Radius [mm]	**Relative burn-up**																
1.5550	0.8212	0.8187	0.8196	0.8218	0.8266	0.8316	0.8366	0.8417	0.8518	0.8618	0.8647	0.8792	0.8842	0.8863	0.8884	0.8966	0.9040
2.0070	0.8400	0.8377	0.8385	0.8406	0.8450	0.8496	0.8542	0.8588	0.8680	0.8770	0.8797	0.8926	0.8971	0.8989	0.9007	0.9077	0.9141
2.3740	0.8712	0.8693	0.8700	0.8717	0.8755	0.8793	0.8832	0.8870	0.8945	0.9018	0.9039	0.9140	0.9174	0.9188	0.9201	0.9254	0.9301
2.6910	0.9078	0.9063	0.9069	0.9082	0.9110	0.9139	0.9168	0.9196	0.9250	0.9302	0.9316	0.9383	0.9405	0.9414	0.9422	0.9454	0.9481
2.9750	0.9490	0.9481	0.9485	0.9493	0.9510	0.9527	0.9544	0.9560	0.9589	0.9615	0.9622	0.9650	0.9658	0.9661	0.9663	0.9672	0.9677
3.2340	0.9951	0.9949	0.9950	0.9951	0.9955	0.9958	0.9960	0.9961	0.9961	0.9958	0.9956	0.9942	0.9935	0.9932	0.9928	0.9913	0.9897
3.4740	1.0478	1.0483	1.0481	1.0475	1.0461	1.0447	1.0431	1.0415	1.0381	1.0344	1.0332	1.0271	1.0248	1.0238	1.0228	1.0187	1.0148
3.6980	1.1083	1.1098	1.1091	1.1076	1.1042	1.1006	1.0970	1.0934	1.0861	1.0787	1.0765	1.0655	1.0616	1.0599	1.0583	1.0519	1.0460
3.9090	1.1807	1.1834	1.1822	1.1795	1.1738	1.1679	1.1620	1.1562	1.1448	1.1338	1.1307	1.1156	1.1105	1.1084	1.1063	1.0984	1.0914
4.1100	1.2789	1.2836	1.2821	1.2786	1.2712	1.2638	1.2566	1.2497	1.2367	1.2250	1.2219	1.2085	1.2047	1.2033	1.2019	1.1973	1.1941

Appendix III

RESULTS OF GAS PUNCTURING AND GAS ANALYSIS

Table A.5. Results of gas puncturing

Rod		1 (solid)	2 (hollow)
Measured free volume at time of PIE	[cm^3]	2.84	3.13
As fabricated free volume (calculated)	[cm^3]	2.90	3.20
Measured pressure (at 0°C)	[MPa]	1.36	1.03*
Total gas amount	[cm^3]	35.1	29.6

* Corrected 17 June 2005 (error in previous version of this report; old value: 3.20).

Table A.6. Results of mass spectrometry of extracted gas

Rod		1 (solid)	2 (hollow)
^{83}Kr	[%]	14.93	14.66
^{84}Kr	[%]	31.79	32.23
^{85}Kr	[%]	5.88	5.80
^{86}Kr	[%]	47.30	47.32
Total Kr	[mg]	5.66	4.55
Total Kr	[cm^3]	1.50	1.20
^{131}Xe	[%]	11.45	11.15
^{132}Xe	[%]	19.94	20.07
^{134}Xe	[%]	26.84	26.60
^{136}Xe	[%]	41.77	42.18
Total Xe	[mg]	106.14	85.96
Total Xe	[cm^3]	17.75	14.38
N_2/CO	[mg]	0.08	0.10
N_2/CO	[cm^3]	0.07	0.08
O_2	[mg]	<0.02	<0.02
O_2	[cm^3]	<0.01	<0.01
Ar	[mg]	0.10	0.08
Ar	[cm^3]	0.06	0.05
CO_2	[mg]	N.D.	N.D.
CO_2	[cm^3]	N.D.	N.D.
He	[mg]	2.81	2.48
He	[cm^3]	15.76	13.91
H_2	[mg]	N.D.	N.D.
H_2	[cm^3]	N.D.	N.D.
Total gas amount	**[cm^3]**	**35.14**	**29.63**

Table A.7. ORIGEN calculations of inventory of fission gases at end of life

Rod		1 (solid)	2 (hollow)
^{83}Kr	[mg]	3.81	3.67
^{84}Kr	[mg]	7.41	7.17
^{85}Kr	[mg]	1.50	1.44
^{86}Kr	[mg]	11.63	11.23
Total Kr	[mg]	24.35	23.51
^{128}Xe	[mg]	0.30	0.30
^{130}Xe	[mg]	0.86	0.86
^{131}Xe	[mg]	67.28	64.57
^{132}Xe	[mg]	128.10	124.20
^{133}Xe	[mg]	1.23	1.16
^{134}Xe	[mg]	169.40	163.70
^{136}Xe	[mg]	253.80	246.70
Total Xe	[mg]	620.97	601.49

Table A.8. Fission gas release from fuel

Rod		1	2
Total Kr released	[mg]	5.66	4.55
Total Xe released		106.14	85.96
Total Kr + Xe released		111.80	90.51
Total Kr generated		24.35	23.51
Total Xe generated		620.97	601.49
Total Kr + Xe generated		645.32	625.00
Fraction Kr + Xe released		0.1732	0.1448

Appendix IV

RESULTS OF “LIMITED” SENSITIVITY STUDY FOR THE SOLID AND HOLLOW MOX PELLETS BEHAVIOUR BENCHMARK

In order to get a picture of the effect of the rod power uncertainty on the calculated fuel centreline temperature and fuel pin pressure, a sensitivity study was performed at the ORNL. The codes used in the study were FRAPCON-3 and TRANSURANUS.

In this study both code-to-code and code-to-experiment comparisons are made. In the following, the results of the sensitivity study are presented.

The basis for the sensitivity study are the uncertainties in the linear heat generation rates which show an uncertainty varying from 5% initially to 10% at EOL. In the ORNL calculations, however, a 5% uncertainty is assumed throughout the irradiation.

The results of the sensitivity study are presented in Figures A5 to A20:

Figure	
A5, 6	FRAPCON-3, fuel centerline temperature
A7, 8	FRAPCON-3, rod internal pressure
A9, 10	FRAPCON-3, fission gas release
A11, 12	FRAPCON-3, effect of ±5% power variation on fuel centerline temperature
A13, 14	FRAPCON-3, effect of ±5% power variation on rod internal pressure
A15, 16	TRANSURANUS, fuel centerline temperature
A17, 18	TRANSURANUS, rod internal pressure
A19, 20	TRANSURANUS, effect of ±5% power variation on fuel centerline temperature

The main features and outcomes are listed below.

Objectives of the sensitivity study

- Determination the effect of the rod power uncertainty on the calculated fuel centreline temperature and fuel pin pressure.

- A code-to-code comparison of FRAPCON-3 and TRANSURANUS as well as code-to-experiment comparisons for each code.

- Study of the effect of fuel thermal conductivity correlations.

General code-to-code-to-experiment conclusions

- The TRANSURANUS temperature predictions compare more favourably with data than FRAPCON-3 (Figures A5, A6, A15 and A16).

- The FRAPCON-3 pressure predictions are much better than TRANSURANUS (Figures A7, A8, A17 and A18).

- TRANSURANUS does not predict significant fission gas release (throughout the irradiation); therefore, the code significantly underpredicts the rod pressure response.

- The FRAPCON-3 MOX thermal conductivity correlation [5] and the ITU correlation [6] within the same framework (i.e. code) yield essentially equivalent fuel centreline temperatures (figure not shown).

- Code-to-code modelling differences (for example, fuel densification and swelling, fuel relocation, FGR models) account for the significant differences in the code-to-code predictions.

General conclusions on power uncertainty effects

- Without the FGR feedback, an uncertainty of ±5% in the power generation results in an uncertainty of <±5% in the calculated fuel centreline temperature (see FRAPCON-3 results, Figures A11 and A12 at times <175 days, or TRANSURANUS results, Figures A19 and A20 throughout the irradiation).

- Realistically, the temperature differences (produced by ±5% power uncertainty) significantly affect the fission gas release models and FGR which in turn affects the pellet-to-clad gap conductance. This can result in:
  - -10 to +15% range on the computed fuel centreline temperature (see Figures A11 and A12);
  - -30 to +40% range on the computed fuel rod pressure (see Figures A13 and A14).

- The inclusion of power uncertainties does produce calculated temperatures and pressures (FRAPCON-3) which envelope the experimental data (see Figures A5 through A8).

Figure A.5. FRAPCON-3 Rod 1 (solid) centreline temperature

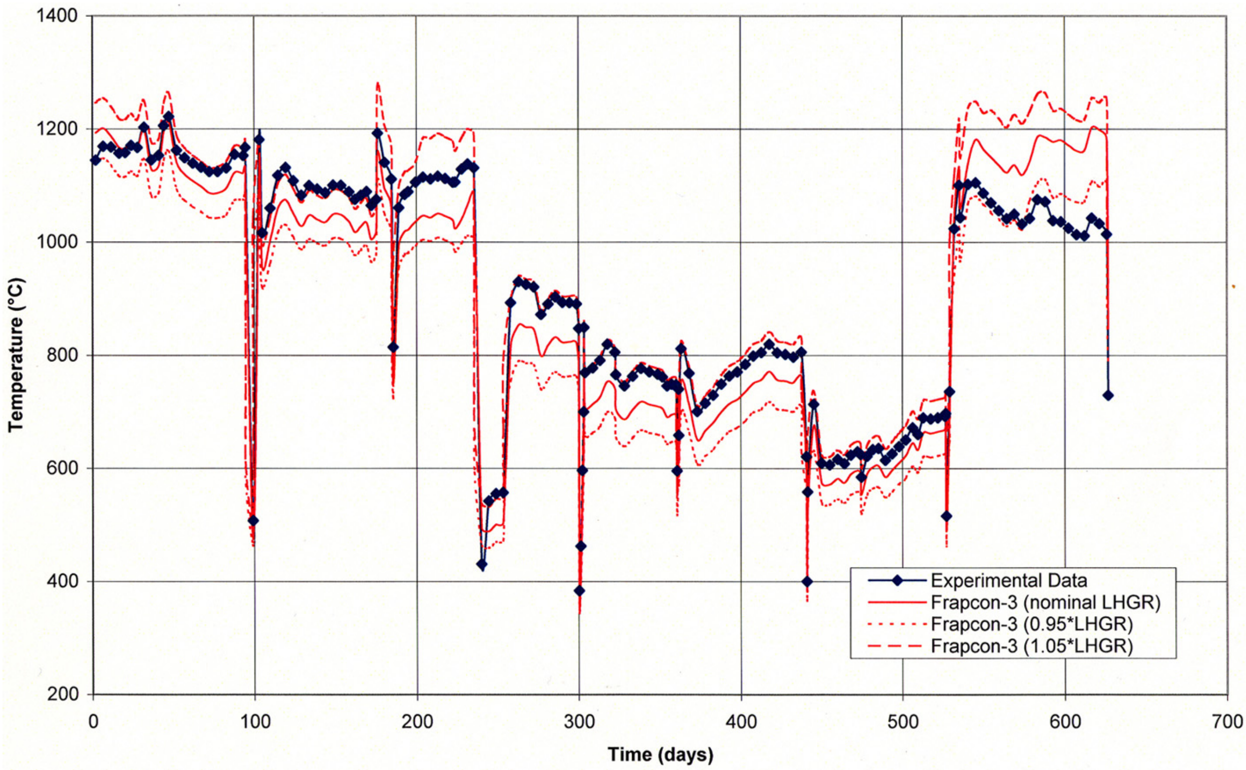

Figure A.6. FRAPCON-3 Rod 2 (hollow) centreline temperature

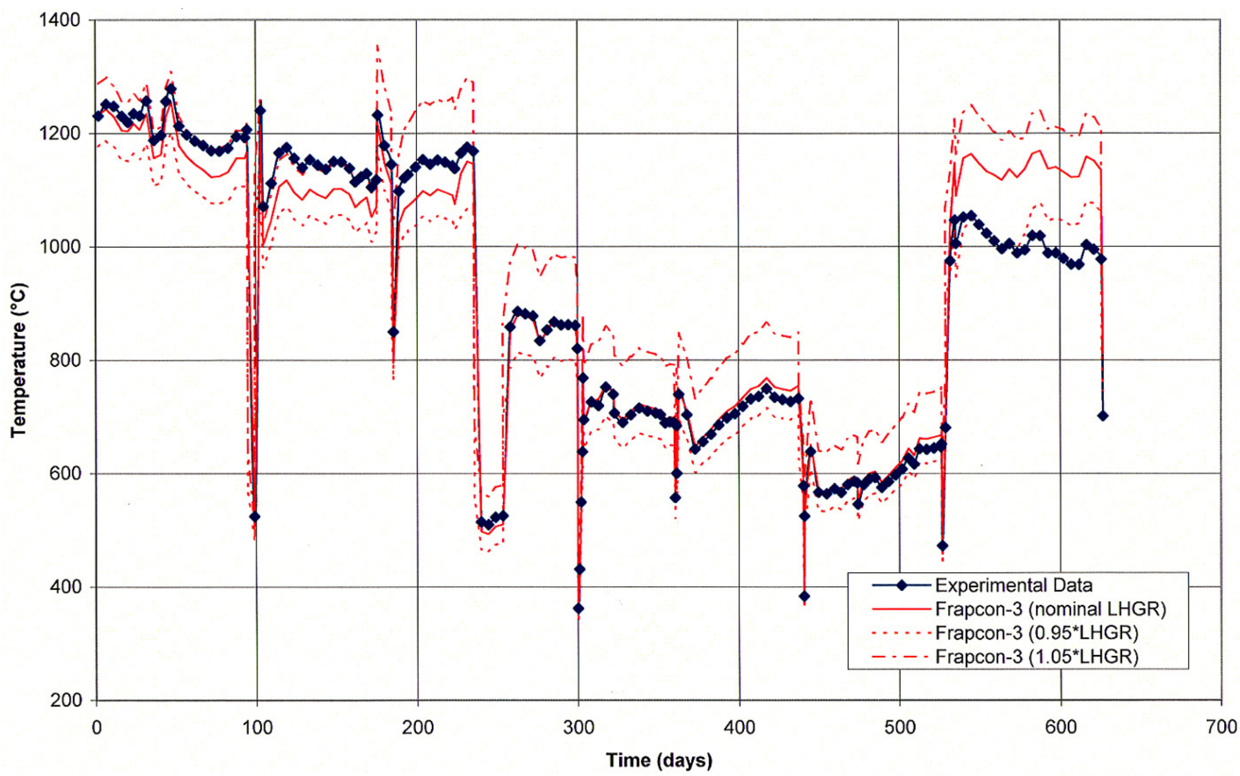

Figure A.7. FRAPCON-3 Rod 1 (solid) internal pressure

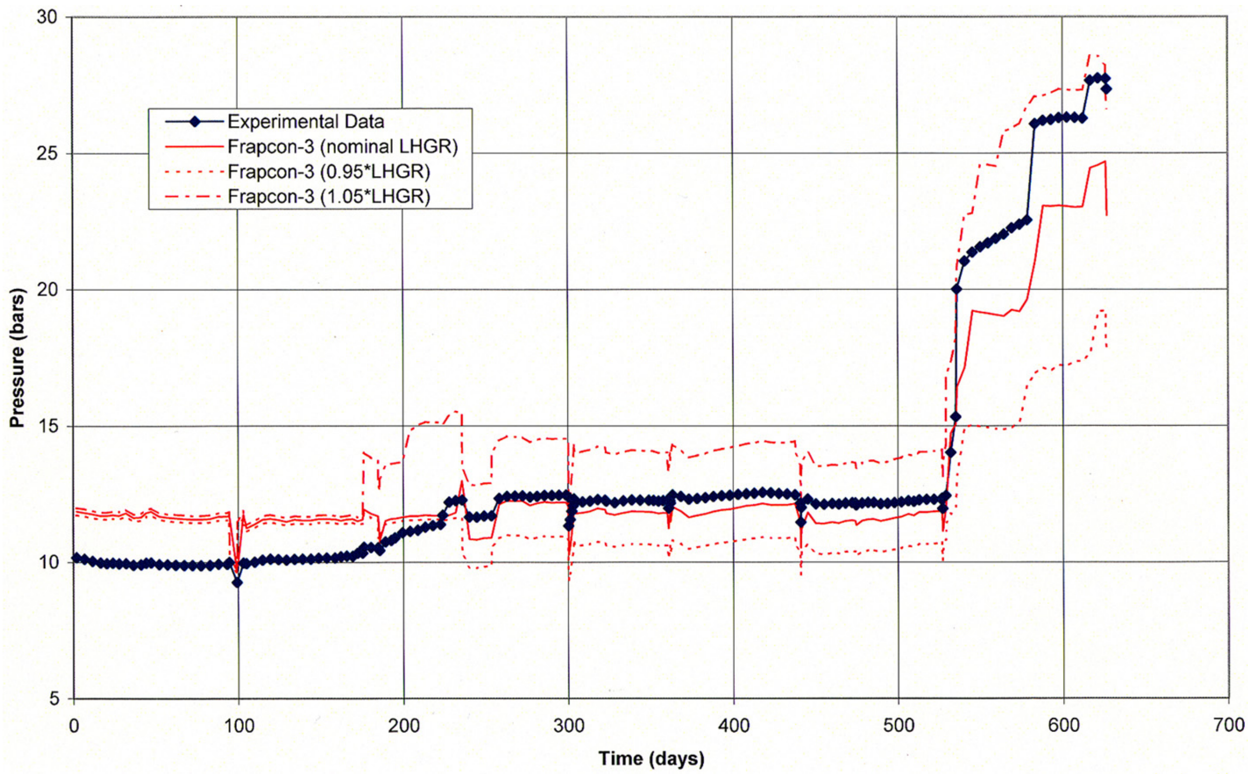

Figure A.8. FRAPCON-3 Rod 2 (hollow) internal pressure

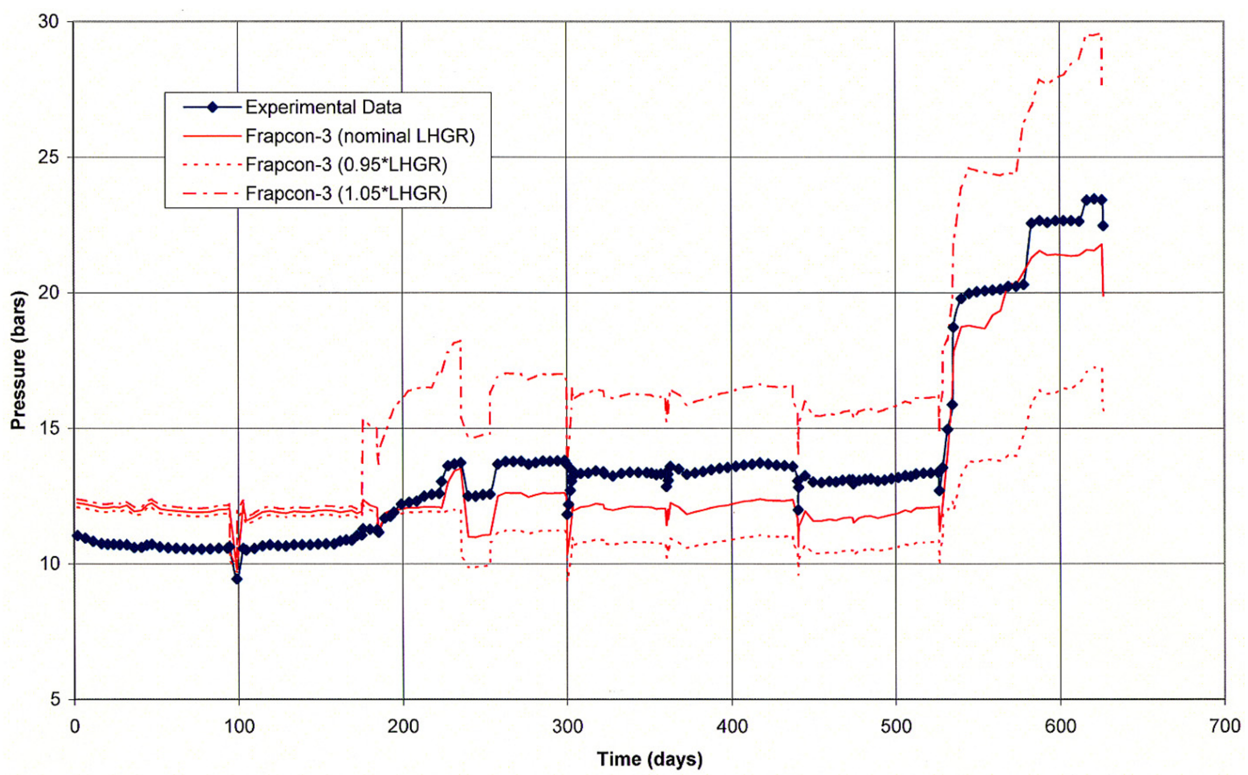

Figure A.9. FRAPCON-3 Rod 1 (solid) calculated fission gas release

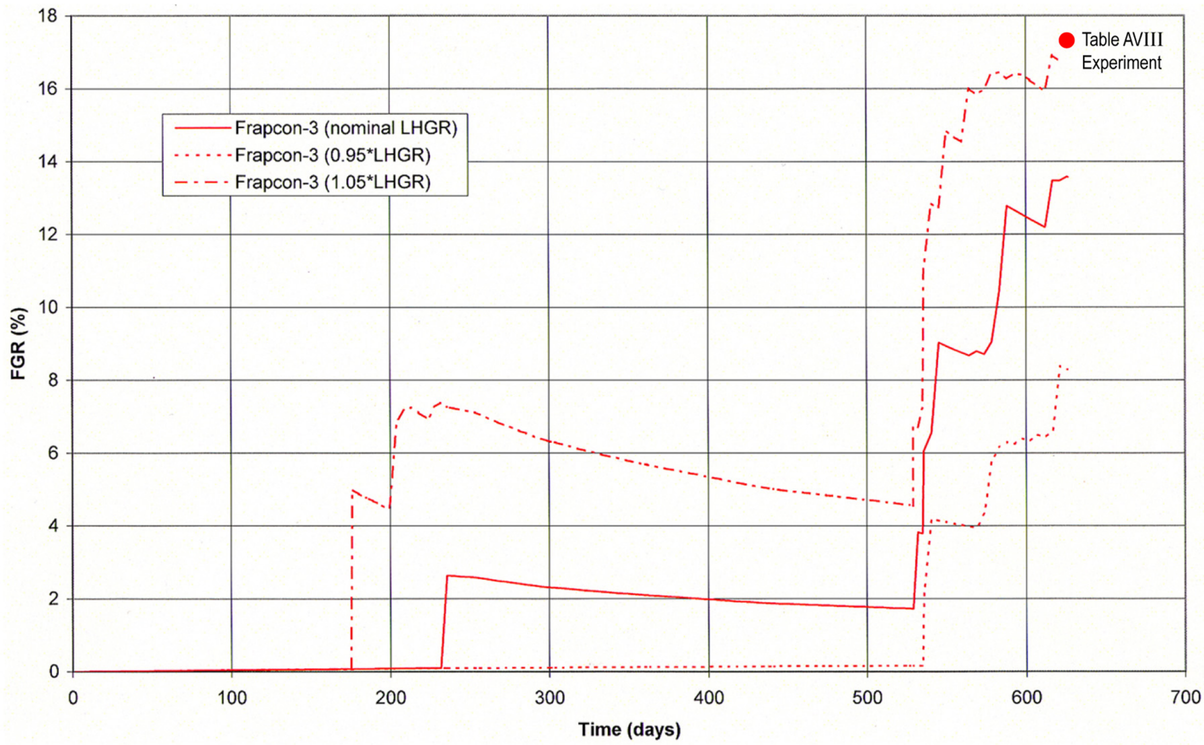

Figure A.10. FRAPCON-3 Rod 2 (hollow) calculated fission gas release

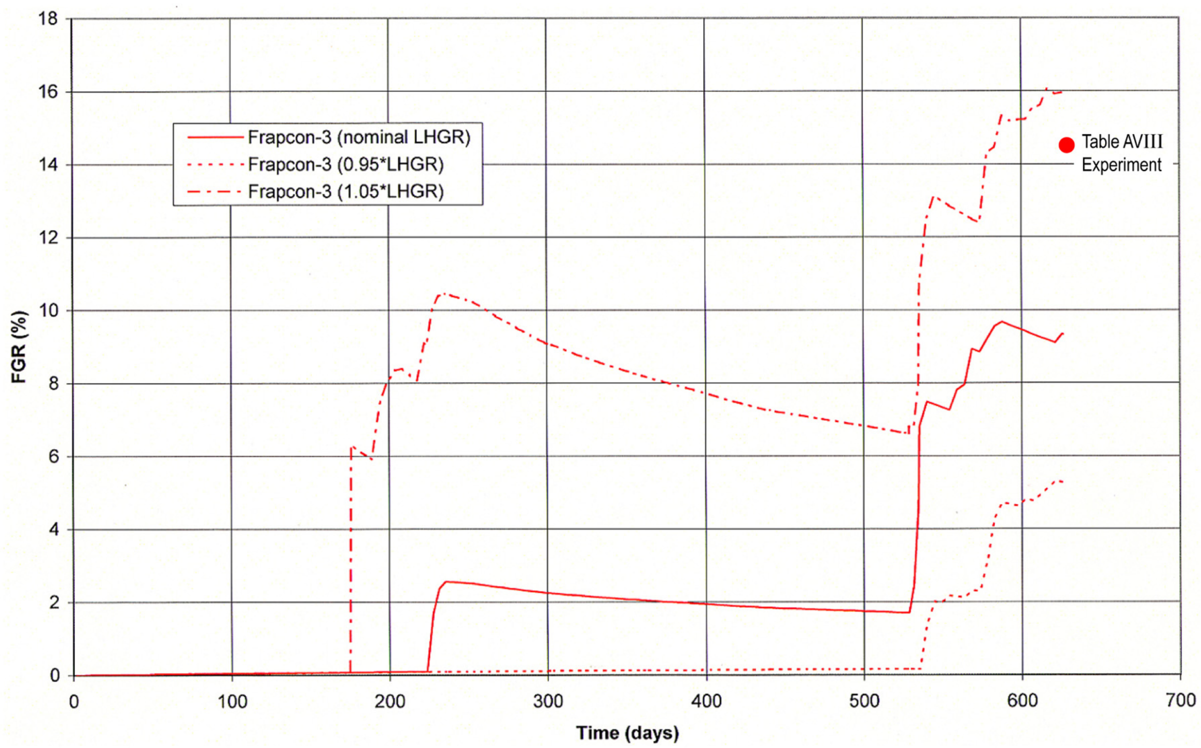

Figure A.11. Effect of ±5% power variation on Rod 1 (solid) FRAPCON-3 calculated temperature

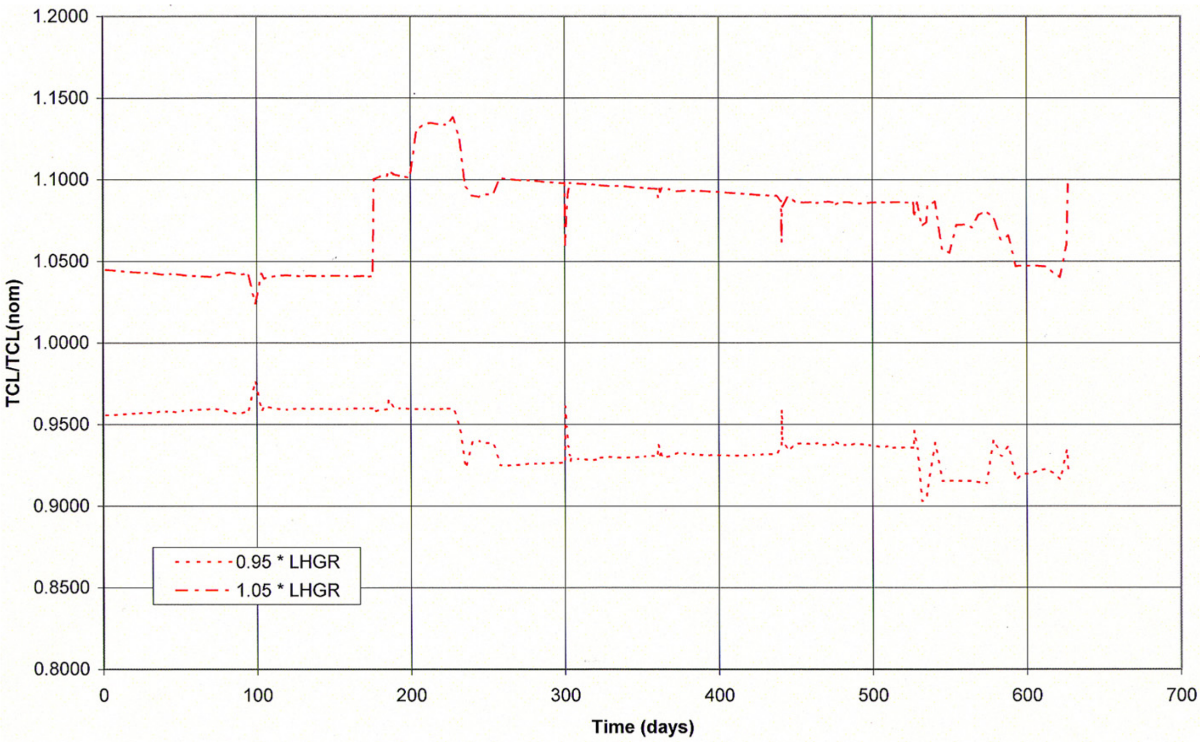

Figure A.12. Effect of ±5% power variation on Rod 2 (hollow) FRAPCON-3 calculated temperature

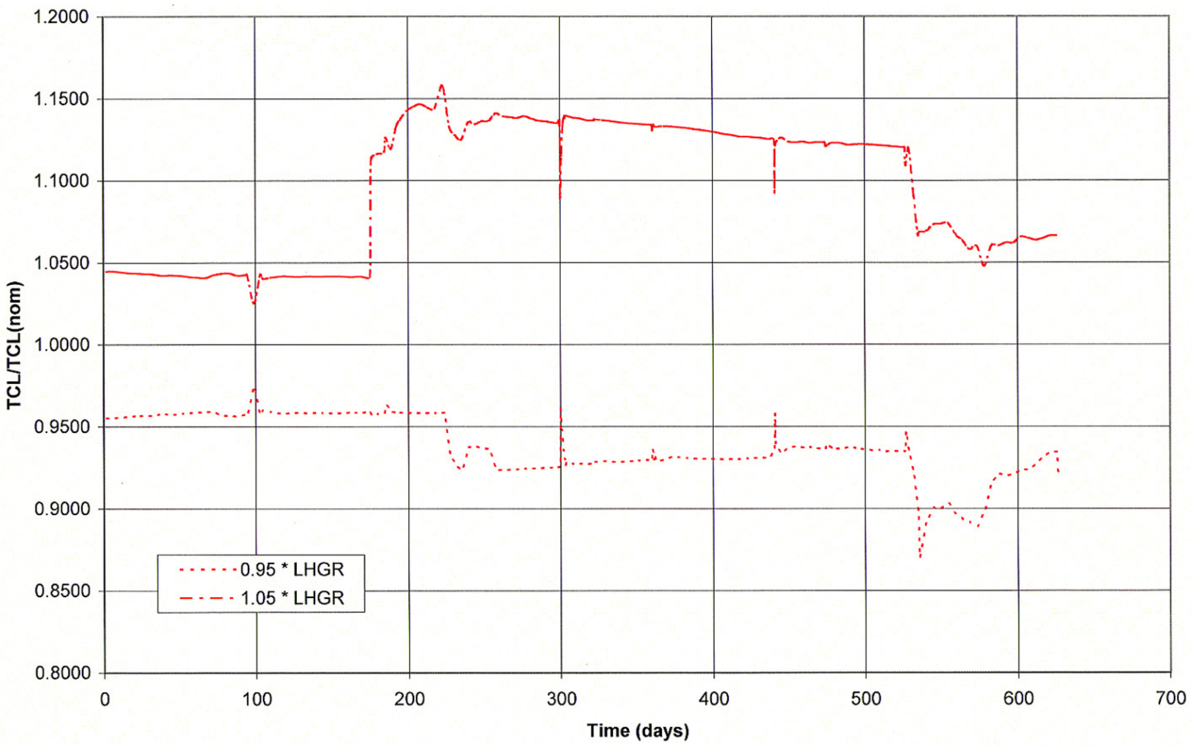

Figure A.13. Effect of ±5% power variation on Rod 1 (solid) FRAPCON-3 calculated pressure

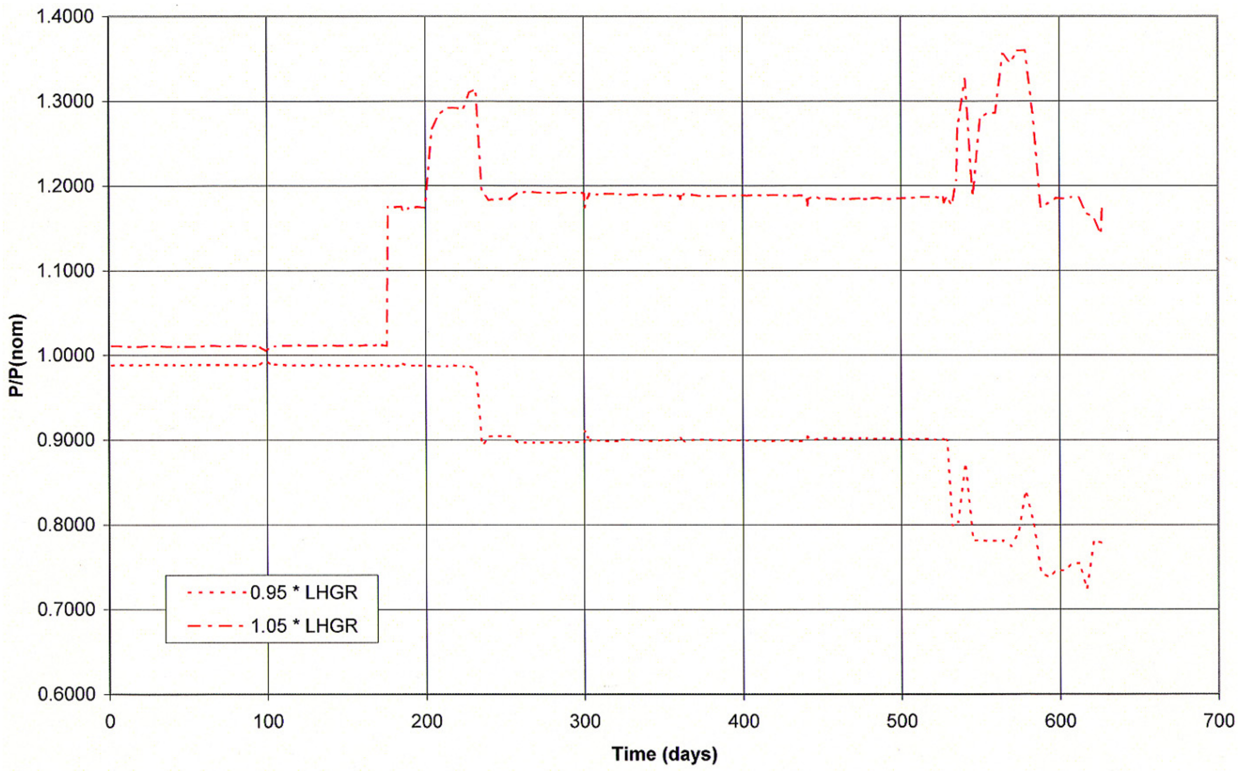

Figure A.14. Effect of ±5% power variation on Rod 2 (hollow) FRAPCON-3 calculated pressure

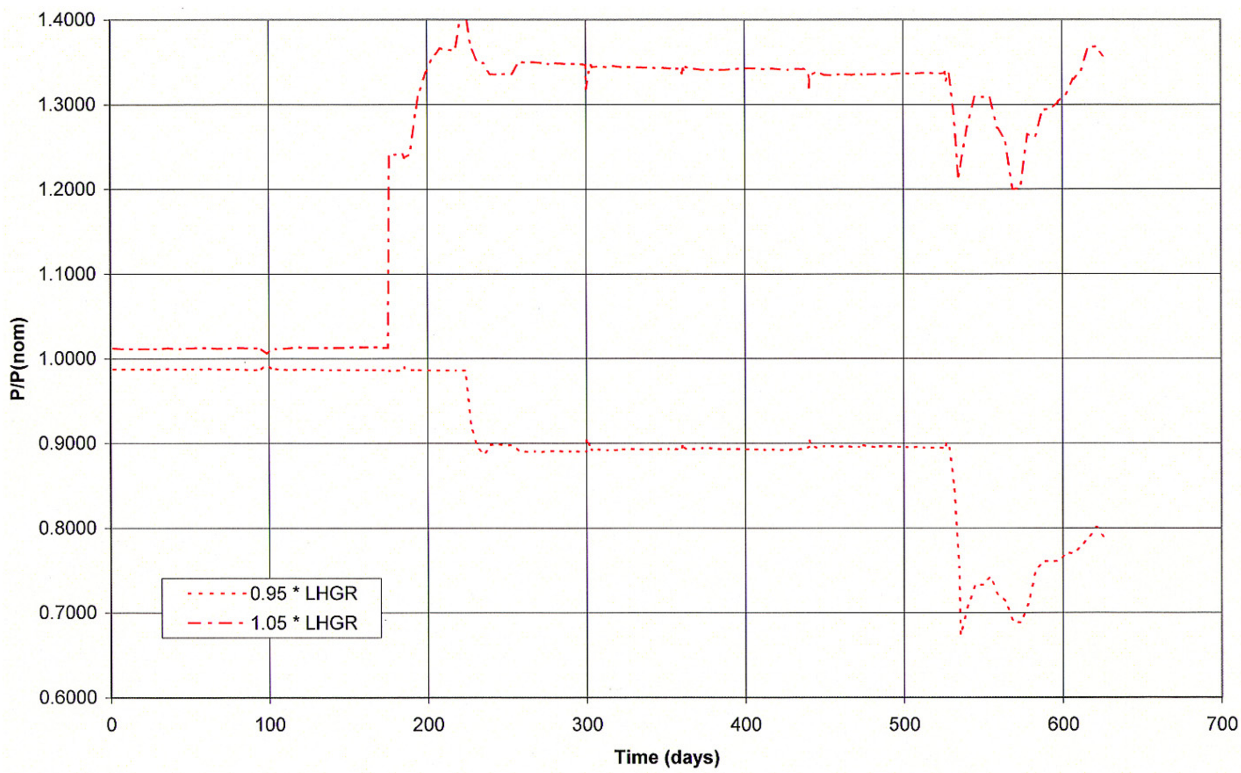

Figure A.15. TRANSURANUS Rod 1 (solid) centreline temperature

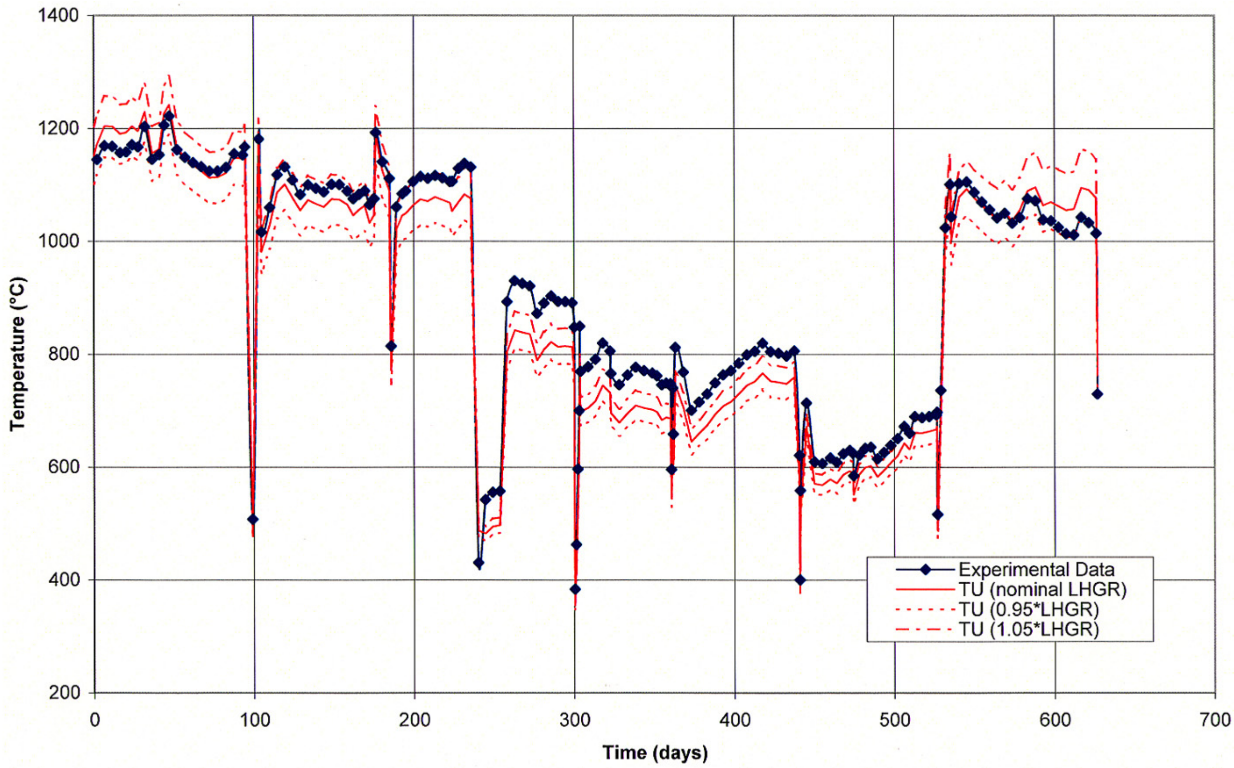

Figure A.16. TRANSURANUS Rod 2 (hollow) centreline temperature

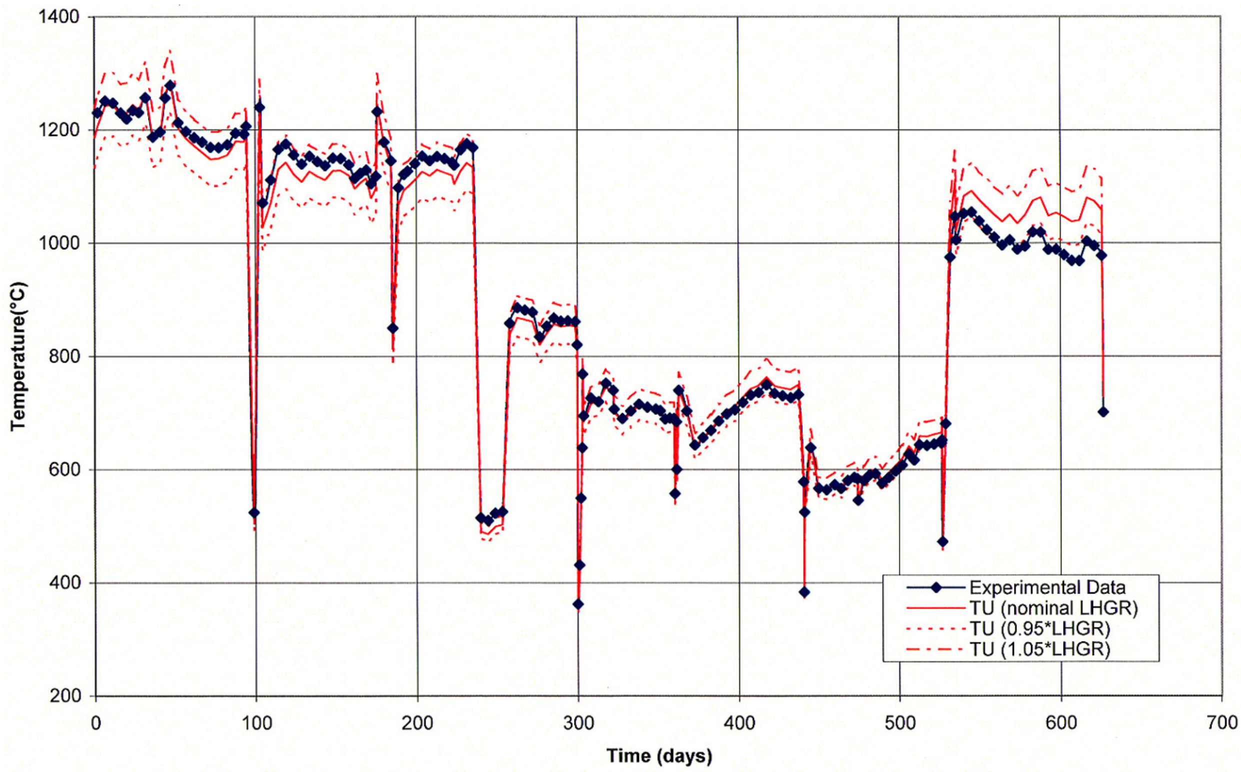

Figure A.17. TRANSURANUS Rod 1 (solid) internal pressure

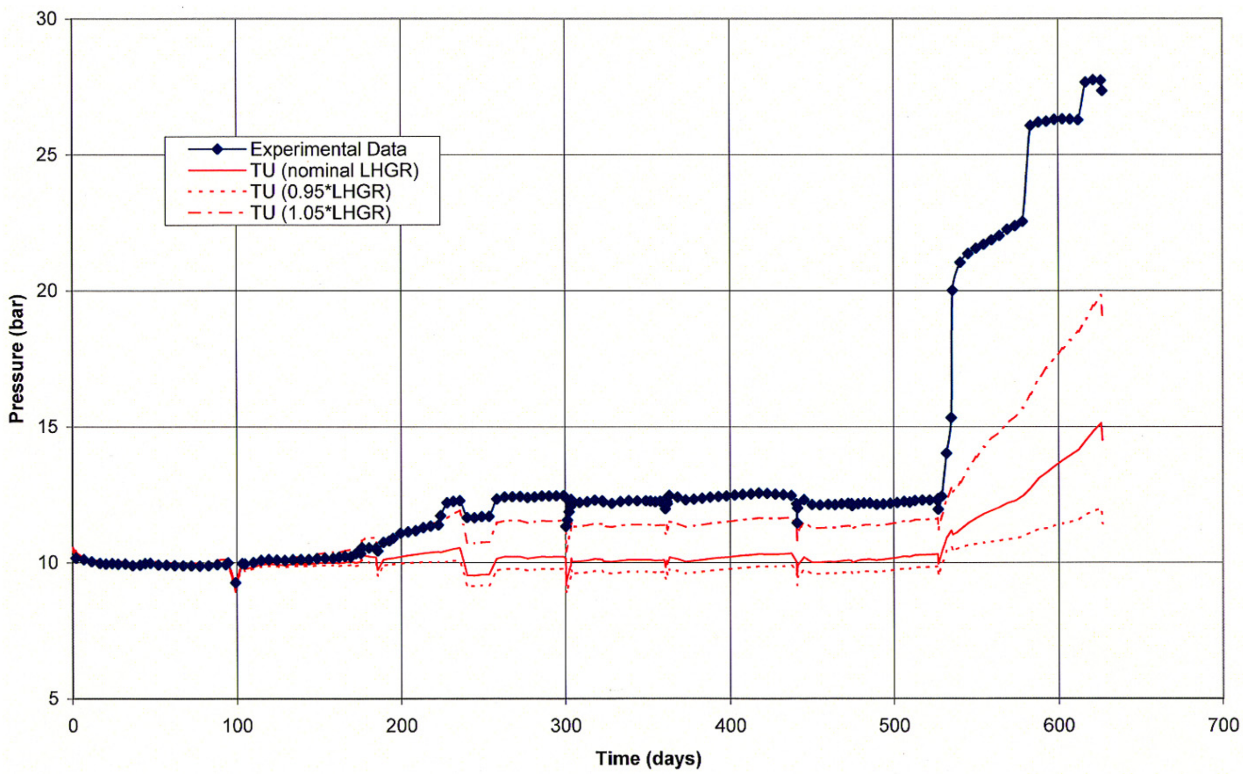

Figure A.18. TRANSURANUS Rod 2 (hollow) internal pressure

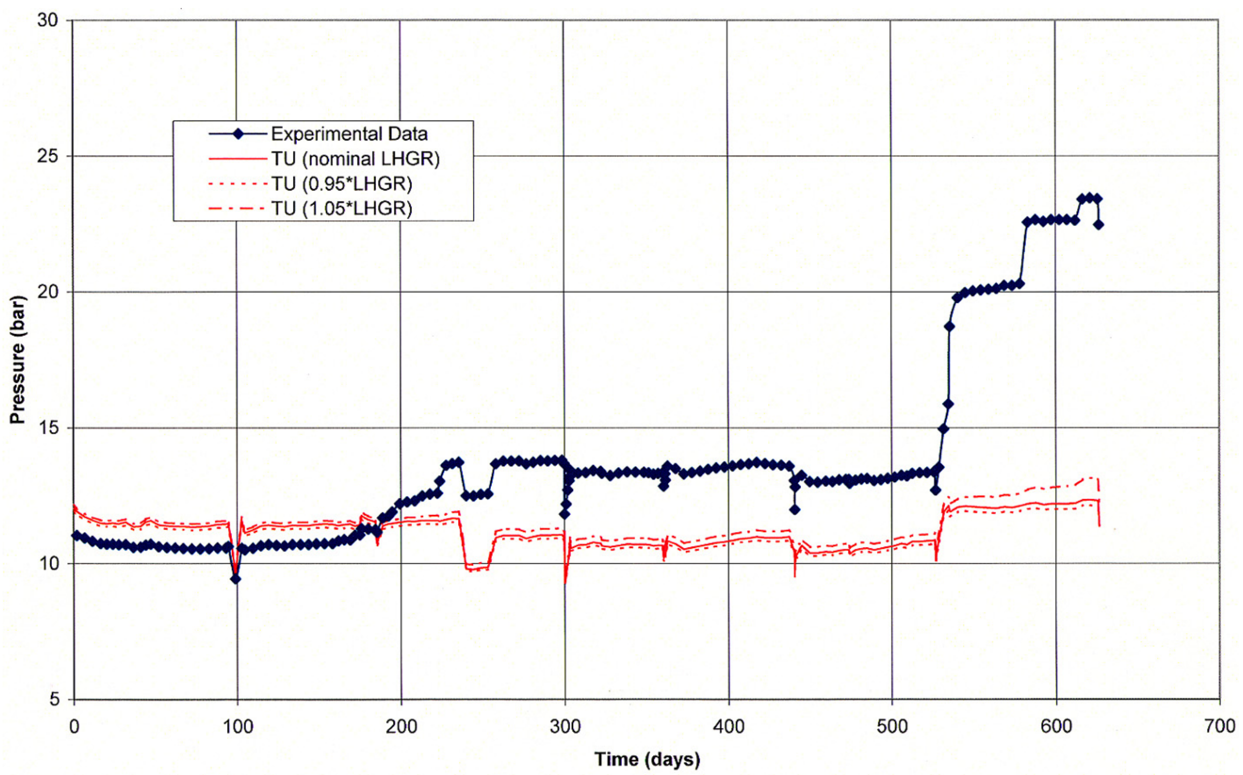

Figure A.19. Effect of ±5% power variation on Rod 1 (solid) TRANSURANUS calculated temperature

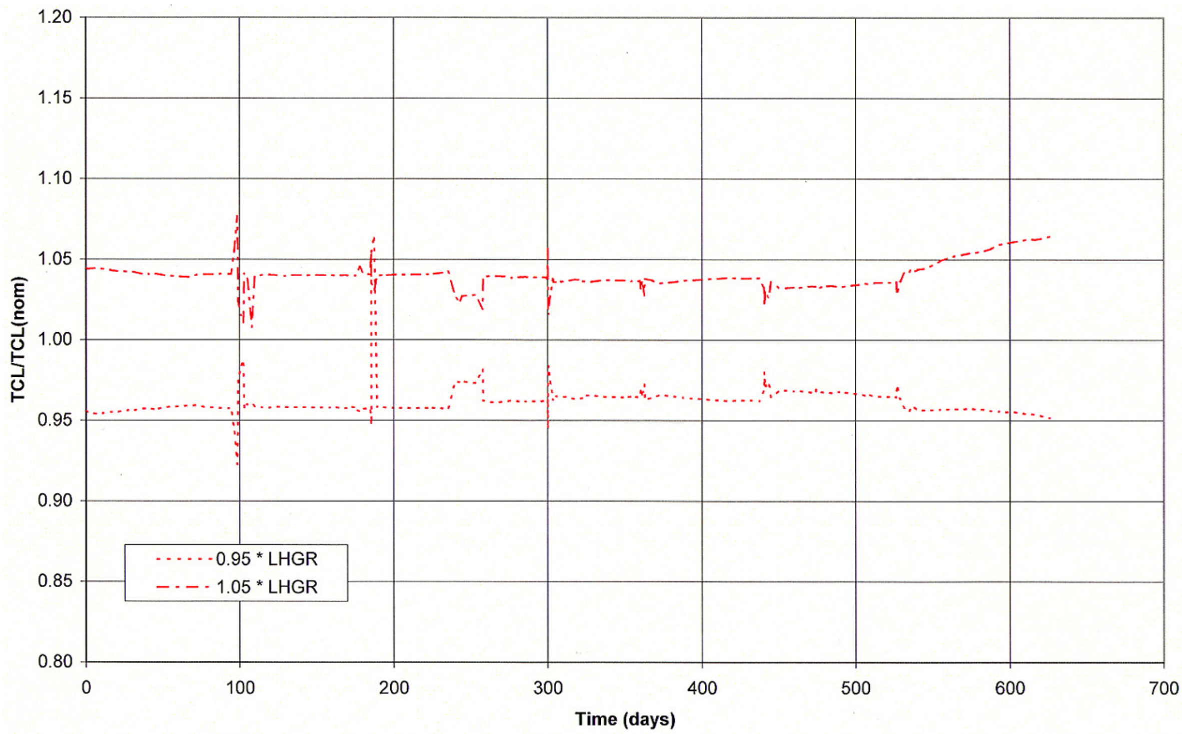

Figure A.20. Effect of ±5% power variation on Rod 2 (hollow) TRANSURANUS calculated temperature